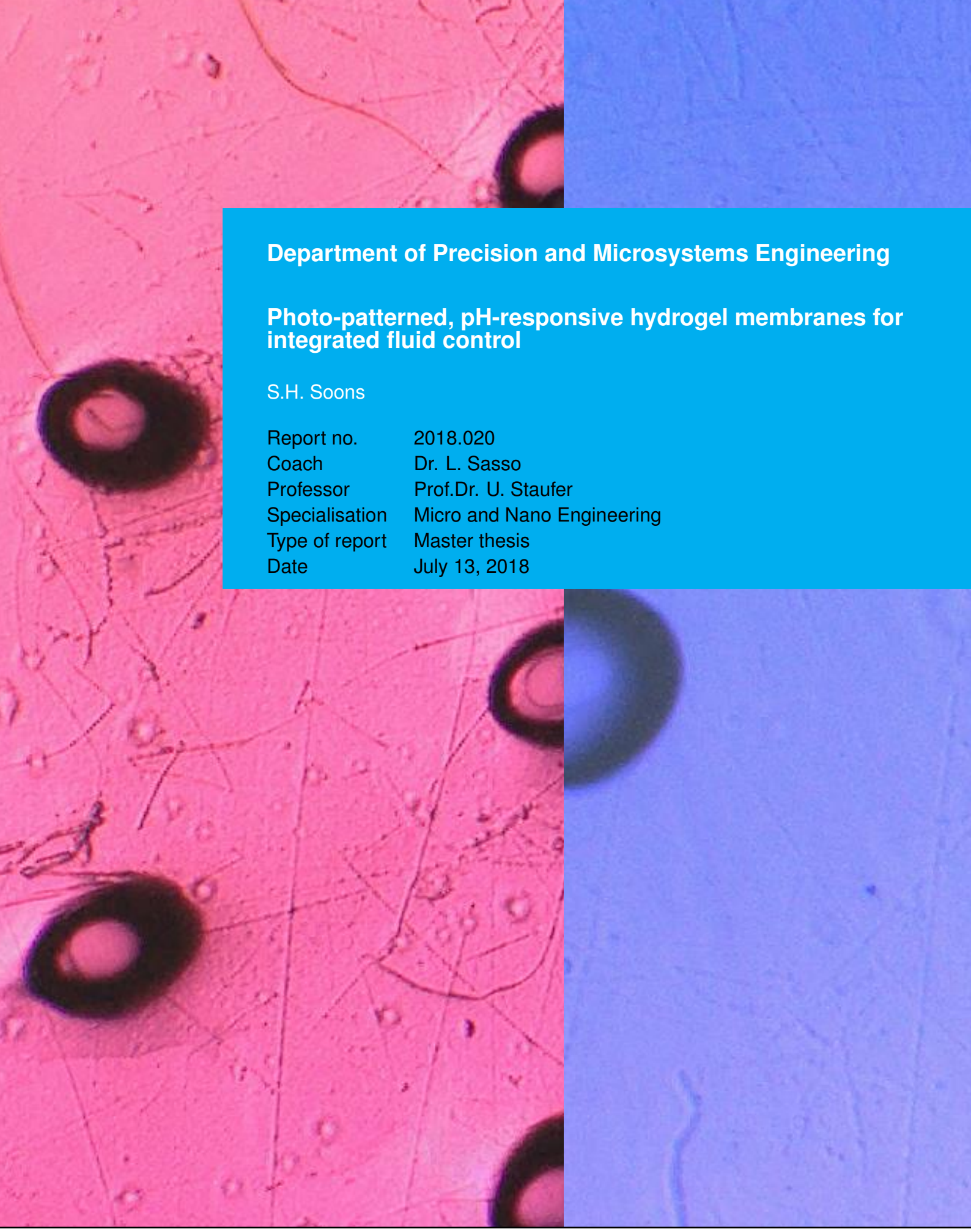

Department of Precision and Microsystems Engineering

Photo-patterned, pH-responsive hydrogel membranes for integrated fluid control

S.H. Soons

Report no.	2018.020
Coach	Dr. L. Sasso
Professor	Prof.Dr. U. Staufer
Specialisation	Micro and Nano Engineering
Type of report	Master thesis
Date	July 13, 2018

Photo-patterned, pH-responsive hydrogel membranes for integrated fluid control

by

S.H. Soons

to obtain the degree of Master of Science
at the Delft University of Technology,
to be defended publicly on Friday July 27, 2018 at 11:00 AM.

Student number: 4090187
Project duration: October 12, 2017 – July 27, 2018
Thesis committee:

Prof. dr. U. Staufer,	TU Delft, chair
Dr. L. Sasso,	TU Delft, supervisor
Dr. Ir. M. Langelaar,	TU Delft

TU Delft

Summary

To control fluid transport, microfluidic systems often make use of pressure driven flow and pneumatically actuated valves. However these require bulky external instrumentation. An integrated fluid control mechanism would make microfluidic systems more portable, closed and automated. The aim of this project was to create a pH-responsive membrane for integrated fluid control in microfluidic systems. pH-responsiveness will allow the membrane to interact directly with analytes in a microfluidic system.

First pH-responsive materials and fluid control mechanisms to create a pH-responsive membrane were reviewed. Cross-linked polymer hydrogels with pH-dependent volumetric swelling were identified as the most suitable material for the membrane. These materials respond to changes in pH by large volumetric transitions, which creates potential for control over a wide range of flow rates. Furthermore they have an inherent interaction with water and are permeable to small molecules such as H^+ ions. The material is synthesized from a liquid precursor that can be cured through photo-initiated free radical polymerization.

We tested a system for measuring the pH response of the material that consisted of a hydrogel disk that was vertically constrained inside a fluidic channel. Due to this constraint, expansion only occurred in the lateral direction and could be measured using an optical microscope. Furthermore, we developed a method for manufacturing macro-porous hydrogel membranes that gives control over pore size, shape and position. A photo-lithography approach was used to pattern the membranes and thereby create pores, using a photo-mask that was manufactured on an office printer in a very fast and low-cost process.

The resulting membranes had a thickness of 140-190 µm and pore diameters of 100-400 µm. The pore size was measured for environmental pH of 1.6 and 7.1, within this range the pores doubled in diameter. Furthermore the pH-responsive deformation ratio of the pores increased significantly with increasing curing time and decreasing pore diameter. The results suggest that there is a difference in material properties around the pores that develops due to a local difference in received exposure dose during curing.

The fluidic properties and pH-response of the membrane can be adjusted to suit a specific application by changing the design, the curing time or the chemical composition of the membrane. The constrained disk system can then be used to measure and compare the pH-response of different potential materials.

Contents

1 Introduction

The aim of this project is to create a pH-responsive membrane for integrated fluid control in microfluidic systems. Microfluidic systems are a promising technology for applications in fields such as (bio)chemical analysis and cell biology. They can best be described as miniaturized lab equipment. In microfluidic systems, fluids are manipulated in channels with sub-millimetre dimensions. The small size creates unique and useful characteristics such as laminar flow, while requiring very low volumes of samples and reagents. By making use of these characteristics, microfluidic systems can perform separations and detections with high resolution and sensitivity, while allowing for parallel testing of large numbers of compounds.

To control fluid transport, many microfluidic systems make use of pressure driven flow and pneumatically actuated valves. However this requires bulky external instrumentation and a large number of connectors [69]. An alternative is to integrate fluid control mechanisms into the system. This would make microfluidic systems more portable and more closed. Furthermore microfluidic processes could be made more automated and be simpler to operate, which lowers the barriers for adoption by prospective users [60]. To be suitable for implementation in a microfluidic system, an integrated fluid control mechanism should be able to sense and respond to local conditions, be flexible in design so that it can be used in different processes and microfluidic system configurations and achieve the required (precision in) transport rates.

Membranes are semi-permeable barriers, that are designed to control transport of species [17]. Since the 1990's the interest in membranes for microfluidics has grown [17]. With the rise of organ-on-chip technology this interest has increased even further. Organ-on-chip systems are microfluidic devices that mimic a chemical and physiological micro-environment inside a human organ. They are used to culture cells to create human organ and disease models for (bio)medical and pharmaceutical research. Within organ-on-chip systems membranes often have a critical function as a support for cell culturing [31]. A further benefit to membranes is that they can simultaneously perform different functions, such as fluid control and filtration and they have a large surface area that can be used to hold a catalyst. Membranes can be dense or porous. Porous membranes have empty spaces (pores) in the membrane, through which transport occurs. In this case transport is mainly governed by membrane morphology [17].

Typically membranes are passive; the material, the morphology and thus the barrier properties of

Tissue or organ	pH
Blood	7.35-7.45
Stomach	1.0-3.0
Duodenum	4.8-8.2
Colon	7.0-7.5
Tumor, extracellular	7.2-6.5

Table 1.1: pH variations in tissue. Adapted from [61, 75].

the membrane do not change over time. The rate of transport over the membrane can only be controlled trough the driving pressure. However, a membrane could be made active by using an active, or stimuli-responsive material. Stimuli-responsive materials are materials that see a change in one or more of their properties in response to a stimulus from the environment. To achieve tunable control over the flow through a membrane, the barrier or resistance to flow must be altered reversibly, for example by a stimuli-responsive change in pore size [80]. There are a few fundamental classes of stimuli which can induce responses in materials. These include: temperature, pH and various chemicals, electric fields, electromagnetic radiation (light) and mechanical forces [74].

For integrated fluid control, pH is an especially interesting stimulus because it could allow membranes to interact directly with analytes in a microfluidic system. In biological systems and processes in the human body, pH is often an important factor. Many organs and diseases within the human body are characterised by a specific (change in) pH, as illustrated in table 1.1. Also for non-biological applications pH is a useful stimulus that will create a direct interaction with chemical processes, whereas many other stimuli would still have to come from an external source.

This report starts with a literature review to identify the best mechanism to achieve pH-responsive fluid control. The review also provides information on the properties and synthesis of the pH-responsive swelling hydrogel that constitutes this mechanism. Methods for simulation of pH-responsive hydrogel swelling were also reviewed, these are included in appendix B. Based on the insights from the literature review, a plan of approach for the lab phase of this project was made. This is discussed in section 1.4.

The second chapter of this report consists of a paper that describes the manufacturing and characterization of the photo-patterned, pH-responsive hydrogel membranes for integrated fluid control that gave this report its title. Next to this, a system to measure the pH-response of a hydrogel material is also discussed.

Appendix A, 'Disk and membrane manufacturing; Investigation of optimal curing time and evaluation of results' was included to give a more in depth understanding of the different factors that played a role in membrane manufacturing and the system to to measure material pH-response. The appendices also contain detailed descriptions of the manufacturing methods, measurement methods and designs that were used.

1.1. Materials and mechanisms for pH-responsive fluid control

For this project, pH is the selected stimulus, so as to make the membrane compatible and able to interact with fluidic and biological systems. In this section a mechanism to achieve pH-responsive fluid control will be selected.

1.1.1. Stimuli-responsive polymer hydrogels

Because of their inherent interaction with water and permeability to small molecules such as the H^+ ions that provide the stimulus, polymer hydrogels are a very suitable material.

Polymers

Polymers are a commonly used membrane material, since they have many advantageous properties. They are inherently biocompatible and can be modified to tailor made properties. Furthermore they allow for easy and low-cost manufacturing, because they can be processed through well-established micro- and nanofabrication methods such as as photolithography and micromoulding [33].

Polymers are macromolecules composed of a large number of repeating units; monomers. They can consist of one or multiple different monomeric units. Additionally they can have different structures: linear, closed and circular, branched or even cross-linked. The properties of a polymer material are determined by the monomeric units and their sequence, the size and structure of the polymer molecules, the relative orientation of molecules to one-another and the interactions (binding) between molecules. These attributes can give rise to characteristic mechanical properties, but can also bring about unique behaviours, such as allowing the attachment of specific molecules, providing programmable molecular interactions.

Polymer hydrogels

When polymer molecules are linked to each other by covalent bonds, crosslinked polymer networks are formed. This usually increases the strength and toughness of the material. Hydrogels are cross-linked polymeric materials that swell in water. They can absorb large amounts of water due to hydrophilic groups that are incorporated in the network. The crosslinking between chains prevents dissolution and provides structure and physical integrity [54]. It provides an elastic restoring force that counters the expansion of the network. The liquid that is incorporated also helps in retaining the network from collapsing [66].

Hydrogel networks can absorb and retain up to 99% water. At the same time, a hydrogel can be porous for the diffusion of small molecules, like oxygen. These properties give the material a resemblance to biological tissues, making it a good candidate for bioengineering applications [66].

Stimuli-responsiveness

A stimulus responsive material is a material that changes (one of) its properties when exposed to an external stimulus. For example: a material that, when irradiated with a specific wavelength of light, changes colour. In this case the light is the stimulus and the change in colour is the response. The stimuli-responsive material can be seen as a signal transducer; it converts one signal (the stimulus) into a different type of signal (the change in property).

Such a change in material properties arises from a shift in the conformation of molecular components of the material. This shift in conformation alters the properties of the molecule, which in turn affect the properties at the macro scale. So the key to stimuli-responsiveness is the ability of molecular components of a material to change their conformations in such a way that the properties of the material at the macro-scale are affected. Consequently a stimuli-responsive material needs to contain molecular entities with a dual character [76]. A system requires energy to go from one state to another. The energy requirement depends on the initial, transition and final physical and chemical states [77]. For a shift in conformation to take place, the stimulus must provide this energy.

The stimuli-responsive shift in materials is not necessarily reversible, but for the creation of a stimuli-responsive membrane reversibility is required. Moreover it is important to achieve responsiveness at the right lengths scales, while maintaining mechanical integrity of the network. Other vital aspects of the response are controllability and predictability.

1.1.2. Response mechanisms for fluid control

In order to use a responsive material for fluid control, the response of the material needs to be one that can influence the flow of a fluid. In literature there are several examples of responsive polymer hydrogels being used for this purpose. The applications vary from membranes to microchannels to paper-microfluidics [33, 63, 80].

Response mechanisms are often classified into surface or bulk responsiveness (sometimes called volumetric or solid responsiveness). A surface response can exhibit the transition of various surface properties. In this case one can take advantage of the high surface-to-volume ratio of micro-scale structures. A volumetric response generally leads to a collective deformation of the bulk. In addition to this, other properties are sometimes also altered.

Stemming from these two response mechanism, there are four main mechanisms by which responsive polymers have been used for fluid control. These are: actuation of the hydrogel, permeability of the hydrogel, obstruction by polymer brushes, and surface wettability. These can also occur simultaneously within the same system. These mechanisms will be discussed below, and are summarized in figure 1.1.

Actuation of the hydrogel: Swelling or shrinking through the absorption or expulsion of water causes a hydrogel structure to expand or contract. This actuation of the hydrogel can obstruct or open a channel or pore, as illustrated in figures 1.1 (III), (V) and (VI). Hydrogel pattens which alter their volumetric structure in this way have been applied to microfluidic components such as valves and pumps [33] and to porous membranes [67]. A hydrogel structure in its swollen state can block the path of fluid (”off state”) and reversibly in shrunken state the fluid path is opened (”on state”).

Permeability of the hydrogel: In concert with a volumetric expansion, swelling also increases the average mesh size of the hydrogel network. Hereby permeation through the hydrogel can be increased [23], as is shown in figure 1.1 (IV).

Obstruction by polymer brushes: A polymer brush consists of polymer chains whose ends are grafted (anchored) to a polymer surface. The conformation of these chains depends on their interaction with the surrounding medium. A change in the affinity between the brush hairs and the medium can cause the brushes to extend or collapse, thus changing the brush height [45]. If these polymer brushes are located on the inside walls of pores, this extension or collapse will decrease or increase the radii of the pores, as can be seen in figure 1.1 (I).

Surface wettability: In micro-scale fluidics the high surface-to-volume ratio allows the wettability of hydrogel surfaces to govern fluidic behaviours. Thus hydrophilic surfaces can attract flow in a micro channel through capillary forces, while hydrophobic surfaces can resist and stop flow [33]. The use of changes in wettability for fluidic control is illustrated in figure 1.1 (II).

1.1.3. Evaluation of response mechanisms

As discussed earlier, the focus of this project is on physically opening and closing pores/channels. Hereto simplified assumptions will be made with respect to the behaviour of the medium flowing through these pores. The fluid control mechanisms of permeability and wettability strongly rely on the interaction between the fluid and the material. Therefore these mechanisms are out of the scope of this project. Hydrogel actuation and polymer brushes both fit within the scope. A comparison of these two mechanism will be made below.

Length scale of response

Swelling hydrogels often display large physiochemical reactions to relatively small stimuli [81]. The degree of swelling can be very large, as high as 20,000 (for poly [acrylamide-stat-(acrylic acid)] hydrogels [81]). Pore sizes of swelling-based responsive membranes reported in literature range from 200 nm to 3.7 µm in open state [25, 51, 67, 70, 71].

The height of a grafted polymer brush is affected by the grafting density and the interaction with the solvent [6], but it can never be more than the length of the grafted polymer chains. Pore sizes of polymer brush-based responsive membranes reported in literature range from 400 Å to 204 nm (in open state) [29, 49].

Switching kinetics: time scale of response

According to Kocak et al. [35], swelling of a ph responsive hydrogel is very slow (up to hundreds of hours to reach equilibrium), but de-swelling is very fast (minutes). Suthar [66] states that hydrogels

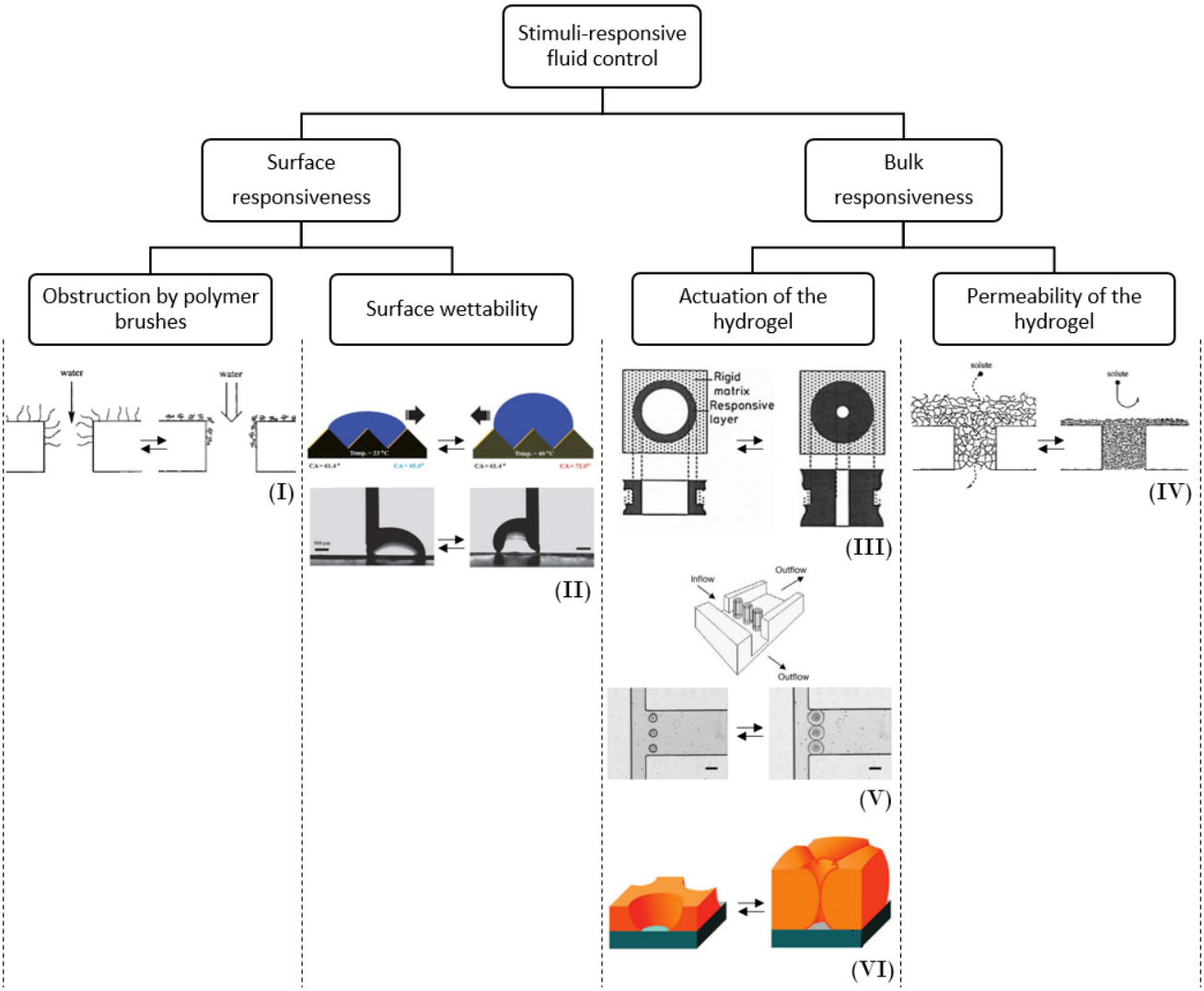

Figure 1.1: Mechanisms for stimuli responsive fluid control; schematic overview with examples from literature. (I) Schematic drawing of the permeation mechanism through PAA-grafted glass pores. Adapted from [53]. (II) Illustrations and movie-cuts showing the temperature dependent directional liquid flow on a two-face prism array. Water flows toward the less hydrophobic surface. Adapted from [34]. (III) Principle of a pH responsive pore consisting of a rigid matrix and a responsive layer. Adapted from [67]. (IV) Schematic drawing of the permeation mechanism through PAA-based hydrogel. Adapted from [53]. (V) Prefabricated posts with hydrogel jackets inside a microfluidic channel. The hydrogel jackets block the side channel branch in their expanded state. Adapted from [8]. (VI) Schematic representations of a single pore of a polyelectrolyte membrane switched between the closed and open states. Adapted from [72].

have a relatively large time constant when responding to an applied stimulus, because the response is limited by the rate of dissociation and association of mobile ions across the solvent-hydrogel interface. However, according to other sources, the response is limited by the diffusion through the hydrogel structure [8, 24]. In this case, scaling down the dimensions of a hydrogel structure could improve the response time, which is confirmed by Stuart et al. [63], who state that hydrogel thin films have fast kinetics of swelling and shrinking in comparison to bulk gels.

In discussions of response time in literature, no clear distinction is made between swelling and grafted layers, since the extension of brush hairs is often also called swelling. From this point of view the only difference between polymer brushes and bulk swelling is that polymer brush layers are inherently thin, thus limiting the diffusion time. Moreover for both swelling and polymer brushes, quantitative results on response times are difficult to find.

1.1.4. Discussion and conclusions

Polymer hydrogels are an ideal material for pH-responsive fluid control because of their inherent interaction with water and permeability to small molecules such as H^+ ions. Hydrogel swelling actuation and obstruction by polymer brushes are two mechanisms by which polymer hydrogels have been used for stimuli-responsive fluid control, that fit within the scope of this project.

Bulk swelling can create responses with larger length-scales, permitting higher flow rates and control over a wider range. The time-scale of the response is a possible downside, although a conclusive evaluation of this aspect could not be found. However, there are possibilities for improving the switching dynamics, such as decreasing the diffusion time [24].

Considering research opportunities, the use of polymer brushes is more of a chemical, manufacturing problem rather than a mechanical, design problem. The length of the brush-hairs has a significant effect, but control over this depends on the synthesis and grafting processes, which are outside of the field of interest for this project.

The use of swelling on the other hand introduces an interesting aspect; that of distributed actuation. Aside from fluid control, this type of actuation could also be interesting for other applications, using other stimuli. Another advantage of bulk swelling is that the material can be modelled as a continuum, which simplifies simulations and gives the opportunity to experiment with different pore geometries. Furthermore, by incorporating the responsive mechanism in the bulk of the material, the surface is free to be functionalized for other applications, such as sensing.

All things considered, bulk swelling of pH-responsive polymer hydrogels is selected as the most suitable fluid control mechanism for this project.

1.2. pH-responsive swelling hydrogels

As discussed, hydrogels absorb and retain water, because they consist of networks of hydrophilic polymers. Hydrophilic polymers contain polar or charged functional groups [2]. The amount of water absorbed by a hydrogel, or the degree of swelling, depends on the density of these polar or charged groups. If this density changes in response to a stimulus, the hydrogel will swell or shrink in response to that stimulus.

1.2.1. pH-responsive swelling mechanism

A pH responsive polymer generally contains weakly basic or weakly acidic groups, which protonate or deprotonate (ionize) in response to the pH of the medium [35]. In literature these are also referred to as ionizable or electrolyte groups and the molecules that contain them as polyelectrolytes (PELs) [80]. During this ionization, electro-neutrality of the gel on a macroscopic scale is preserved because the polymer-network charge is compensated by the charge of small counter-ions. Thus the ionization of PELs in a hydrogel is paired with a diffusion of counter-ions into or out of the gel [66].

The ionization of side groups affects the swelling of the gel in two ways: It changes both the hydrophilicity and the osmolarity of the gel. Firstly, ionization changes the amount of charge groups and thus the wettability of the polymer molecules that make up the gel. Secondly, the diffusion of mobile counter-ions into or out of the gel changes the osmotic pressure within the gel network [55]. If the osmotic pressure inside the gel is different from the surrounding medium, this this causes the gel to absorb or release water.

However, swelling or de-swelling does not necessarily continue until the osmotic pressures of the gel and medium are equal. The swelling ratio of the gel is determined by an equilibrium between the osmotic pressure in the gel and the elasticity of the gel network, which counteracts the absorption of water.

pH-responsive groups

As mentioned above, pH responsive polymers generally contain ionizable groups, which can be acidic or basic. A list of acidic and basic pH-responsive polyelectrolyte groups is given in table 1.2. Hydrogels that contain acidic monomers become negatively charged by releasing protons at high pH and thereby swell. Similarly, basic hydrogels become positively charged by accepting protons at low pH and thereby swell [35]. Amphoteric hydrogels contain both basic and acidic monomers. They swell at low and high pH, but de-swell at isoelectric point [35], which is the pH at which the gel contains no net electrical charge. The swelling and de-swelling behaviour of these three types of pH responsive hydrogels is illustrated in figure 1.2.

Acid dissociation constant

The behaviour of pH responsive groups is usually summarized using one value, the acid dissociation constant pKa. The pKa is a quantative measure of the strength of an acid in solution, that is characteristic for that acid. It is the pH at which the solution contains exactly the same amount of the protonated

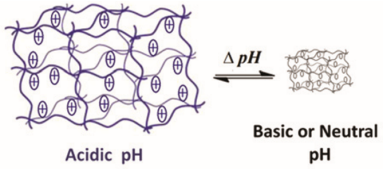

(a) Basic hydrogel

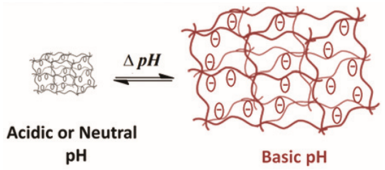

(b) Acidic hydrogel

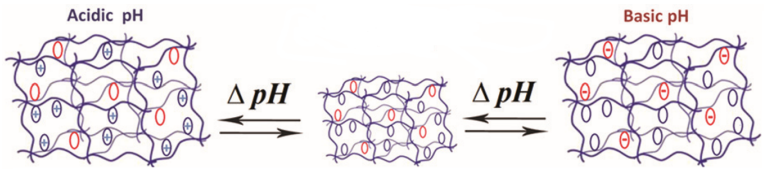

(c) Amphoteric hydrogel

Figure 1.2: The swelling and de-swelling behaviour of basic, acidic and amphoteric hydrogels. Figures adapted from [35].

	Type	Characteristic group	Polymers containing this group
Acidic	Carboxylic acid	-COOH	PAAc, PMAAc, PEAAc, PPAAc, PVBA, PIA
	Phosphoric / phosphonic acid	-OPO3H2 or -PO3H2	PEGAP, PVPA, PEGMP, PVBPA
	Sulfonic acid	-SO3H	PVSA, PSSA, PAMPS, PKSPMA
	Amino acid	-NH2 and -COOH	PASA, PLGA, PHIS
	Boronic acid	-BOOH	PVPBA, PAAPBA
Basic	Tertiary amine	R3-N	PDMA, PDEA, PDPAEMA, PDPA, PDMAPMAm, PDMAEA, PtBAEMA, poly(N,N-dialkylvinylbenzylamine), PDEAm
	Morpholino	-NC4O (cyclic)	PMEMA, PAM, PMEMAm
	Pyrrolidine	-NC4 (cyclic)	PEPyM
	Piperazine	R-NC4N-R (cyclic)	poly(N-acryloyl-N'-alkenyl piperazine)
	Pyridine	-C5N (cyclic)	P4VP, P2VP
	Imidazole	-NC3N (cyclic)	PVI, PImHeMA

Table 1.2: pH responsive electrolyte groups and polymers that contain these groups. Adapted from [35].

acidic form (HA in equation 1.1) and its deprotonated basic form ($\mathrm{A^-}$). The lower the pKa, the larger the equilibrium constant and the stronger the acid [15].

To clarify; the dissociation of an acid AH in water is described by:

$$\mathrm{HA + H_2O \rightleftharpoons A^- + H_3O^+} \tag{1.1}$$

The dissociation constant is defined as a quotient of the equilibrium concentrations (in mol/L):

$$K_a = \frac{[\mathrm{A^-}][\mathrm{H_3O^+}]}{[\mathrm{HA}][\mathrm{H_2O}]} \tag{1.2}$$

Unless the solution is very concentrated, the concentration of water can be taken as a constant. Therefore the dissociation can be written as:

$$K_a = \frac{[\mathrm{A^-}][\mathrm{H^+}]}{[\mathrm{HA}]} \tag{1.3}$$

The pKa is the negative log of this equilibrium constant:

$$\mathrm{p}K_a = -\log_{10}(K_a) \tag{1.4}$$

1.2.2. Predicting polyelectrolyte dissociation

To simulate the pH response of a hydrogel structure, it is very useful to know the degree of dissociation inside the hydrogel for every pH of the surrounding medium. Furthermore, if it were possible to predict the pH for a hydrogel based on its monomer composition, this allows for the design of polymer hydrogel materials that respond exactly when a predesignated pH is reached. Therefore in this section it will be investigated what factors affect the pKa of a molecule and to which degree the pKa of a material can be predicted.

pKa of small molecules

When it comes to measuring pKa values of small molecules, a precision of two decimals is considered very good [57]. pKa values of these molecules have been predicted numerically with precisions of 0.5 to 1 decade [36, 68].

The strength of an acid is influenced by [15]:

1. The intrinsic stability of the conjugate base (anion A-). Stability can arise from:

   Having the negative charge on an electronegative[1] atom.

   Spreading the charge over several atoms (delocalization).

2. Bond strength A-H.

3. The solvent; more specifically how well the solvent stabilizes the formed atoms.

An important item on this list is the first, which indicates that pKa depends on the structure of an entire molecule, not just on that of a single ionizable group. For example, the presence of electronegative atoms somewhere in an acidic molecule can stabilize the conjugate base [15].

In spite of being universally referred to as a constant, the dissociation constant pKa is not in fact truly constant; it depends on temperature, ionic strength[2], and solvent dielectric constant [57]. Reporting pKa values therefore requires that these conditions are exactly stated.

pKa of polymers

The dissociation of polymers in solution is more complex than that of small molecules or monomers in solution. In small molecules that are separated in solution, the protonation of individual species occurs independently [12]. However the protonation (and hence pKa) of different sites on a polymer are directly affected by the immediate environment within the molecule of that group [12]. The electrostatic interaction between the nearby ionized groups on the chain can restrict further ionization. Therefore ionization of weak polyelectrolytes is suppressed compared to the corresponding monomer and the pKa of acidic groups on a polymer can increase with increasing degree of ionization [12, 48].

Apart from the distribution and ionization state of the neighbouring units, the pKa values of the acidic groups in a polymeric system can be affected by the bond formed between the monomeric units, additional van der Waals and electrostatic interactions, any potential hydrogen bonds formed among the functional groups and the hydrophobicity of the environment [12, 18].

The pKa of a polymer in solution can be measured through similar methods as for monomers, but pKa becomes a parameter that depends on the degree of ionization of the chain, its length, concentration, etc. It is impossible to characterize the non-ideality of a polyelectrolyte chain by a single value of effective pKa (pKeff) [48]. Theoretical prediction of pKa values is an active area in computational chemistry. Until about ten years ago theoretical calculations were focussed on monomer acids or macromolecules such as proteins and no attempt had been made to predict the pKa of polymeric acids [18]. Recently, computer simulations have been used to analyze the pKa of weak polyelectrolytes [12, 48]. This work is viewed as groundwork for using molecular dynamics simulations to help assist in the design of new polymers.

pKa of hydrogels

The interactions between polymer molecules in a hydrogel network are stronger than those between polymers in solution. In a solution of polyelectrolytes, the continuous transition between collapsed and swollen regimes occurs in a very narrow range of bath pH, around pKa, whose width depends on the salt concentration. A polyelectrolyte gel however, responds less abruptly to changes in bath pH, and there is a wider range of pH values for which protonated and unprotonated monomers are mixed.

Longo et al. [40] describe a theory to analyse the response of weak polyelectrolyte gels to changes in pH and salt concentration of the surrounding medium. They find that the acid-base equilibrium in a hydrogel behaves in a nontrivial way as compared to the surrounding solution. There is a nonlinear dependence of the gel pH with respect to the pH of the medium and the gel pH can be several units smaller, depending on the salt ion concentration.

1.2.3. Discussion and conclusions

A pH responsive polymer contains weakly basic or weakly acidic groups, which dissociate in response to the pH of the medium and thereby initiate swelling. The behaviour of these 'electrolyte' groups is usually summarized using one value, the acid dissociation constant pKa.

[1] Electronegativity is a property that describes the tendency of an atom to attract electrons towards itself [44].

[2] The ionic strength (I) is defined as the sum of concentrations (c) of all ionic species, corrected for their charge number (z): $I = \frac{1}{2}\sum z^2 \cdot c$ [57].

To simulate pH-responsive behaviour, it would be very useful to be able to calculate the pKa of a polymer hydrogel. However the pKa depends on the structure of an entire molecule, not just on that of the ionizable group. Because of this it is impossible to characterize the non-ideality of a polyelectrolyte chain by a single value of effective pKa. Instead, for polymers pKa is a parameter that depends on the distribution and ionization state of the neighbouring units. A polyelectrolyte gel responds even less abruptly to changes in bath pH than a polymer strand in solution, and there is a wider range of pH values for which protonated and unprotonated monomers are mixed.

Therefore it is not feasible to calculate the pKa of a hydrogel based on the molecular structure of its monomers. In the future it might become possible to design polymers to have a specific pKa, but to do so for hydrogels is still one step further in complexity. Also it is difficult to use measured pKa values from literature, if they can be found, because the composition of the hydrogel and the conditions of the measurement have a large effect on the measured properties.

To include pH dependent dissociation in the simulation of a hydrogel structure, the best alternative is to first measure this behaviour on the same material used for that hydrogel structure and include the measured material properties in the model. This could be done by varying the pH and for each pH measuring the potential difference between the gel and the bath, or measuring the swelling ratio of the gel. From this the degree of dissociation could be calculated.

1.3. Synthesis of pH-responsive hydrogels

To create a hydrogel, hydrophilic monomers are polymerized and the polymer chains are cross-linked. This can either be done in the presence of water, or be followed by swelling of the dry gel in water. These processes are crucial, because all characteristics of hydrogels, such as the mechanical properties, swelling kinetics and solute permeation, are strongly affected by the processing conditions [59]. For the realization of pH-responsive fluid control, there are several requirements that need to be met by the hydrogel material:

- The material is pH responsive, it responds by a measurable change in swelling ratio and the response is reversible.
- The material does not decompose in acidic or basic aqueous environments.
- The material has homogeneous properties.
- The material components are available at a reasonable price and shipping time.

Synthesis of the hydrogel material and manufacturing of the final hydrogel structure usually take place simultaneously, in one process. For this project a fabrication method is desired that allows simple fabrication of 2D structures that are about a hundred micron in size. However, to allow for the fabrication of 3D scaffolds in the future, this method must be extendible to smaller resolutions and 3D structures.

Therefore light-induced fabrication processes will be used. These processes make use of photo-polymerization, where the polymerization reaction is induced by irradiation with light. This leaves a lot of flexibility for manufacturing, as there is a broad range of well-established fabrication processes that make use of photo-polymerization. Simple designs can be manufactured with photolithography or casting and UV curing, while more complicated three-dimensional structures, with smaller resolutions can be made by using stereolithography or 2-photon-polymerization.

1.3.1. Hydrogel synthesis

Light-induced polymerization takes place by a free-radical polymerization reaction. This is a well-established mechanism and the most common mechanism used for the synthesis of hydrogels [43, 59].

Free-radical polymerization mechanism

Free radical polymerization or chain polymerization as it is also called, typically occurs between unsaturated monomers (containing a carbon double bond) [43, 47]. It consists of three phases: initiation, propagation and termination.

Initiation: The reaction begins with the generation of an active centre, a free radical. Active centre generation may be based on heat, γ-radiation, electron beams or light [43]. Most monomers are not sensitive to light. Therefore a photo-initiator is added. Irradiation of the photo-initiator generates exited states, which produce the initiating species; free radicals [19, 43]. The initiating species will react with monomers, opening the double bond to yield a new species that is also a free radical.

Propagation: Free radicals continue to react with monomers, rapidly propagating through the carbon double bonds, without extinguishing the active centre. Thus each reactive centre is responsible for the reaction of many monomer units onto a growing polymer chain [43, 47]. Free radicals are highly reactive, giving rise to a high reaction rate. As a result no species of intermediate size are found in such a reacting system, only monomers and polymers [47].

Termination: These chain reactions do not continue indefinitely. Free radicals are so reactive that they are likely to react in ways that destroy the radical activity [43, 47]. Two growing molecules may combine to extinguish both radical centres with formation of a chemical bond (combination). They can also react to generate end groups in two molecules, one of which is unsaturated (disproportionation). Apart from other radicals, active centres may also find other molecules to react with, such as solvents or impurities.

Cross-linking

Cross-links are what renders a hydrogel insoluble. The physical properties of a hydrogel can be adjusted by controlling the cross-linking density [82]. An increased cross-linking density results in the formation of mechanically stronger, but more brittle gels [52]. Furthermore it increases the glass transition temperature and decreases swelling ability.

Monomer(s)	Crosslinking agent	Ref.
acrylic acid (AAc)	ethyleneglycol dimethacrylate (EGDMA)	[7]
methacrylic acid (MAAc)	tri(ethylene glycol) dimethacrylate (TEGDMA)	[27]
methacrylic acid (MAAc)	tetraethylene glycol dimethyl acrylate (TEGDMA)	[83]
acrylic acid (AAc) and 2-hydroxyethyl methacrylate (HEMA)	ethyleneglycol dimethacrylate (EGDMA)	[7, 8, 39]*
2-(dimethylamino)ethyl methacrylate (PDMA) and 2-hydroxyethyl methacrylate (HEMA)	ethyleneglycol dimethacrylate (EGDMA)	[8]

Table 1.3: Components of photo-initiated, pH responsive, macrogels. All listed polymers were cured with UV light using photoinitiator 2,2-dimethoxy-2-phenylacetophenone (DMPA / Irgacure 651).
*De et al. [16] also describe using a UV-cured HEMA and AAc hydrogel with a diacrylate crosslinker, for their models, experiments and simulations of the equilibrium swelling and kinetics of pH-responsive hydrogels, but the photoinitiator and specific crosslinking agent are not mentioned.

Cross-linking in hydrogels is usually classified as chemical or physical and may occur intra- and intermolecularly. Chemical, or 'permanent', cross-linking involves the formation of covalent bonds, often via a cross-linking agent. Physical, or 'reversible' cross-linking can be based on physical interactions, molecular entanglement, ionic interaction, hydrophobic interaction and hydrogen bonding between the polymeric chains [30, 52, 73]. Physical gels are often reversible, meaning that they can be dissolved by changing environmental conditions such as pH or temperature [14, 73]. Within physical hydrogels, clusters of molecular entanglements or hydrophobically- or ionically- associated domains can create inhomogeneities. Furthermore free chain ends or chain loops create transient network defects [30].

Due to the reversibility and inhomogeneity of physical gels, chemical cross-linking is more suitable for this project. The free-radical reaction scheme described in the previous section is very versatile and may also be used to create chemical cross-links. Hereto a cross-linking agent is included in the pre-polymer mixture, which can participate in the propagation of two radical chains and produce a cross-link [43].

1.3.2. Hydrogel composition

Apart from monomers, hydrogels (can) have several other components, such as a cross-linking agent, (photo)initiator, inhibitor and solvent. Furthermore functional groups or nano-particles can be included [66]. Industrial polymers often also contain fillers, pigments and plasticizers [58].

To get insight into which compositions allow for photo-curing and lead to functional pH responsive structures, a search of pH responsive, photo-cured macrogels[3] used in literature was conducted. The monomers and cross-linking agents used in these gels are listed in table 1.3. In the following sections the most vital components of a photo-cured polymer hydrogel will be discussed.

Monomer

Monomers are the primary building blocks of polymeric hydrogels. In order to obtain a pH-responsive hydrogel, (part of) the monomeric units need to be hydrophilic and pH responsive. The higher the density of electrolyte monomers, the larger the pH-responsive swelling ratio will be. To create other functionalities or specific mechanical properties, other monomers can be added as well. Furthermore each monomer needs to contain a carbon double bond to allow for free radical polymerization [43].

pH responsive mono- and polymers, polyelectrolytes, have been discussed in section 1.2.1. The most frequently reported polyacids are PAAc and PMAAc. These are inexpensive and can easily be polymerized via various polymerization techniques [35]. Sulfonic acid containing PAMPS[4] and PSSA[5] and phosphorus-containing (meth)acrylate monomers are also common in the synthesis of acidic pH responsive hydrogels. The most frequently used polybase is PDMA[6], which is pH- and thermo-responsive.

[3] Classification of hydrogels based on to their size: nanogel (gel nanoparticle) $1 - 100$ nm [4], microgel (gel microparticle) $0.1 -$ 100 □m [4], macrogel ≥ 100 □m [35].
[4] PAMPS: poly(2-acrylamido-2-methylpropane sulfonic acid)
[5] PSSA: poly(4-styrenesulfonic acid)
[6] PDMA: poly[(2-dimethylamino)ethyl methacrylate]

(a) Ethylene glycol dimethacrylate (b) Di(ethylene glycol) dimethacrylate

Figure 1.3: Cross-linking agent length; ethylene glycol dimethacrylate (EGDMA) has one ethylene glycol unit separating the end groups, while di(ethylene glycol) dimethacrylate (DEGDMA) has two, so it is longer. Figures adapted from [1].

The hydrogels listed in table 1.3 all consist of these most commonly used pH responsive monomers, AAc, MAAc and PDMA. Another monomer that is mentioned in the table is HEMA. Water swollen PHEMA gel is a widely used and extensively studied biomedical hydrogel [13, 14, 43]. It is resistant to degradation and inert to normal biological processes. [13, 43].

Cross-linking agent
A cross-linking agent for free-radical polymerization is a molecule containing two or more polymerizable double bonds. The chemical structure and concentration of the crosslinking agent strongly affect the degree of cross-linking and thus the properties and pH-responsive swelling of a hydrogel. A higher cross-linking density will result in a stiffer, more brittle material, a lower equilibrium water content an a lower pH responsive swelling ratio. Moreover the swelling characteristics can be controlled by choosing the length of the cross-linking agent [43], which is illustrated in figure 1.3. Gels synthesized with a longer cross-linking agent may exhibit a higher degree of swelling.

Considering the cross-linking agents in table 1.3, EGDMA, TEGDMA ('tetra...') and TEGDMA ('tri...'), it can be seen that there is a difference in length between the cross-linkers that are listed. EGDMA has one ethylene glycol unit separating the double bond-containing groups at the ends of the molecule, while TEGDMA ('tri...') has three and TEGDMA ('tetra...') has four.

Photo-initiator
A photo-initiator is molecule that generates an initiating species, such as a free radical, when irradiated with light. These free radicals can then start a chain of polymerization reactions. An initiator is sensitive to a specific range of wavelengths; the absorption spectrum. This is important to keep in mind since it means an initiator that is used in UV curing, will probably not be effective in laser-based polymerization techniques (e.g. the Nanoscribe uses a wavelength of 780 nm [46]).

Process dependent requirements for initiators for example The initiators used for two-photon-polymerization are more specific than those used in most photo- polymerization processes. For these it is required that the the transition energy between the ground and excited states of the photoinitiator is equal to the combined energy of two photons [9]. In this case the absorption has a quadratic dependence on the light intensity, confining it to the area of the focal point.

Inhibitor
An inhibitor is a molecule that reacts with initiating or propagating free radicals to form non-radical products or radical products of low reactivity [5]. By quenching radicals polymerization and cross-linking are prevented.

Inhibitors are usually added to monomer stocks to prevent spontaneous polymerization during storage [3]. Also, inhibitors are used in pre-polymer mixtures for micro-stereo lithography to minimize radical diffusion from the focal volume of the laser in order to control the polymerized layer thickness and achieve a lower resolution [9, 28].

Solvent
Macrogels can be fabricated by solution polymerization and bulk polymerization. In solution polymerization the pre-polymer mixture contains a solvent. This can be advantageous because it helps dispel heat produced by the reaction. Typical solvents used for solution polymerization of hydrogels include water, ethanol, water-ethanol mixtures, and benzyl alcohol [43]. After synthesis the solvent can be removed by washing the hydrogel in deionized water. Alternatively hydrogels can be fabricated by bulk polymerization, using a pre-polymer mixture without solvents, and swollen in water afterwards.

An important consideration is the compatibility of each hydrogel component with the solvent. These must be soluble in, but not react with the solvent. Furthermore the solvent and solvent to monomer

ratio during synthesis can strongly affect the chemistry and physical characteristics of the final product [43].

1.3.3. Discussion and conclusions

In this project, light-induced free-radical polymerization will be used for the manufacturing of hydrogel structures. This can be achieved by adding a photo-initiator molecule to the pre-polymer mixture, which will start the polymerization reaction upon irradiation by light.

Many photo-cured pH-responsive hydrogels in literature have very similar compositions. The most frequently used combination is that of AAc and HEMA monomers, crosslinked with EGDMA and cured with photo-initiator DMPA (Irgacure651). PAAc is amongst the most frequently used pH-responsive polymers. It is inexpensive and can easily be polymerized via various polymerization techniques. PHEMA hydrogels are also widely used. They are resistant to degradation and inert to normal biological processes. Combining AAc and HEMA will dilute the acidity of the AAc, making it somewhat safer to handle. Furthermore using a mixture of the two makes it possible to vary the density of pH-responsive groups in the gel, which might be interesting from a research perspective. The cross-linking agent EGDMA creates chemical cross-links, which are formed by the same free-radical mechanism as the polymerization reaction. Chemical cross-linking is preferred over physical cross-linking because it results in more homogeneous hydrogels, that are less likely to decompose.

These materials are readily available and have already been shown to produce hydrogels that show reversible pH-responsive swelling and can withstand acidic and basic conditions [16, 39]. Using a tried and tested hydrogel composition will make it easier to come to a succesfull manufacturing process and will allow for the comparison of experimental results to literature. Therefore the combination of AAc and HEMA monomers, crosslinked with EGDMA and cured with DMPA (Irgacure651) was chosen for use in this project.

1.4. Conclusions and approach for lab-phase

A literature review was conducted to identify the best mechanism to achieve pH-responsive fluid control and gain knowledge on the properties and synthesis of the pH-responsive materials that constitute this mechanism.

Polymer hydrogels were found to be an ideal material for pH-responsive fluid control, because of their inherent interaction with water and permeability to small molecules such as H^+ ions. Bulk swelling of polymer hydrogels will be used to create pH-responsive fluid control, because it can create responses with large length-scales, thus permitting higher flow rates and control over a wider range of flow rates. However the time-scale of this response mechanism is a possible downside.

A pH responsive hydrogel contains weakly basic or weakly acidic groups, which dissociate in response to the pH of the medium and thereby initiate swelling. The behaviour of these 'electrolyte' groups is usually summarized by one value, the acid dissociation constant pKa. However, this single value is not enough to accurately describe the pH-response. Rather, dissociation of electrolyte groups in a hydrogel occurs over a range of pH. An alternative is to measure the pH response and include the measured properties in the model.

Light-induced free-radical polymerization will be used for the manufacturing of the hydrogel structures. This can be achieved by adding a photo-initiator molecule to the pre-polymer mixture, which will start a polymerization reaction upon irradiation by light. A cross-linking agent will be added to create chemical cross-links, which are formed by the same free-radical mechanism. Many photo-cured pH-responsive hydrogels in literature have similar compositions. A frequently used combination is that of AAc and HEMA monomers, crosslinked with EGDMA and cured with photo-initiator DMPA (Irgacure651). These materials are readily available and have been shown to produce hydrogels with reversible pH-responsive swelling. Therefore this combination is chosen for use in this project.

Based on these insights and decisions, an approach for the lab-phase of the project was devised. This is summarized in table 1.4. The approach was divided into six stages and for each stage a set of milestones were defined. To what degree these milestones could be fulfilled determined which course of action was taken in the next stage. The first three stages relied mostly on insights gained in the literature review. The last three stages relied mostly on the results of the first three stages. In the next few sections, the plans for each stage are discussed in more detail.

1.4.1. Material properties (stage 1 - 3)

Constrained disk set-up for measuring material pH-response

The pH-response of the selected material will be investigated in a set-up similar to that used by De et al. [16], using protocols based on the work of Liu et al. [39]. The results will be compared to results obtained in literature to validate that the methods that were selected from literature are appropriate for the continuation of this project.

To measure the pH-responsive swelling of the circular samples, a hydrogel disk with a diameter of 300 µm and a thickness of 180 µm. will be placed inside a fluidic channel with a height of 180 µm. The top and bottom walls of the channel will constrain the hydrogel from expanding in the height direction, so that only deformations in the radial direction are allowed (figure 1.4).

The channel will then be filled with buffered pH solutions of different pH, that should cause the material to swell to different degrees. Swelling will be determined by measuring the diameter of the disk, using an optical microscope.

Disk manufacturing

To manufacture the hydrogel disks, they will be cured in-situ, inside the channel. For this a protocol by Liu et al. [39] will be used. The channel will be filled with a liquid phase precursor (pre-polymer) mixture. It is covered with a glass slide and the precursor is photo-patterned by exposure with UV light, through a mask with a circular, 300 µm diameter, opening in it. After patterning the excess polymer precursor is washed away.

Measurement of disk pH-response

The pH dependent swelling of the material will be measured by immersing the constrained disk in a series of buffered pH-solutions and for each pH recording the diameter of the disk when swelling has reached equilibrium. This will be done for pH 2 to 12 at intervals of approximately 1 pH unit. The most

Stage	Milestones	Activities to reach milestone
1	Succesfully preparing the precursor, curing it with UV light testing if it swells in water	Make precursor Test UV-curing of precursor Test swelling in water of cured material
2	Patterning the precursor (into a disk shape), inside a micro-channel, using a mask that was printed using an office printer and removing the non-cured precursor from the channel.	Make microchannel Make mask Pattern material inside microchannel (in disk shape) Create method to wash out non-cured resist and replace it by water
3	Measuring the disk behaviour by using the constrained disk set-up and comparing to literature.	Investigate shape of cured disk Make buffer solutions of different pH Calculate required swelling times Create method to analyze images and measure disk size Disk swelling measurements
4	Using the same patterning method to cure membranes	Adjust curing system and approach to make membranes Create method to release membranes from system Inspect membranes
5	Measuring the pH-response of these membranes	Create method to swelll membranes in different pH Create method to measure membrane pH response Create method to analyze membrane images Membrane swelling measurements
6	Understanding how the membrane pH response is influenced by design and manufacturing parameters.	Design experiments to investigate effect of design and manufacturing parameters on membrane response Manufacture membranes using different parameters Measure pH response of these different membranes

Table 1.4: Approach for lab phase. The lab phase is divided into six stages. For each stage, milestones are defined and some activities needed to reach these milestones are listed.

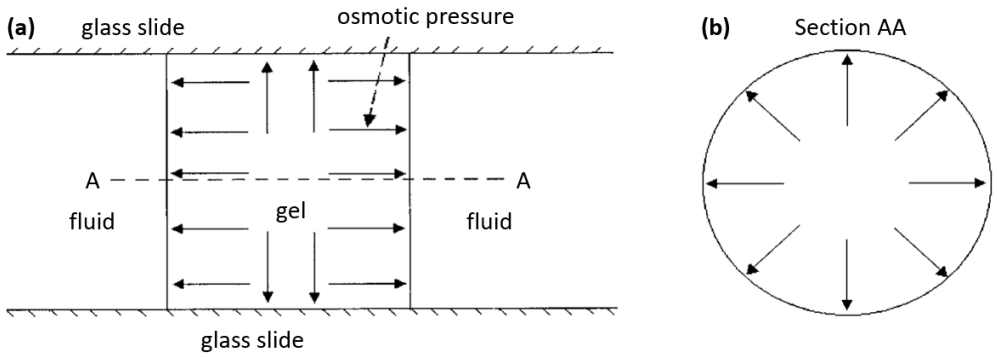

Figure 1.4: Illustration of the cylindrical sample constrained by two glass slides. the cross-section of the disk shown in section AA depicts the gel under radial osmotic pressure. Adapted from [16].

significant swelling is expected between pH 4 and 7 [16], if possible smaller intervals will be used in this range.

Knowledge of the time it takes for a sample to reach equilibrium is important for the planning of experiments and to ensure that measurements are always taken in equilibrium. The time to reach equilibrium is reported to be about 20 000 s for swelling resulting from a pH change from 3 to 6 and 2000 s for de-swelling for a pH change from 6 to 3 [16]. These numbers will be used to estimate a required time for our disks to reach equilibrium swelling.

Comparison of material swelling results to literature
The measurement results will be compared to measurements of pH-dependent swelling reported by De et al. [16] and Li et al. [37] to verify that the material shows the same type of pH-responsive swelling behaviour. The comparison will focus on:

- Initial diameter (at pH ≤ 3).
  Differences in initial diameter may be caused by manufacturing or swelling of the gel when it is first moved from a dry to a liquid environment.
- pH range within which swelling occurs.
  This depends on the type and density of acidic groups in the gel and the length and structure of polymer chains in the gel.
- Final diameter (at pH≥ 8).
  This is likely to deviate from values in literature, because it depends on several factors such as the Young's modulus and electrolyte group density of the gel and the ionic strength of the bath.

1.4.2. Membrane (stage 4 - 6)

When the precursor can be patterned and the pH-responsive behaviour of the material is known, the manufacturing method and set-up will be adjusted towards making membranes.

The pH response of these membranes will be measured and the effect of design and manufacturing parameters on this response will be investigated. Parameters that will be investigated are:

- Pore size
- Pitch
- Curing time

Other parameters that could be interesting to investigate are:

- Membrane thickness
- Membrane thickness distribution
- Pore shape
- Material composition

1.4.3. Risks and alternative approaches

Manufacturing

- Incomplete curing:
  Can be caused by oxygen that is dissolved in the precursor mixture, which functions as an inhibitor. The AAc and HEMA monomers need to be vacuum distilled prior to use. If this is not sufficient other measures can be taken to prevent contact of the polymer precursor with air, such as curing in a vacuum environment.

- Problems with manufacturing or replication of the features on the mask:
  Use a 3D-printed mould instead.

- Adhesion of membrane to glass slide or container:
  Could be solved by using an anti-stick coating or using a different material for the slide or container

Experimental setup

- No swelling visible:
  Swelling can also be determined by measuring the change in weight.

- The time to reach equilibrium is very long:
  Swelling dynamics are diffusion limited. Diffusion time scales with distance squared. So an effective way to speed up swelling is by decreasing the diffusion distances. This can be done by making the sample diameters smaller or the top and bottom slides porous, so that the pH solution can pass through them. Otherwise, swelling could be measured not when it has reached equilibrium, but when the rate of deformation is below a certain threshold value. This would however require continuous monitoring of the sample diameter.

Material

- Large variation in measurement results:
  This may indicate that the manufacturing conditions were not constant. Hydrogel properties, such as the degree of cross-linking, are highly dependent on the curing conditions.
  Swelling is also affected by environmental factors other than pH, such as ionic concentration and electric fields.

- The gel does not swell:
  The swelling ratio can be increased by using a higher percentage of electrolyte (AAc) groups, or decreasing the stiffness of the gel by decreasing the cross-linking density.
  If this is not effective using a different polymer precursor mixture or buying ready-made pH responsive hydrogel must be considered.

- Swelling is not reversible or the gel deteriorates during swelling experiments:
  To counteract this, very acidic and very basic pH baths may be avoided. Alternatively it may be possible to improve the resistance to degradation of the hydrogel network by using a higher fraction of HEMA, which is non-degradable, or cross-linking agent.

2

Paper

Photo-patterned, pH-responsive hydrogel membranes for integrated fluid control

S.H. Soons

Department of Precision and Microsystems Engineering, Faculty of Mechanical, Maritime and Materials Engineering (3mE), Delft University of Technology, Delft, The Netherlands

Abstract

To control fluid transport, microfluidic systems often make use of pressure driven flow and pneumatically actuated valves. However these require bulky external instrumentation. An integrated fluid control mechanism would make microfluidic systems more portable, closed and automated. We created an active membrane for integrated, pH-responsive fluid control. pH-responsiveness allows the membrane to interact directly with analytes in a microfluidic system. The membrane material is a 2-Hydroxyethyl methacrylate and Acrylic acid based, cross-linked polymer hydrogel that swells with increasing pH. We tested a system for measuring the pH response of the material and we developed a method for manufacturing pH-responsive hydrogel membranes that gives control over pore size, shape and position. A photo-lithography approach was used to pattern the membranes and thereby create pores, using a photo-mask that was manufactured on an office printer in a very fast and low-cost procedure. The resulting membranes had a thickness of 140-190 µm and pore diameters of 100-400 µm. The pore size was measured for environmental pH of 1.6 and 7.1, within this range the pores doubled in diameter. Furthermore the pH-responsive deformation ratio of the pores increased significantly with increasing curing time and decreasing pore diameter. The results suggest a difference in material properties around the pores that develops due to a local difference in received exposure dose during curing. The fluidic properties and pH-response of the membrane can be adjusted to suit a specific application by changing the design, the curing time or the chemical composition of the membrane. The testing system can then be used to measure and compare the pH-response of different potential materials.

Keywords: membrane, porous, hydrogel, microfluidics, pH-responsive, pH-sensitive, smart materials, active materials

1. Introduction

The aim of this work is to create a pH-responsive membrane for integrated fluid control in microfluidic systems. Microfluidics is a promising technology for applications in fields such as (bio)chemical analysis and cell biology. It can be used to perform separations and detections with high resolution and sensitivity, while allowing for parallel testing of large numbers of compounds. In microfluidic systems, fluids are manipulated in channels with sub-millimetre dimensions. The small size creates unique and useful characteristics such as laminar flow while requiring very low volumes of samples and reagents.

To control fluid transport, many microfluidic systems make use of pressure driven flow and pneumatically actuated valves. However this requires bulky external instrumentation and a large number of connectors [1]. An alternative is to integrate fluid control mechanisms into the system. This enables microfluidic systems to be more portable and more closed. It also allows for more automated systems that are simpler to operate, which lowers the barriers for adoption by prospective users [2]. To be suitable for implementation, an integrated fluid control mechanism should be able to sense and respond to local conditions, be flexible in design so that it can be used in different processes and microfluidic system configurations and achieve the required (precision in) transport rates.

Membranes are semi-permeable barriers, that are designed to control transport of species [3]. A benefit to membranes is that they can simultaneously perform different functions, such as fluid control and filtration and they have a large surface area that can be used to hold a catalyst or as a support for cell culturing. Membranes can be dense or porous. Porous membranes have empty spaces (pores) in the membrane, through which transport occurs. In this case transport is mainly governed by membrane morphology [3]. Typically membranes are passive; the material, the morphology and thus the barrier properties of the membrane do not change over time. The rate of transport over the membrane can only be controlled trough the driving pressure. However, a membrane could be made active by using an active, or stimuli-responsive material.

Stimuli-responsive materials are materials that see a change in one or more of their properties in response to a stimulus from the environment. To achieve tunable control over the flow through a membrane, the barrier or resistance to flow must be altered reversibly, for example by a stimuli-responsive change in pore size [9]. There are a few fundamental classes of stimuli which can induce responses

Reference	Composition	Constraints	Membrane thickness*	Pore diameter*	Pore creation	Curing proces	pH response: change in pore size
Tamada et al. [4]	heterogeneous	free	100 µm**	3.7 µm	track etching	Heated to 75 C for 24 h. Hydrolyzed with 1 M NaOH solution for 40 min at 25 C.	Pores close at maximum swelling.
Tokarev et al. [5] and Orlov et al. [6]	homogeneous	attached to surface	0.15-0.25 µm	0.3-1.4 µm	phase separation	Temperature annealing under vacuum at 120 C for 48 h.	Pores close at maximum swelling.
Gopishetty et al. [7]	homogeneous	attached to surface	0.2-1 µm	0.1-0.2 µm	phase separation	Crosslinked by immersion in 0.3 M calcium chloride.	Pores close at maximum swelling.
You et al. [8]	homogeneous	free	5 mm	approx. 180 µm	microsphere template	UV light for 90 s. Immersed in dichloromethane and shaken vigorously for 48 h to remove PMMA microspheres.	Pore size nearly doubles compared to the non-swollen state.

Table 1: Overview of porous, pH-responsive swelling hydrogel membranes.
* Of the dry / non-swollen membrane. ** Thickness of hydrolyzed layer ≈ 0.5 µm.

in materials. These include: temperature, pH and various chemicals, electric fields, electromagnetic radiation (light) and mechanical forces [10].

For integrated fluid control, pH responsiveness is especially interesting because this could allow systems to interact directly with a broad range of analytes and processes, without need for an external stimulation source. pH-responsive hydrogels respond to pH by a dramatic change in volume [11]. This makes these materials especially interesting for integrated fluid control, because it means that control over a wide range of pore sizes or flow rates could be possible. Furthermore there are many different polymer compositions that can be used to make such hydrogels [12, 13], making it possible to tune the material properties and pH response range to suit an application.

Hydrogels are crosslinked polymer networks that absorb water due to hydrophilic groups that are incorporated in the network. For pH-responsive hydrogels the amount of water that is absorbed is influenced by the pH and ion concentrations of its environment [14, 15]. The polymer network of a pH-responsive hydrogel contains weak acidic or basic (poly)electrolyte (PEL) groups, whose (de)protonation is pH dependent [12]. When acidic PEL dissociate, the network becomes charged. This increases hydrophilicity of the network and attracts ions into the gel. [16, 17]. The ions raise the osmotic pressure inside the material, which causes absorption of water and thus swelling. The equilibrium swelling volume is governed by a chemo-electro-mechanical relation [18, 19, 20]: there is a balance between the electrostatic attraction of ions into the material and a concentration gradient that causes ions to diffuse in the opposite direction. And there is an equilibrium between osmotic pressure driving water transport into the material which leads to swelling and the elastic properties of the hydrogel network, which counteract swelling .

Asides from environmental conditions, the behaviour of a pH-responsive swelling hydrogel depends on its composition. The pH-range where swelling occurs depends on the dissociation constant (pK_a) of the PEL component and the chemical structure of the gel. Moreover, acidic PEL dissociate at high pH while basic PEL become charged at low pH. The degree of swelling depends partly on the chemical structure and hydrophilicity of the gel network, but is strongly affected by the density of electrolyte groups and cross-links [21, 22]. The density of electrolyte groups sets the attainable charge density inside the hydrogel, therefore a higher density will increase swelling. A higher density of cross-links decreases swelling, by increasing the mechanical strength and thus resistance to swelling of the polymer network.

A number of studies have been devoted to manufacturing membranes from pH-responsive swelling hydrogels. An overview is given in table 1. Homogeneous, porous, pH-responsive membranes have been made from solutions containing a PEL polymer and a volatile additive, using phase separation to create the pores [5, 6, 7]. Another approach, which has been used to create pores in a pH-responsive tissue engineering scaffold, is casting the polymer precursor into a mold filled with packed polystyrene spheres, whose removal after curing results in a network of interconnected cavities [8]. Heterogeneous, porous, pH-responsive membranes have been manufactured from pristine, non-responsive membranes by track etching to create pores and subsequently hydrolyzing to create a pH-responsive hydrogel surface layer [4]. However all these methods provide limited control over the pore position, size and shape. If it were possible to exactly control these parameters, the design of a membrane could be better tuned towards specific fluid control applications.

Hydrogel swelling has also been used for in-channel fluid control [23]. In that work, hydrogel structures were cured in a lithography process. The pH-responsive precursor was exposed to uv light through a mask to create pillars of different shapes [24]. This method could be applicable to create pH-responsive membranes with better control over pore size, shape and location.

In this work, we propose a macroporous[1], pH-responsive hydrogel membrane for integrated fluid control. First the pH-responsive swelling of the hydrogel material was investigated using a set-up in which a hydrogel disk was vertically constrained inside a fluidic channel. Due to this constraint, expansion only occurred in the lateral direction and could be measured using an optical microscope. Membranes were then manufactured from this same material, using a lithography-based curing approach that allows control over pore position, size and shape. The influences of pore diameter, distance between pores (pitch) and curing time on the pH response of the membrane were investigated. The pore size was measured for environmental pH of 1.6 and 7.1, within this range the pores doubled in diameter. Furthermore the pH-responsive deformation ratio of the pores increased with increasing curing time and decreasing pore diameter.

2. Methods

Materials

The pH-responsive material was a cross-linked polymer hydrogel that has previously been studied and modelled by the group of Beebe et al. [26, 27, 28, 29]. It swells with increasing pH. The volume transition occurs between pH 5 and 6 and is reversible and repeatable [30]. The material was produced from a liquid precursor that cures when exposed to ultraviolet light (UV). Preparation of the precursor was based on a recipe described by the group of Beebe et al. [30, 28]. The precursor was made by combining 2-Hydroxyethyl methacrylate (HEMA) and Acrylic acid (AAc), which induces the pH-responsive behavior, in a 4:1 mol ratio and adding 1 wt % of crosslinker Ethylene glycol dimethacrylate (EGDMA) and 3 wt % of photoinitiator 2,2-Dimethoxy-2- phenylacetophenone (DMPA). All chemicals were purchased at Sigma-Aldrich. An inhibitor (4-Methoxyphenol (MEHQ)) was present in the liquid components: 200 ppm in AAc, 250 ppm in HEMA and 90-110 ppm in EGDMA. The precursor was mixed ultrasonically for 20 min to dissolve the DMPA crystals and stored under refrigeration in an amber bottle.

To pattern the precursor, it was exposed to UV light through a negative photomask that was made in a fast, low-cost process [31, 24]: the mask designs were printed in black ink onto transparencies using a 1200 x 1200 dpi laserprinter. It was found that two mask layers were needed to sufficiently block the light. These ware aligned manually with the help of alignment marks and fixed with adhesive tape.

Curing of the precursor was done with a Light curing unit (Photopol A5406(B)), in which the sample was placed on a rotating plate and illuminated from the top by two

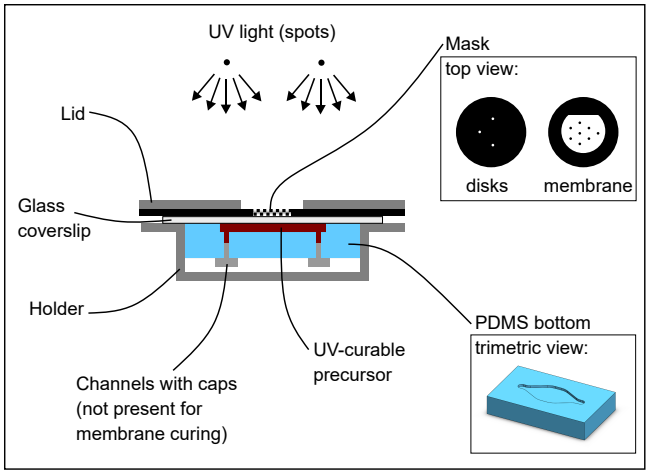

Figure 1: Schematic diagram showing a cross-section of the curing set-up used to make the disks. After curing, the disks remain inside the channel, which consist of a PDMS bottom and a glass coverslip bonded together. The non-cured precursor is removed and the channel can be filled with different buffer solutions. The set-up for curing a membrane is very similar, only the PDMS bottom is not bonded to the glass coverlip. Therefore there is no need for channels through the PDMS to fill the channel with precursor. Thus these channels and caps are not present, instead the PDMS bottom is supported by an extra block of PDMS, so that it is raised and slightly sticks out of the holder. The glass coverslip then rests on top of the PDMS.

spots with different light spectra from 320 to 550 nm. Curing times were optimized for the mask design, by testing times between 100 and 170 s for the disks and 60 and 100 s for the membranes. The details of this are described in appendix A.

Disks and membranes were both cured inside a channel consisting of a Polydimethylsiloxane (PDMS) bottom with a 180 µm deep, 6 mm wide slot, covered by a 0.17 mm thick borosilicate glass slide. The PDMS bottom was made by casting PDMS in a 3D-printed mold. The mold was manufactured on a desktop stereolithography system with 30 µm lateral and 25 µm vertical resolution (Envisiontec Micro Plus HD, material: HTM 140 V2).

During curing, the channel was placed inside a holder and covered by a lid. These helped to align the mask to the precursor-filled channel and blocked UV light coming from the sides. Both were printed on the same Envisiontec 3D-printer, using lower resolution settings.

To investigate the pH response, disks and membranes were swollen at room temperature in 0.1 M phosphate buffers of pH 1.6 - 12.2. For each pH, NaH_2PO_4, Na_2HPO_4, HCl and NaOH, were used to obtain a buffer molarity of 0.1 M, then NaCl was added to adjust the total molarity to 0.2 M. Thus buffers of pH 1.6, 2.5, 3.5 contained NaH_2PO_4, HCl and NaCl; buffers of pH 5.0, 6.1, 7.1, 8.2 contained NaH_2PO_4, Na_2HPO_4 and NaCl; and buffers of pH 12.2 contained Na_2HPO_4, NaOH and NaCl.

Manufacturing

The approaches used to manufacture the disks and membranes were very similar. The main difference was

[1] Macroporous membranes: membranes that consist of a solid matrix with defined holes or pores which have diameters larger than 50 nm [25]

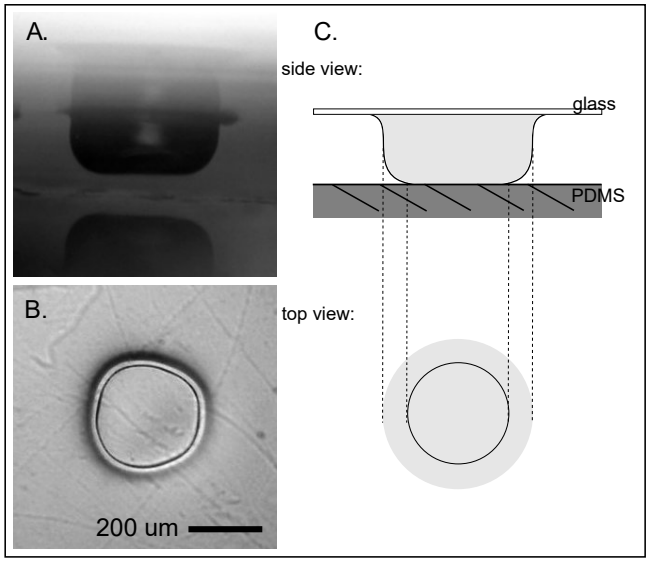

Figure 2: Disk shape. A. and B. are images of the same disk. A. Side profile (After curing and emptying the channel). B. Top view (After curing, before removing non-cured precursor, so here the disk is immersed in liquid precursor). C. Schematic diagram to demonstrate how the double border that is visible in the top view can be explained by the curvature in the side walls of the disk.

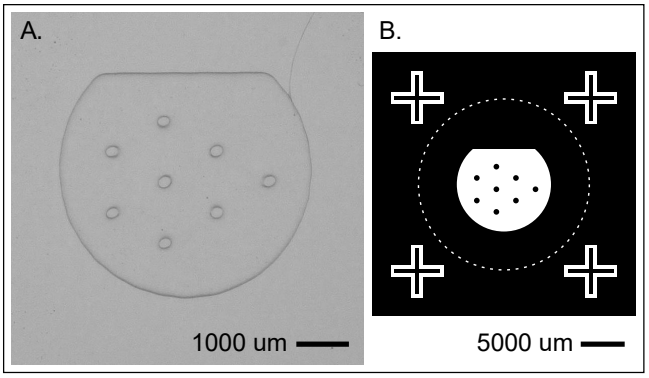

Figure 3: Membrane. A. Dry membrane, attached to glass slide. The membrane was cured with an UV exposure time 80s. The non-cured precursor was washed away, the membrane was dried and subsequently imaged with an optical microscope. B. The mask design that was used to pattern the membrane. Pore diameter = 300 µm, pitch = 1200 µm. The + signs are alignment marks that were used to align the two mask layers. The dashed circle was used to align the membrane to the lid of the curing-holder.

that the channel in which the disks were cured was permanently closed and the disks remained inside it for the swelling measurements, while the membranes were removed from the channel after curing. The general manufacturing procedure for both disks and membranes was as follows: The channel was filled with the UV-curable precursor and placed in a holder to block light from the bottom and the sides. The top was covered by the mask, which was held in place by a lid that was clamped to the holder with small pegs. This stack was then placed in the curing unit to pattern the polymer, after which the cured structures were post processed. The specific procedures for disk and mask manufacturing are detailed below.

To manufacture the constrained disks, an inlet and outlet were made at each end of the PDMS channel bottom, by punching a hole with a 1.3 mm (outer diameter) blunt needle. The PDMS bottom was then bonded to the glass slide using air plasma treatment (3.5 mbar, 40 W, 60 s). The resulting channel was filled with the precursor using a syringe with a 0.75 mm blunt needle, after which the openings were closed with caps. The filled channels were placed in the holder as described above and cured for 130 s, using a mask design that created 3 disks per channel. After curing the disks were imaged to determine their non-swollen size. Then the excess precursor was washed away by flushing the channel first with ethanol and subsequently with deionized (DI) water. To further remove traces of non-cured precursor, the channel was filled with DI water and disks were left to swell overnight.

The resulting disks had a diameter (measured after curing) of $311 \pm 3\,\mu m$ (mean $\pm$ SD). Figure 2 B. shows the top view of a disk after curing, before removing the excess precursor from the channel. In the image the disk has a double outer border, which suggests that the the sides of the disks were not perfectly straight and vertical. The side profile of disks was investigated by emptying channels after curing, cutting them in half and imaging disks from the side. A side-profile image is shown in figure 2 A. In the image it can be seen that the bottom side of the disk has detached from the PDMS, most likely due to the cutting of the channel. The sides of the disk are partly straight, but have a convex curvature where the disk touches the glass and a concave curvature where the disk touches the PDMS. The double disk border as seen from the top is thought to be the result of these curvatures, as illustrated in figure 2 C.

To manufacture the membranes, the channel bottom was placed in the holder, which was partly filled with a stack of flat PDMS pieces so that the channel rose slightly above the holder (approximately 1 mm). A drop of precursor was placed in the channel and covered with a glass slide. The mask with the membrane design and the lid were placed on top of this and fastened with pegs. This stack was then placed in the Light curing unit. After curing, the lid and mask were removed from the holder. The glass slide, now with the membrane attached to it was lifted off the PDMS bottom. Non-cured precursor was washed away by submerging and flapping the glass slide with the membrane subsequently in ethanol and DI water, for 10 s each. Afterwards the water was blown off using compressed air and the slide with the membrane was left to air-dry. The dry membranes were imaged and inspected while attached to the glass. Hereafter the membrane was removed from the glass slide, by leaving it immersed in DI water overnight. This caused the membrane to swell, which released it from the glass.

To investigate the effect of mask design and curing time on membrane pH-response, a total of 24 membranes was

Manufacturing parameter	Constant value	Variable values
Curing time t_c (s)	80	60, 70, 80, 90, 100
Pore diameter d (µm)	300	250, 300, 400, 500
Pitch p (µm)	$4 \times d$	525, 600, 750, 900, 1200

Table 2: Mask design and curing time; parameters used in membrane manufacturing. A wider range of parameters was tested, but parameters that did not lead to successful membranes ware not included in the table. More details about this are found in appendix A.

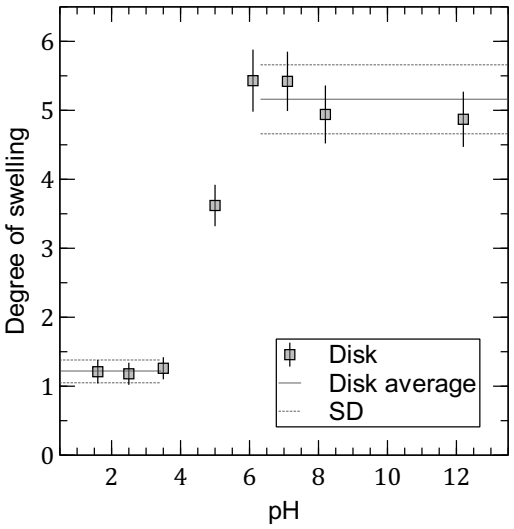

Figure 4: pH-responsive swelling of constrained hydrogel disks; the degree of swelling as a function of pH. The squares represent the average at a specific pH, with error bars for the standard deviation based on a sample with n=6 (2 channels with 3 disks per channel). The solid lines represent the averages of swelling at low and high pH, with dotted lines for the standard deviations of these averages, based on samples of n=18 for low pH and n=24 for high pH.

used. These were manufactured with different curing times and masks with different pore diameter and pitch. An overview of these parameters is given in table 2. When one parameter was varied, the other two were kept constant. For most membranes a curing time of 80 s was used. Times between 60 and 100 s were used to investigate the influence of curing time on pH-response. All masks had the same general design, only the pore diameter and pitch were varied. When varying the pore diameter, a pitch of 4 times the pore diameter was used.

The manufactured membranes had a thickness of 172 ± 18 µm (mean ± SD) when dry. An image of a dry membrane, attached to a glass slide, is shown in figure 3. To check that the pores were open, membranes were inspected using white light interferometry. Membranes with blocked pores were excluded from this paper, only manufacturing parameters that consistently gave open pores were used.

Experiments

To investigate pH-response, only equilibrium swelling was measured. However the dynamic swelling of our pH-responsive material has been measured by De et al. [26]. The swelling rate is generally considered to be diffusion limited [24, 32], so swelling time scales with the cube of the diffusion distance. Thus the the required swelling times to reach equilibrium, for different disk and membrane dimensions, could be estimated based on the measurements of De et al. This resulted in $t = 0.64d^2$ for swelling and $t = 0.11d^2$ for de-swelling with t the time to reach equilibrium in seconds and d the diffusion distance in micron, which is equal to the radius of a disk and half of the thickness of a membrane. The minimum swelling times that were employed for our measurements are multiples of these estimations. For the constrained disks: 9h for swelling and 1.5h for de-swelling, furthermore the buffer inside the channel was replaced once; at least 4.5h and 45 min. respectively before the measurement. For the membranes: 4.3h for swelling and 43 min. for de-swelling.

To measure disk pH-response, the channels holding the disks were filled with the buffer solutions using a syringe with a 0.75 mm blunt needle. When switching buffers, first the previous buffer was washed out with DI water. Then all liquid was removed by injecting air, after which the channel was filled with the new buffer (approximately 1 ml.). An optical microscope with a built in camera was used to image the disks from the top, through the glass coverslip. Images of the same disk at different states of swelling are shown in figure 4. The disk area was measured using 'ImageJ' software. Greyscale images were thresholded to make a binary image, and the disk area was found using the 'analyze particles' function. Each individual binary image was checked manually to correct for gaps in the outline of the disk or connections to surrounding areas (see appendix C). If multiple concentric outlines to the disk were visible, the outermost edge was always used.

To measure membrane pH-response, after being released from the glass slide, membranes were kept free-floating in 5 ml Eppendorf tubes filled with buffer solution. To switch to a buffer of a different pH, the membrane was submerged in DI water to wash of the previous buffer, and placed in a tube filled with the new buffer. To image the swollen membranes, they were placed on the bottom of a Petri dish. A drop of buffer solution was placed on the membrane to maintain the swelling and the membrane was covered with a glass microscopy cover slip, to prevent evaporation of the buffer and keep the membrane flat. The asymmetric membrane design made it easy to always image the membrane from the same side. For all measurements, the area of the central pore and a pitch bordering on the central pore were used. Pore areas were measured using 'ImageJ', by manually tracing the innermost outline of the pore area. Most pores were not round but slightly oval or irregularly shaped (figure 6). However for calculating the different swelling measures it was assumed that they were round and the measured area was

used as if it was the area of a round pore. Pitch, the centre-to-centre distance between pores, was measured using the microscope's built-in tool that allows measurement of the distance between two three-point-circles. More details on these methods are described in appendix C.

3. Results

pH-responsive membranes were manufactured from a pH-responsive polymer hydrogel material. First the pH-response of the material was examined in a constrained disk set-up. These measurements were used to predict the pH-response of the membrane and to relate the results to previous research with a similar material [26, 30, 27, 28, 29]. Then the pH response of the membranes was investigated by measuring both the deformation of the pores and the deformation of the pitch which was used as a measure of the response of the bulk membrane material. Membranes were manufactured with different mask designs and UV curing times to investigate the relation between the pH-response of the membrane and these manufacturing parameters.

Measures of swelling

The pH-responsive hydrogel material swelled with increasing pH. Only equilibrium swelling was considered. It was assumed that the material properties were homogeneous and that swelling was also homogeneous throughout a structure. Thus the same volumetric expansion was expected for constrained and un-constrained structures: if deformation in one direction is constrained, it will be larger in other directions. To express the amount of swelling, two different measures were used: the degree of swelling H and the linear deformation ratio α. These were calculated from each set of measurements. The degree of swelling, or the hydration, was defined as the ratio of the volume of fluid to the volume of solid inside the gel [26]. It describes a swollen state with respect to the initial, dry state.

$$H = \frac{V_1 - V_0}{V_0} \tag{1}$$

Thus if $H = 1$, the volume of the gel has doubled with respect to its dry state.
The linear deformation ratio was defined as:

$$\alpha = \frac{u_2}{u_1} \tag{2}$$

with $u = V^{\frac{1}{3}}$. In these equations, V_0 is the volume of the dry, non-swollen material and subscripts $_1$ and $_2$ refer to different states of swelling. The linear deformation ratio indicates how much the dimensions of a feature change with pH. It can be defined with respect to the dry state [33], but in this case it will be used to represent the difference between two states of swelling. Therefore it describes how much hydrogel features, such as the pores in a membrane, can be expected to change in size with a change in pH.

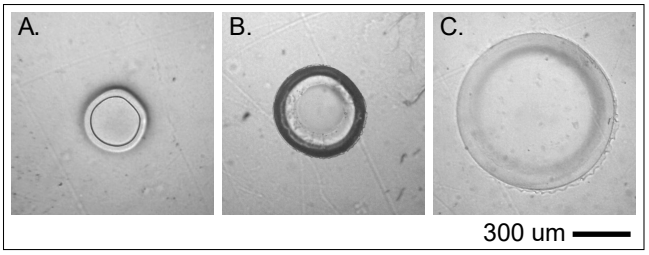

Figure 5: Disk swelling. Images of the same disk at different states of swelling. A. After curing (before washing away excess precursor). B. Equilibrium swelling at pH 1.6. C. Equilibrium swelling at pH 7.1. Images were taken with an optical microscope.

The two swelling measurements were calculated from the different pH-response measurements as follows:

For disk area measurements:

$$H_{\text{disk}} = \frac{A_1 - A_0}{A_0} \tag{3}$$

$$\alpha_{\text{disk}} = \frac{(A_2 h)^{\frac{1}{3}}}{(A_1 h)^{\frac{1}{3}}} = \left(\frac{A_2}{A_1}\right)^{\frac{1}{3}} \tag{4}$$

With $V_{\text{disk}} = \frac{1}{4}\pi d^2 h = Ah$ and h a constant and equal to the height of the channel holding the disk.

For membrane pitch measurements:

$$H_{\text{membrane pitch}} = \frac{p_1^3 - p_0^3}{p_0^3} \tag{5}$$

$$\alpha_{\text{membrane pitch}} = \frac{p_2}{p_1} \tag{6}$$

with p the measured centre-to-centre distance between pores.

For membrane pore area measurements:

$$H_{\text{membrane pore}} = \frac{A_1^{\frac{3}{2}} - A_0^{\frac{3}{2}}}{A_0^{\frac{3}{2}}} \tag{7}$$

$$\alpha_{\text{membrane pore}} = \frac{\sqrt{A_2}}{\sqrt{A_1}} \tag{8}$$

Disk pH response

The pH-responsive swelling behaviour of the hydrogel material was investigated by measuring the swelling of a circular hydrogel disk. The disk was formed inside a fluidic channel by curing it in situ (figure 1). The height of the disk was constrained by the channel, so that expansion could only take place in the lateral direction. Therefore the volume of the disk could be easily determined from its area, which was measured using an optical microscope

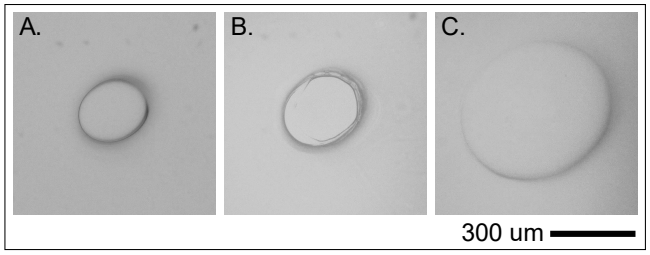

Figure 6: Membrane swelling. Images of the same pore at different states of swelling. A. Dry membrane (after curing and washing away non-cured precursor). B. Equilibrium swelling at pH 1.6. C. Equilibrium swelling at pH 7.1. The membrane was cured for 80s, using a mask with pore diameter 300 µm and pitch 1200 µm. Images were taken with an optical microscope.

with a built in camera. The channel was filled with buffers of different pH and the disk area was measured at each pH.

The degrees of swelling of constrained disks for different pH are plotted in figure 4. The plot shows a region of low swelling at pH 1.6 - 3.5 and a region of high swelling at pH 6.1 - 12.2, with a transition region in between. Within the region of high swelling, the degree of swelling seems to be highest for pH 6.1 - 7.1 and lower for pH 8.2 - 12.2. The average swelling of these regions of low and high swelling is included in the plot as solid lines.

Membrane pH response

The pH response of the membranes was investigated by measuring the deformation of the pores and the pitch. First membranes were manufactured using a mask with pore diameter $d = 300\,\mu m$ and pitch $p = 1200\,\mu m$ and curing time $t_c = 80\,s$. The membranes were submerged in buffers of pH 1.6 and 7.1 until equilibrium swelling was reached. The pore area and pitch were measured in the dry state and at both pH.

Figure 6 shows the same pore dry, at pH 1.6 and at pH 7.1 . The size of the pore increases slightly going from dry to pH 1.6 and drastically between pH 1.6 and pH 7.1. The measurements of membrane swelling are summarized in table 3. The degree of swelling and the linear swelling ratio of the membrane were determined based on the pitch and pore area measurements. The measurements of disk area are also summarized in table 3, as well as swelling data based on disks of the same material, with diameters between 300 and 700 µm, that were similarly vertically constrained [26]. The table shows that for all disk and membrane measurements the degree of swelling at pH 7.1 is significantly larger than the degree of swelling at pH 1.6. The linear deformation ratios of pH 7.1 with respect to pH 1.6 lie between 1.43 and 2.05. Two things stand out: firstly, for the disk area measurements the degree of swelling at pH 1.6 is much larger than for the other measurements. Secondly, for the pore diameter measurements both the degree of swelling at pH 7.1 and the linear deformation ratio are relatively large: it appears that the pore diameter expands more between pH 1.6 and pH 7.1 than the pitch and the disks do.

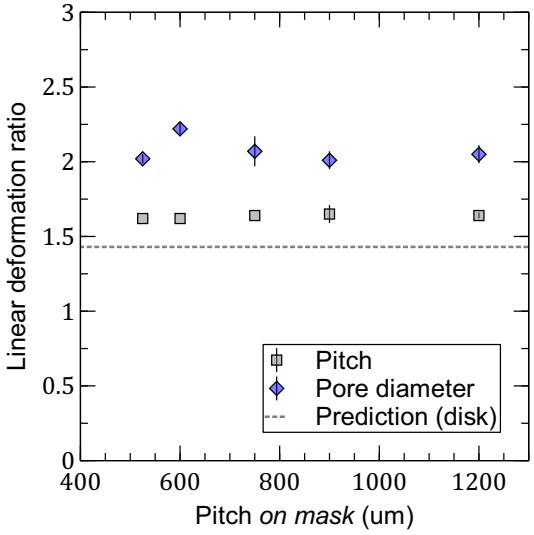

Figure 7: Membrane pH response for varying pore diameter; graph of linear deformation ratio as function of pitch. Linear deformation ratios were calculated from the pitch and pore size at pH 7.1 vs. pH 1.6. Membranes were cured for 80 s, through masks with pore diameter 300 µm and variable pitch. Membrane dimensions were measured at equilibrium swelling, at pH 1.6 and at pH 7.1. The squares and diamonds represent averages with error bars for the standard deviation based on a sample with n=2. For reference, the dotted line represents the linear deformation ratio of the constrained disks, as given in table 3.

Effects of mask design and curing time

The relation between the pH-response of the membrane and different manufacturing parameters was investigated. To do so membranes were manufactured with different curing times and using masks with varying pore diameter and pitch. An overview of these parameters is given in table 2. For each membrane the pore area and pitch were measured while dry, at ph 1.6 and at pH 7.1. Based on these measurements, the linear deformation ratios at pH 7.1 with respect to pH 1.6 were plotted, together with the linear deformation ratio that was found using the constrained disks.

The measured linear deformation ratios for membranes manufactured using masks with varying pitch are shown in figure 7 . The linear deformation ratio of the pitch is higher than the disk prediction and does not vary much. The linear deformation ratio of the pore diameter is also nearly constant, but is significantly higher than that of the pitch.

The measurements of pore diameter and pitch for membranes manufactured using masks with varying pore diameter are shown in figure 8 Again the linear deformation ratio of the pitch is nearly constant and higher than the disk prediction. The linear deformation ratio of the pore diameter is close to that of the pitch for large pore diameters, but increases for smaller pore diameters.

The linear deformation ratios measured for membranes

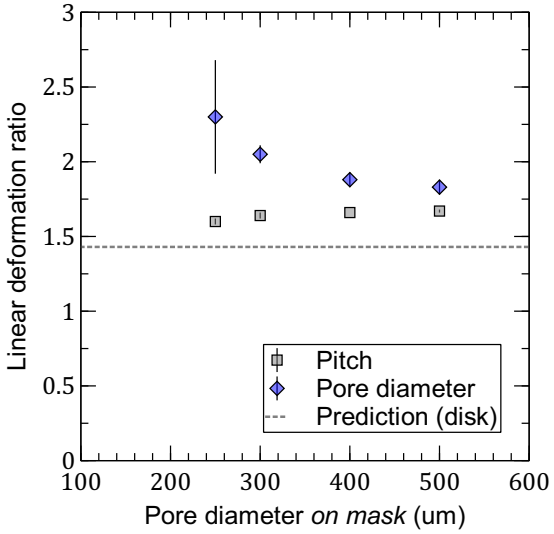

Figure 8: Membrane pH-response for varying pore diameter; graph of linear deformation ratio as function of pore diameter. Linear deformation ratios were calculated from the pitch and pore size at pH 7.1 vs. pH 1.6. Membranes were cured for 80 s, through masks with variable pore diameters and a pitch of four times the pore diameter. Membrane dimensions were measured at equilibrium swelling, at pH 1.6 and at pH 7.1. The squares and diamonds represent averages with error bars for the standard deviation based on a sample with n=2. For reference, the dotted line represents the linear deformation ratio of the constrained disks, as given in table 3.

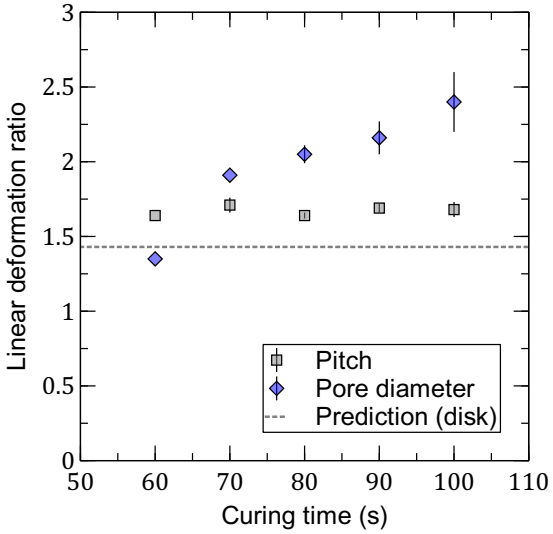

Figure 9: Membrane pH response for varying curing time; graph of linear deformation ratio as function of curing time. Linear deformation ratios were calculated from the pitch and pore size at pH 7.1 vs. pH 1.6. Membranes were cured at variable exposure times, through masks with pore diameter 300 µm pitch 1200 µm. Membrane dimensions were measured at equilibrium swelling, at pH 1.6 and at pH 7.1. The squares and diamonds represent averages with error bars for the standard deviation based on a sample with n=2, with the exception of the data points at 60 s, where n=1. For reference, the dotted line represents the linear deformation ratio of the constrained disks, as given in table 3.

manufactured with the same mask design, but using different UV curing times, are shown in figure 9. Here too the linear deformation ratio of the pitch is nearly constant and well above the disk prediction. The linear deformation ratio of the pore diameter is close to that of the pitch at curing times of 60-70 s and increases with increasing curing time.

4. Discussion

A homogeneous, macro-porous pH-responsive membrane was created for integrated fluid control in microfluidic applications. The material is a 2-Hydroxyethyl methacrylate and Acrylic acid based, crosslinked polymer hydrogel that swells with increasing pH. This allows the membrane to interact directly with analytes, while the large lengths scale of its response will allow for control over a large range of transport rates. A lithography approach was used to pattern the membranes and thereby create the pores. This technique gives control over pore position, size and shape. Furthermore, the masks were manufactured in a very fast and low-cost process, so that it is easy to switch designs.

Disk and membrane pH response

The pH-responsive swelling behaviour of the hydrogel material was investigated by measuring the swelling of a constrained, circular, hydrogel disk. The results agree quite well with the swelling behaviour that was measured by De et al. [26] using a similar material and set-up. In both cases there is a region of low swelling below pH 4 and a region of high swelling above pH 6, with a transition region in between. The only inconsistency is that our measured swelling seems to decrease for the highest pH values (8.2 and 12.2). This could be caused by deviations in the molarity of the used buffers, as molarity is known to affect the degree of swelling [14, 15]. The buffer ingredients were calculated to give all buffers the same molarity, but only the pH and not the molarities of the buffer solutions were measured after preparation.

The degree of swelling and linear deformation ratio of the disk are compared to literature in table 3. This table also summarizes the pH response of the first set of membranes. Similar to the constrained disks, the membrane pores and pitch increased slightly in size going from dry to pH 1.6 and drastically between pH 1.6 and pH 7.1. Pore diameter and pitch were only measured at pH 1.6 and pH 7.1, but based on the disk swelling measurements in figure 5, the largest transition in size is expected to occur between pH 3.5 and 6.1 or within an even narrower range.

One thing that is noticeable in table 3 is that the degrees of swelling measured for the disks are higher than those reported by De et al. [26]. However because the edges of our disks are not perfectly vertical and straight

	Measured values		Degree of swelling H At pH 1.6		At pH 7.1		Linear deformation ratio α pH 7.1/1.6	
Disk	Disk area	n = 6	1.21	±0.18	5.42	±0.47	1.43	±0.01
Disks [26]	*Disk diameter*	*n = 4*	*0.28*	*±0.21*	*4.08*	*±0.54*	*1.59*	*±0.04*
Membrane	Pitch	n = 2	0.54	±0.09	5.75	±0.10	1.64	±0.02
Membrane	Pore area	n = 2	0.49	±0.21	12.01	±2.91	2.05	±0.06

Table 3: Summary of disk and membrane swelling measurements. The errors represent the standard deviation based on a sample, with n as given. The membranes described in the table were cured for 80 s, through masks with pore diameter 300 µm pitch 1200 µm. The data in row '*Disks [26]*' was calculated based on work by De et al. who investigated disks of different sizes (300, 400, 500 and 700 µm), using a set-up and pH-responsive material that were very similar ours. To obtain the disk size at swelling equilibrium, the first datapoints above pH 1.6 and above 7.1 were taken from their graphs. For the size of a dry disk, after curing, they do not give a measured size, so the "designed" disk size was used.

(figure 2), the swelling ratio was expected to be lower, not higher: when a disk expands outwards, the "gaps" in its side-profile are filled first which detracts from the measured swelling, as illustrated in figure 10. One possible explanation could be that there is a difference in material properties that gives our material a higher swelling ratio. Also, De et al. do not give clear values for the diameter of their disks when they are dry. Since the degree of swelling is calculated with respect to the dry state this ambiguity could be another cause of the difference.

Taking a closer look at the values, it can be seen that the degree of swelling for the disks at pH 1.6 ($H = 1.21$) is also much larger than for the membrane measurements. Since these were made using exactly the same material and method, it would be expected that the disk swelling ratios are the same as the membrane swelling ratios. Moreover, if the constrained disk set-up causes any differences, the disk swelling ratios should be lower: simulations have shown that constraints can decrease hydrogel swelling, not increase it [34]. The difference corresponds to an overestimation of the disk diameter at pH 1.6 by approximately 120 µm. It is visible in figure 5 that the appearance of the hydrogel disk changes also with pH. This is caused by the large difference in water content in the gel for different pH. The dark ring in figure 5 B. could have caused the disk size to be overestimated. The ring was assumed to be part of the disk, but it could instead be some kind of meniscus that is not part of the disk.

Another set of values that stands out in table 3 are the results based on the pore diameter; the degree of swelling $H_{(\text{at pH } 7.1)} = 12.01$ and the linear deformation ratio $\alpha = 2.05$. These are much higher than the values based on the pitch and disk measurements. It seems that with increasing pH, the pore size increases much more than the other dimensions of the membrane. At pH 7.1, the pore diameter is about 95 µm larger than would be expected. The images of the pores at this pH do not give reason to suspect this difference is caused by imaging artefacts (figure 6 C.): although the pore edge is more difficult to distinguish at high swelling, its visibility is good enough.

Another possible explanation would be a difference in material properties around the pore, compared to the bulk material. The creation of the pores could locally affect the material, creating a gradient in material properties around the pore. This could cause locally different swelling behaviour. The most likely reason for this is a gradient in exposure dose around the pore, the partial shadow of the mask generating a boundary layer that has received a lower dose. The exposure dose is the amount of electromagnetic energy per unit area that a resist is subjected to, it is found by multiplying the intensity of the incident UV light by the curing time. Research has shown that a lower exposure dose leads to a lower Young's modulus [27, 28]. The equilibrium swelling of a pH-responsive hydrogel is dependent on the Young's modulus of the material [26]. Therefore it logically follows that a lower exposure dose gives a higher degree of swelling. This led us to the hypothesis that the larger than expected pore expansion is caused by the presence of a difference in material properties around each pore, where the degree of swelling is higher than in the bulk material, that develops due to a local difference in received exposure dose. If this is the case then the curing time should have a detectable effect on the pH-response of the membranes.

Effects of mask design and curing time

The relations between the curing time and mask design used to manufacture a membrane and the pH response of that membrane were investigated. To do so membranes were manufactured using the parameters listed in table 2.

It was found that for each set of parameters pH-dependent deformation of the pitch was hardly affected by changes in mask design and curing time. The average linear deformation ratio of the pitch, for all membranes, was 1.65 ± 0.04 (mean±sd). As it is unaffected by these parameters, the pitch is a good indicator of the bulk material response, independently of any divergent material behaviour that might occur around the pores.

In contrast, the expansion of the pores was affected significantly by the design and curing parameters. As is visible in figure 9, the linear deformation ratio of the pores increases with curing time. This supports the theory that there is a curing-induced gradient material properties around the pores. For varying pore diameter, the linear

deformation ratio of the pores increases with decreasing pore diameter (figure 8). A possible explanation for this is that, because of the smaller pore size, the boundary layer relatively has a larger effect. For varying pitch the linear deformation ratio of the pore diameter is approximately constant. This is expected, because neither the exposure dose nor the pore size are varied.

Evaluation of membrane manufacturing method

The disks and membranes were patterned using a lithography-based approach. For this a curing unit with two UV light spots and no focussing system was used, in contrast to most lithography processes, where focussed light is the standard. The non-focussed light could have enhanced the boundary layer effect that is suspected to occur around the pores. The mask replication could also be affected by the non-focussed light, as well as by inconsistent contact between the mask and the glass due to flexibility of the mask material. This is likely what caused some pores to be more oval than round (figure 6). For masks with more complex features or sharp angles, these effects could be even more pronounced than they were for circular shapes.

Compared to the membranes listed in table 1, our manufacturing method is by far the fastest, taking only minutes instead of days. Moreover, ours is the only method that can be used to make pores of different shapes. It also allows for the most control over pore position and size. However only straight pores are possible, in contrast to the tortuous pores and interconnected cavities that are formed with phase separation or micro-sphere templates.

The pore size of our membranes was much larger than that of the other membranes in table 1. It could however be lowered by using masks with smaller features. The limit to this is the resolution of the printer that is used to make the mask [35]. The minimum feature size achievable with commercially available printers is somewhere between 10 and 50 µm (e.g. a 2500 dpi printer can prints dots that are about 10 µm in size, which will allow reliable printing of 50 µm features). Specialized film-mask manufacturers can produce feature sizes down to 5 µm. A second limit is the aspect ratio[2], which means that the achievable pore size is limited by the thickness of the membrane. With UV lithography the maximum aspect ratio is 25 [35]. However this was determined using SU8 photoresist and under special conditions. A more realistic expectation for our material would be a maximum aspect ratio below 10. Khoury et al. patterned liquid phase precursors at aspect ratios between 4 and 8 [36] and Bryant et al. developed a photopolymerization technique to pattern 760 µm thick HEMA hydrogels with an aspect ratio of 4 [37]. The thickness of the membrane can easily be reduced by adapting the curing set-up. However the thinner the membrane is, the more fragile it will be. There are also diffraction related limits to the achievable pore size that may become relevant for pores smaller than 10 µm [38].

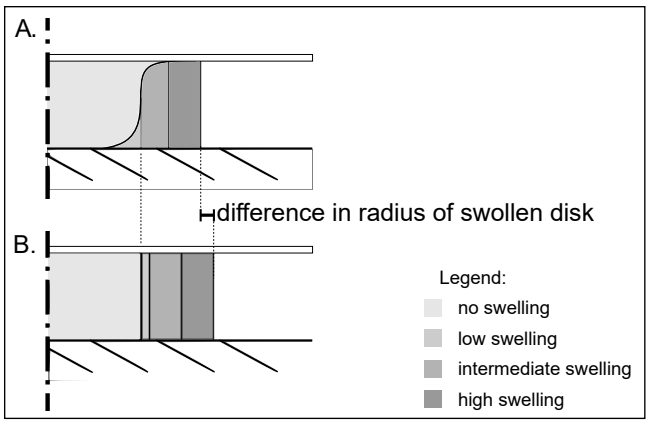

Figure 10: Illustration of the effect of disk side-profile shape on measured swelling. Schematics of half of a disk inside a channel (side view). In A. the side-wall shape is as we suspect it to be for the manufactured disks. In B. the side-walls of the disk are perfectly vertical and straight.

The comparison also shows that the pore size of a hydrogel membrane can only decrease with swelling when the pH-responsive material is somehow constrained. This can be done by making a heterogeneous membrane [4] or attaching the membrane to a rigid surface or scaffold. A scaffold has the additional benefit of making the membrane less fragile. When the membrane is not constrained, the pore size can only increase with swelling.

Constrained disk as system for measuring material response

A constrained disk set-up was used to measure the pH-responsive swelling of the hydrogel material and compare it to literature. The in-situ polymerization of the disk inside a fluidic channel made it simple to constrain the disk and expose it to different pH. Because swelling only occurred in the lateral direction and the top of the channel was made out of glass, it was very easy to image the disk and measure its swelling. Furthermore this method enables manufacturing and investigating very small pieces of pH-responsive material, which greatly decreases the time needed to reach equilibrium swelling.

However it was difficult to manufacture the disk in such a way that the sides were perfectly straight. Where this did not succeed, the measurements were affected. Also the constraints on the disk may have influenced the volumetric swelling of the disk, decreasing it. Measuring the disk size at different states of swelling requires image analysis and interpretation, which is quite prone to errors due to the fact that the appearance of the disk changes with increasing water content. An alternative could have been measuring the change in weight of the swelling material, but this method has many practical limitations due to the fact that it requires for the material to be removed from the pH solution.

[2]Aspect ratio: ratio of feature height (or depth) over width.

It is suspected that the pH-response of the pores is affected by a layer with different swelling properties around the edge of the pore. However if this is the case then this layer must also be present in the disks. Thus the disk material would not be homogeneous, as was assumed. This would also add an error to the measurements.

Overall the constrained disk set-up is a useful tool to get an estimation of the pH response of a material. It can be used to investigate and compare different pH-responsive swelling materials, find the pH at which a material responds and can also be used to measure dynamic swelling. As such it can contribute to the design and development of pH-responsive hydrogel structures. However the swelling measurements do not give a very accurate prediction of bulk material swelling.

5. Conclusion and perspectives

We have developed a method for the fabrication of pH-responsive hydrogel membranes that gives control over pore size, position and shape. The membrane material is a 2-Hydroxyethyl methacrylate and Acrylic acid based, cross-linked polymer hydrogel that swells with increasing pH. This allows membranes to interact directly with analytes in a microfluidic system. A lithography approach was used to pattern the membranes and thereby create pores. A UV-cureable liquid precursor was exposed through a negative photo-mask, that was manufactured in a very fast and low-cost process. The pore size was measured for environmental pH of 1.6 and 7.1, within this range the pores doubled in diameter. The increase in pore size was higher than would be expected based on the measured pH-response of the bulk material. This is attributed to the occurrence of divergent material properties around each pore, which develop due to a local difference in received exposure dose. It was found that the curing time and the mask pore diameter have a significant effect on the pH-response of the pores, which supports our theory of a curing-dependent local difference in material properties.

The next step towards implementation of our membranes should be characterization of the pH-dependent barrier properties of the membrane. This is important because it is thus far unknown how properties such as the permeability of the hydrogel matrix and wettability of the material surface change with pH. Aside from the pore size, these properties could also affect transport through the membrane. The barrier properties of the membrane could be investigated by measuring the pressure drive flow or diffusion driven rate of transport through the membrane at different pH and comparing to pH-responsive hydrogel membranes without pores and porous, non-responsive HEMA membranes.

Next to this it is important to further investigate the cause of the larger-than-expected pore expansion. As a control membranes with the same pore size and geometry could be made from the same material but using a different manufacturing technique, such as mold replication. Then it can be measured how the pores deform when there can not be a curing-related gradient in material properties. Furthermore, previous research has shown that the Young's modulus of the pH-responsive hydrogel that we used is curing dependent, but not how this affects the swelling. Therefore the swelling of samples cured at different times should be investigated. It would also be interesting to model the swelling of pH-responsive hydrogels with gradients in material properties, to better understand how this can affect pore deformation.

The fluidic properties and pH-response of the membrane can be adjusted in several ways to suit a specific application. First of all, the pore size, shape and position can easily be changed, because of the fast, low-cost mask-manufacturing method that was used. The thickness of the membrane can be changed by adjusting the design of the PDMS bottom. Additionally, the pH at which the membrane responds can be altered by using a different electrolyte monomer than acrylic acid to synthesize the gel. The membrane can even be made to swell at low pH instead of high pH by using a basic monomer. The swelling ratio can be tuned by altering the PEL and cross-linker concentrations. The Young's modulus of the material is dependent on the cross-linker concentration, but can also be adjusted by using a different cross-linking agent or replacing HEMA by another base material. The constrained disk set-up can then be used to test and compare the pH-response of different potential materials.

References

[1] Y. Temiz, R. D. Lovchik, G. V. Kaigala, E. Delamarche, Lab-on-a-chip devices: How to close and plug the lab?, Microelectronic Engineering 132 (2015) 156–175. doi:10.1016/j.mee.2014.10.013.

[2] E. K. Sackmann, A. L. Fulton, D. J. Beebe, The present and future role of microfluidics in biomedical research, Nature 507 (7491) (2014) 181–189. doi:10.1038/nature13118.
URL http://dx.doi.org/10.1038/nature13118

[3] J. de Jong, R. G. H. Lammertink, M. Wessling, Membranes and microfluidics: a review, Lab on a Chip 6 (9) (2006) 1125. doi:10.1039/b603275c.
URL http://xlink.rsc.org/?DOI=b603275c

[4] M. Tamada, M. Asano, R. Spohr, J. Vetter, C. Trautmann, M. Yoshida, R. Katakai, H. Omichi, Preparation of hydrolyzed pH responsive ion track membrane, Macromol. Rapid Commun. 51 (1995) 47–51.

[5] I. Tokarev, M. Orlov, S. Minko, Responsive polyelectrolyte gel membranes, Advanced Materials 18 (18) (2006) 2458–2460. doi:10.1002/adma.200601288.

[6] M. Orlov, I. Tokarev, A. Scholl, A. Doran, S. Minko, pH-responsive thin film membranes from poly(2-vinylpyridine): Water vapor-induced formation of a microporous structure, Macromolecules 40 (6) (2007) 2086–2091. doi:10.1021/ma062821f.

[7] V. Gopishetty, Y. Roiter, I. Tokarev, S. Minko, Multiresponsive biopolyelectrolyte membrane, Advanced Materials 20 (23) (2008) 4588–4593. doi:10.1002/adma.200801610.

[8] J. O. You, M. Rafat, D. Almeda, N. Maldonado, P. Guo, C. S. Nabzdyk, M. Chun, F. W. LoGerfo, J. W. Hutchinson, L. K. Pradhan-Nabzdyk, D. T. Auguste, pH-responsive scaffolds generate a pro-healing response, Biomaterials 57 (2015) 22–32.

doi:10.1016/j.biomaterials.2015.04.011.
URL http://dx.doi.org/10.1016/j.biomaterials.2015.04.011

[9] D. Wandera, S. R. Wickramasinghe, S. M. Husson, Stimuli-responsive membranes, Journal of Membrane Science 357 (1-2) (2010) 6–35. doi:10.1016/j.memsci.2010.03.046.
URL http://dx.doi.org/10.1016/j.memsci.2010.03.046

[10] M. W. Urban, Biologically Responsive Polymers, The Royal Society of Chemistry, 2016.

[11] E. M. White, J. Yatvin, J. B. Grubbs, J. A. Bilbrey, J. Locklin, Advances in smart materials: Stimuli-responsive hydrogel thin films, Journal of Polymer Science, Part B: Polymer Physics 51 (14) (2013) 1084–1099. doi:10.1002/polb.23312.

[12] G. Kocak, C. Tuncer, V. Bütün, pH-Responsive polymers, Polym. Chem. 8 (1) (2017) 144–176. doi:10.1039/C6PY01872F.
URL http://xlink.rsc.org/?DOI=C6PY01872F

[13] D. H. Kang, S. M. Kim, B. Lee, H. Yoon, K.-Y. Suh, Stimuli-responsive hydrogel patterns for smart microfluidics and microarrays., Analyst 138 (21) (2013) 6230–42. doi:10.1039/c3an01119d.
URL http://www.ncbi.nlm.nih.gov/pubmed/24029824

[14] G. S. Longo, M. Olvera De La Cruz, I. Szleifer, Molecular theory of weak polyelectrolyte gels: The role of pH and salt concentration, Macromolecules 44 (1) (2011) 147–158. doi:10.1021/ma102312y.

[15] J. Reijenga, A. van Hoof, A. van Loon, B. Teunissen, Development of methods for the determination of pKa values, Analytical Chemistry Insights 8 (1) (2013) 53–71. doi:10.4137/ACI.S12304.

[16] A. R. Khokhlov, S. G. Starodubtzev, V. V. Vasilevskaya, Conformational Transitions in Polymer Gels: Theory and Experiment, in: K. Dušek (Ed.), Responsive Gels: Volume Transitions I, Vol. 109, Springer, 1993, pp. 123–171. doi:10.1007/BFb0021125.
URL http://link.springer.com/10.1007/BFb0021125

[17] O. E. Philippova, D. Hourdet, R. Audebert, A. R. Khokhlov, pH-Responsive Gels of Hydrophobically Modified Poly(acrylic acid), Macromolecules 30 (26) (1997) 8278–8285. doi:10.1021/ma970957v.
URL http://pubs.acs.org/doi/abs/10.1021/ma970957v

[18] T. Wallmersperger, B. Kröplin, J. Holdenried, R. W. Guelch, Coupled multifield formulation for ionic polymer gels in electric fields, Proceedings of SPIE 4329 (Smart Structures and Materials 2001: Electroactive Polymer Actuators and Devices).

[19] K. J. Suthar, Simulation, Synthesis, and Characterization of Hydrogels and Nanocomposite Gels, Ph.D. thesis, Western Michigan University (2009).
URL http://scholarworks.wmich.edu/dissertations

[20] T. Wallmersperger, Modelling and Simulation of the Chemo-Electro-Mechanical Behaviour, in: G. Gerlach, K.-F. Arndt (Eds.), Hydrogel Sensors and Actuators, Springer, 2010, pp. 137 – 163. arXiv:arXiv:1011.1669v3, doi:10.1007/978-3-540-75645-3.
URL http://link.springer.com/10.1007/978-3-540-75645-3

[21] A. M. Mathur, S. K. Moorjani, A. B. Scranton, Methods for Synthesis of Hydrogel Networks: A Review, Journal of Macromolecular Science, Part C: Polymer Reviews 36 (2) (1996) 405–430. doi:10.1080/15321799608015226.
URL http://www.tandfonline.com/doi/abs/10.1080/15321799608015226

[22] S. Dai, P. Ravi, K. C. Tam, pH-Responsive polymers : synthesis , properties and applications, Soft Matter 4 (2008) 435–449. doi:10.1039/b714741d.

[23] D. J. Beebe, J. S. Moore, Q. Yu, R. H. Liu, M. L. Kraft, B. H. Jo, C. Devadoss, Microfluidic tectonics: a comprehensive construction platform for microfluidic systems., Proceedings of the National Academy of Sciences of the United States of America 97 (25) (2000) 13488–93. doi:10.1073/pnas.250273097.
URL http://www.pnas.org/content/97/25/13488.full

[24] D. J. Beebe, J. S. Moore, J. M. Bauer, Q. Yu, R. H. Liu, C. Devadoss, B.-H. Jo, Functional hydrogel structures for autonomous flow control inside microfluidic channels, Nature 404 (6778) (2000) 588–590. doi:10.1038/35007047.
URL http://www.nature.com/doifinder/10.1038/35007047{%}5Cnpapers3://publication/doi/10.1038/35007047

[25] L. Giorno, E. Piacentini, F. Bazzarelli, Macroporous, Mesoporous, and Microporous Membranes, Springer Berlin Heidelberg, Berlin, Heidelberg, 2016, pp. 1–2. doi:10.1007/978-3-642-40872-4_2244-1.
URL https://doi.org/10.1007/978-3-642-40872-4{_}2244-1

[26] K. S. De, N. R. Aluru, B. Johnson, W. C. Crone, D. J. Beebe, J. Moore, Equilibrium swelling and kinetics of pH-responsive hydrogels: Models, experiments, and simulations, Journal of Microelectromechanical Systems 11 (5) (2002) 544–555. doi:10.1109/JMEMS.2002.803281.

[27] B. Johnson, D. Niedermaier, W. C. Crone, J. Moorthy, D. J. Beebe, Mechanical properties of a pH sensitive hydrogel, Society for Experimental Mechanics, Annual proceedings (2002) 14–17.
URL http://scholar.google.com/scholar?q=intitle:Mechanical+Properties+of+a+pH+Sensitive+Hydrogel{#}1

[28] B. Johnson, D. J. Beebe, W. C. Crone, Effects of swelling on the mechanical properties of a pH-sensitive hydrogel for use in microfluidic devices, Materials Science and Engineering C 24 (4) (2004) 575–581. doi:10.1016/j.msec.2003.11.002.

[29] B. Johnson, J. M. Bauer, D. J. Niedermaier, W. C. Crone, D. J. Beebe, Experimental Techniques for Mechanical Characterization of Hydrogels at the Microscale, Experimental Mechanics 44 (1) (2004) 21–28. doi:10.1177/0014485104039629.
URL http://www.ingentaselect.com/rpsv/cgi-bin/cgi?ini=xref{&}body=linker{&}reqdoi=10.1177/0014485104039629

[30] R. H. Liu, Q. Yu, D. J. Beebe, Fabrication and characterization of hydrogel-based microvalves, Journal of Microelectromechanical Systems 11 (1) (2002) 45–53. doi:10.1109/84.982862.

[31] D. Qin, Y. Xia, G. M. Whitesides, Advanced Materials, Advanced MaterialsMaterials 9 (11) (1997) 639–643.

[32] R. Gemeinhart, C. Guo, Fast Swelling Hydrogel Systems, in: Nobuhiko Yui, Randall J. Mrsny, K. Park (Eds.), Reflexive Polymers and Hydrogels: Understanding and Designing Fast Responsive Polymeric Systems, CRC Press LLC, 2004, Ch. 13, pp. 245–257. doi:doi:10.1201/9780203485354.ch13.

[33] O. Okay, General Properties of Hydrogels, in: G. Gerlach, K.-F. Arndt (Eds.), Hydrogel Sensors and Actuators, Springer, 2010, pp. 1–14. arXiv:arXiv:1011.1669v3, doi:10.1007/978-3-540-75645-3.
URL http://link.springer.com/10.1007/978-3-540-75645-3

[34] A. D. Drozdov, J. deClaville Christiansen, Swelling of pH-sensitive hydrogels, Physical Review E 91 (2) (2015) 022305. doi:10.1103/PhysRevE.91.022305.
URL https://link.aps.org/doi/10.1103/PhysRevE.91.022305

[35] M. J. Madou, Lithography (Part I), in: Fundamentals of Microfabrication and Nanotechnology, volume II, 2011, pp. 2 – 147.

[36] C. Khoury, G. A. Mensing, D. J. Beebe, Ultra rapid prototyping of microfluidic systems using liquid phase photopolymerization, Lab on a Chip 2 (1) (2002) 50–55. doi:10.1039/b109344d.

[37] S. J. Bryant, K. D. Hauch, B. D. Ratner, Spatial patterning of thick poly(2-hydroxyethyl methacrylate) hydrogels, Macromolecules 39 (13) (2006) 4395–4399. doi:10.1021/ma060145b.

[38] S. Franssila, Optical Lithography, in: Introduction to Microfabrication, 2nd Edition, John Wiley & Sons, Ltd, 2010, pp. 103–113.

A

Disk and membrane manufacturing; Investigation of optimal curing time and evaluation of results

A.1. Background: photolithography

How lithography-approach may influence results Ihe disks and membranes are patterned using a photolithographic approach. Photolithography, or optical lithography, uses UV light to expose photosensitive resist films through photo-masks. The pattern that is formed in the resist is usually not a one to one copy of the mask. Below different factors that can affect the cured result are discussed.

Curing time / exposure dose

The exposure dose is the amount of electromagnetic energy per unit area that a resist is subjected to. It is found by multiplying the intensity of the light source by the exposure time.

Resist / precursor

The precursor is comparable to a negative photo-resist. Here 'negative' indicates that the resist cures (becomes solid/insoluble) when exposed to light. The main difference between our precursor and conventional resists is than conventional resists usually contain a solid base resin that is dissolved in a solvent. When such a resists is spin-coated onto a wafer, the solvent evaporates and a solid resist layer is formed. This makes them easier to process than our liquid precursor.

Resist is not an on/off material, which cures as soon as it is touched by light of the right wavelength. It has a threshold exposure energy. This threshold energy is often refered to as the dose-to-print or dose-to-size, meaning the amount of exposure energy that is required to produce the proper feature dimensions in resist [20].

The resist is also an optical material and part of an optical system, which means we must consider its absorption. Generally in a resist, the exposure dose is higher at the top of a layer than at the bottom, because part of the light is absorbed at the top and never reaches the bottom. In negative resists, this effect creates an undercut, which means that the top of a cured structure will be wider than the bottom [21]. How strong this effect is also depends on the absorbency of cured resist. If this is high, very high exposure times are needed to cure the resist layer throughout its thickness.

Resolution and resist profile

The optics of a lithography system affect the achievable resolution and the shape and side profile of the cured structures. Generally in lithography pattern transfer is limited by diffraction. However in our process, the relevant wavelengths (Light source: 320 - 550 nm, DMPA absorbency: below 380 nm [62]) are over 250 times smaller than the smallest mask dimensions. Therefore we deduce that diffraction can not have a significant effect.

The coherence, or lack thereof, will probably have a much larger influence. To cure the disks and membranes, UV light coming from two spots is used. Since this light is scattered, it probably causes

considerable exposure underneath the mask. Replacing the light source by one that is focussed would reduce this. For large resist layer thicknesses and large aspect ratios, using colliminated light would be even better [22].

Proximity effect

Proximity effects are variations in the shape of a cured pattern that are caused by the proximity (or absence) of other nearby features on the mask [41]. These can arise from different causes, such as diffraction, or diffusion of chemical components in the resist. However, because of the relatively large size of our features, there is one main effect that we need to consider: This is that a section of resist will receive additional exposure energy through any nearby transparent areas on the mask.

An example of this is the difference in printed line-width between an isolated line and a line in a dense array of lines [41]. The line in an array will be wider, because exposure dose is added by the surrounding lines.

For our method, this effect is enhanced by the fact that the UV light is not focussed. Any section of resist will receive light through the mask area directly above it ánd through any nearby transparent areas on the mask, within a certain radius. This means that if there are more nearby transparent areas, the cured feature will receive a larger exposure dose, which will cause it to become larger than if it were an isolated feature.

A.2. Curing time optimization

Because of the proximity effect described above, the optimal curing time for a mask design depends on the density of features on that mask. For disk and membrane manufacturing, this density of features is very different: the disk masks are mostly opaque, while the membrane masks are mostly transparent, which is equivalent to a high density of features. Therefore the optimal curing times for these designs are expected to be different. The effect of curing time on disk and pore dimensions was investigated. These measurements were used to select the optimal curing time.

For disks, the results are shown in figure A.1. The disk size increases with curing time. It equals the mask size at a curing time between 120 and 130 s. Based on this 130 s was selected as the optimal curing time for the disks.

For membranes, the results are shown in figure A.2. The pore size decreases with curing time, thus the size of the cured area increases with curing time. The pore size equals the mask size at curing times between 60 and 70 s. However for these times, membranes were not properly cured throughout their full thickness, creating a sticky semi-cured residue. Therefore 80 s was selected as the optimal curing time for the membranes.

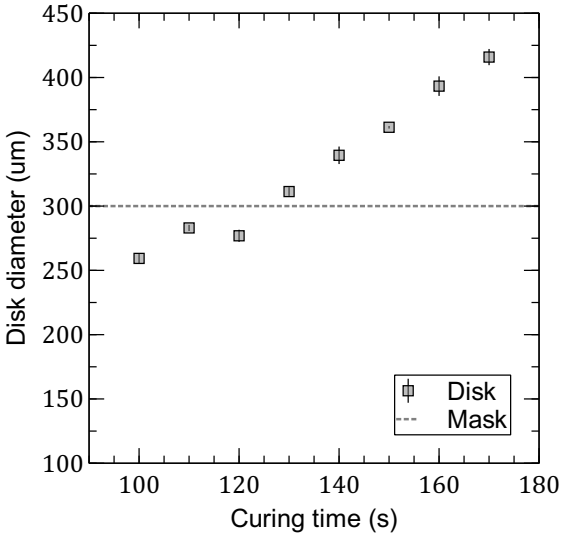

Figure A.1: Effect of curing time on size of cured disk;
Graph of disk diameter as function of curing time. Disk diameters were measured after curing, before flushing the non-cured precursor out of the channel. Disks were cured using masks with 300 um openings, as indicated by the dotted line. Squares: Average, error bars: standard deviation based on a sample with n=3 (one channel per curing time, with 3 disks per channel).

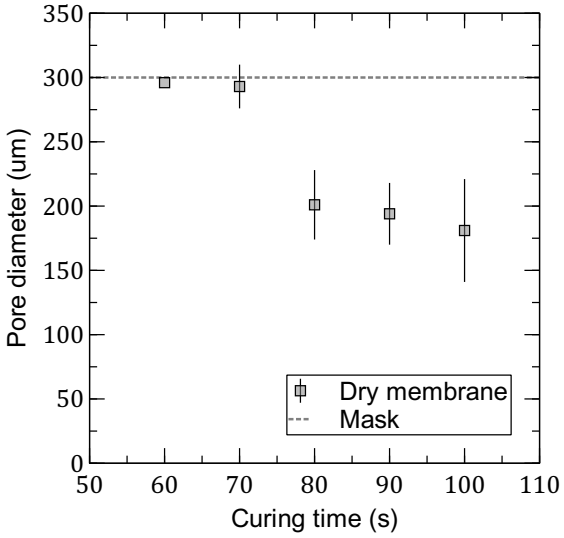

Figure A.2: Effect of curing time on pore size of cured membrane;
Graph of pore diameter as function of curing time. Pore diameters were measured on dry membranes (after curing and washing away non-cured precursor). Membranes were cured using masks with 300 um pores, as indicated by the dotted line, and 1200 um pitch. Squares: Average, error bars: standard deviation based on a sample with n=2.

A.3. Disk manufacturing; evaluation of results

A.3.1. Influence of curing time on shape of disk

When imaged from the top, disks appeared to have a double border.

To investigate how these borders are affected by curing time, disks were cured using different curing times. After curing, for each disk the diameters of the outer border and inner ring were measured and subtracted. The difference between these diameters was plotted with respect to curing time. As can be seen in figure A.3, the distance between the two borders changes with curing time. The difference first decreases, then increases, with a minimum at 130 s. With (overly) long curing times, disks were found to develop star-like spikes.

The side profile of the disk was also imaged, which was made possible by cutting the channel in half near a disk. An image of a disk viewed from the side is shown in figure A.4 A. The side-walls of the disk are partly vertical, but have a concave curvature where the disk touches the glass and a convex curvature where the disk touches the PDMS.

Based on the measurements described above and the images taken of disks from the side, it seems that the double border is related to the shape of the disk side-walls. This is illustrated in figure A.4 C. Figure A.3 suggests that the side-walls of the disk are the most vertical and straight for a curing time of 130 s.

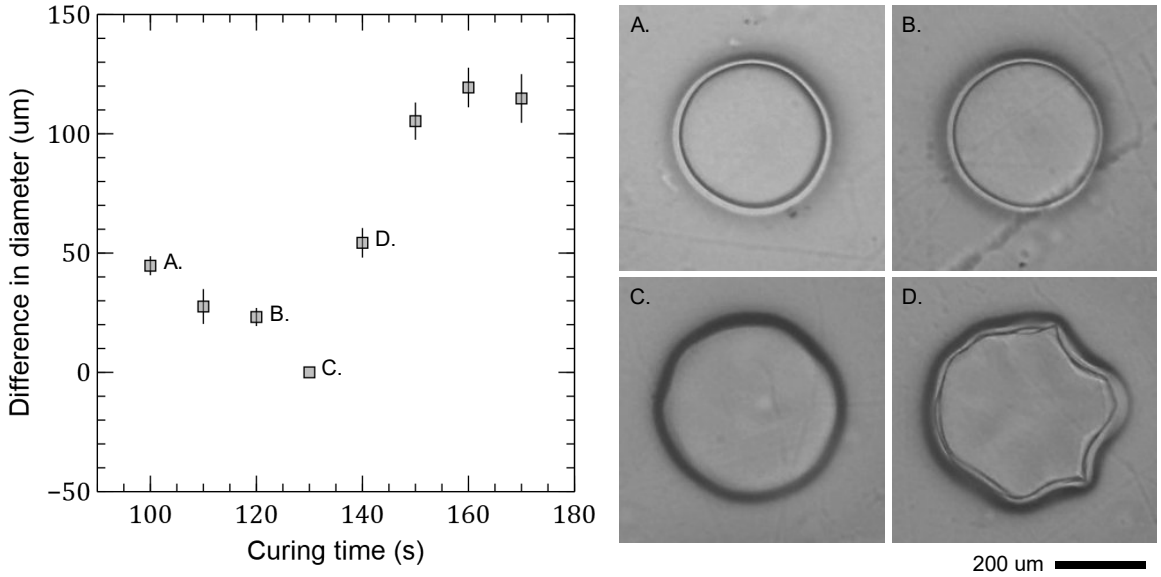

Figure A.3: Graph: Effect of curing time on double border of disk; Plot of the difference between the diameter of the outer border and the diameter of the inner border ($d_o - d_i$) as function of curing time. Diameters were measured after curing, before flushing the non-cured precursor out of the channel. Disks were cured using masks with 300 um openings. Squares: Average, error bars: standard deviation based on a sample with n=3 (one channel per curing time, with 3 disks per channel). A. - D.: Images of disks with different curing times, as indicted in the graph.

A.3.2. Influence of shape of disk on disk swelling

If the side-walls of the disk are not straight and vertical, this would affect the measured swelling. When the disk expands outwards due to swelling, the ”gaps” in the side-profile are filled, as illustrated in figure A.5. This leads to a measured volumetric swelling that is lower than the true volumetric swelling.

To investigate this whether this takes place, disk that were manufactured using different curing times, were swollen in DI water. The disk diameter was measured after curing (AC) and at equilibrium swelling in DI. For each disk, the ratio of the diameter AC to the diameter in DI was plotted with respect to the curing time that was used for the disk.

The results are shown in figure A.6. The plot shows that the relative diameter is influenced by the curing time. The highest swelling occurs at a curing time of 120 s. This observation confirms the

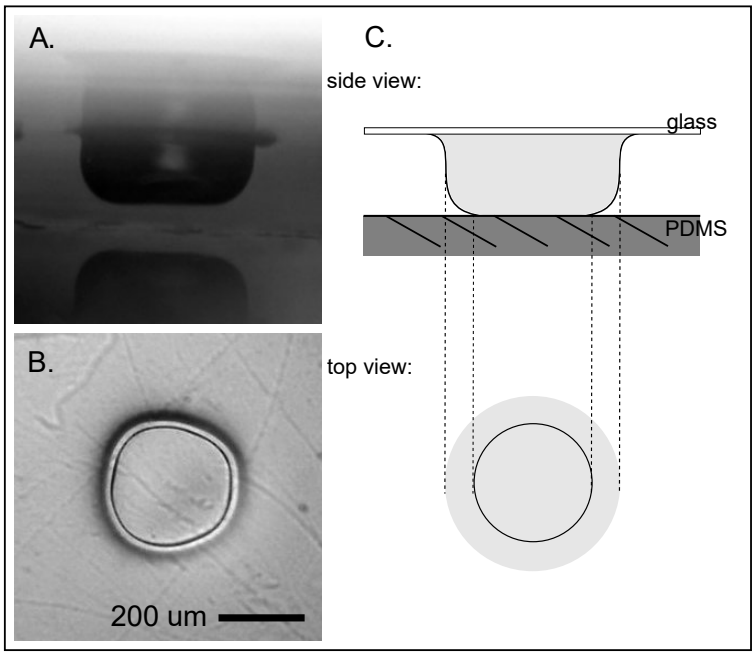

Figure A.4: Disk shape. A. and B. are images of the same disk. A. Side profile (After curing and emptying the channel). B. Top view (After curing, before removing non-cured precursor, so here the disk is immersed in liquid precursor). C. Schematic diagram to demonstrate how the double border that is visible in the top view can be explained by the curvature in the side walls of the disk.

suspected shape of the disk side-walls. It also suggests that 120 would have been a more optimal curing time than 130 s. However the difference is not large.

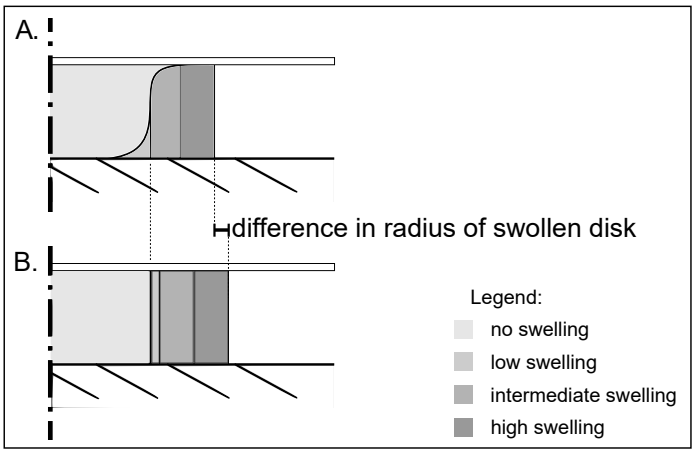

Figure A.5: Illustration of the effect of disk side-profile shape on measured swelling. The images show half of the side view of a disk inside a channel. In A. the side-wall shape is as we suspect it to be for the manufactured disk. In B. the side-walls of the disk are perfectly vertical and straight.

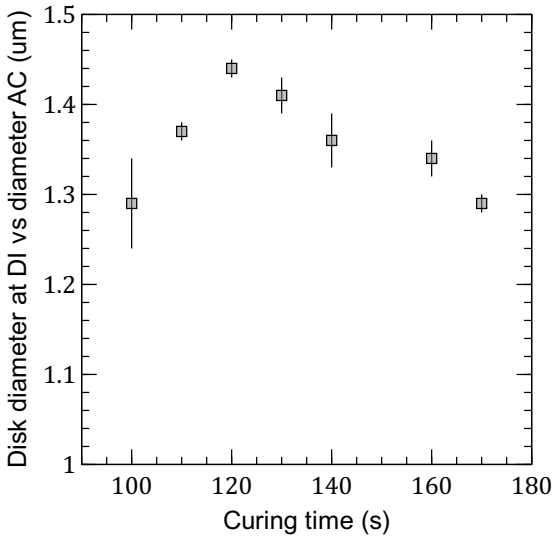

Figure A.6: Effect of curing time on disk swelling; Graph of the ratio of disk diameter after curing (AC) over the disk diameter at equilibrium swelling in DI water, as function of curing time. Squares: Average, error bars: standard deviation based on a sample with n=3 (one channel per curing time, with 3 disks per channel).

A.4. Membrane manufacturing; evaluation of results

A.4.1. Influence of mask design on pore size

Because of the proximity effects described above, the mask design could influence the pore size of the cured membrane.

In figure A.7 the pore diameter of the cured membrane is plotted with respect to the pore diameter of the mask used to cure the membrane. Membranes were cured for 80 s, using masks with different pore diameters and a pitch of four times the pore diameter. It can be seen that for all pore sizes, the pores are smaller on the membrane than on the mask, similar to what we observed for a curing time of 80 s in figure A.2. The pore size of the membrane follows the same slope as the pore size of the mask, except for the smallest pore diameter (250 um). Here the pore size of the membrane seems to be smaller than could be expected. This could be caused by the proximity effect, because a smaller pore is surrounded by relatively more transparent mask area.

In figure A.8 the pore diameter of the cured membrane is plotted with respect to the pitch of the mask used to cure the membrane. Membranes were cured for 80 s, using masks with a pore diameter of 300 um and different pitches. The graph shows that for pitch below 800 um, the pores are approximately 50 um smaller than for pitch above 800 um. This is the opposite of what would be expected if there was a proximity effect: For a smaller pitch, the ratio of transparent mask area to opaque mask area decreases.

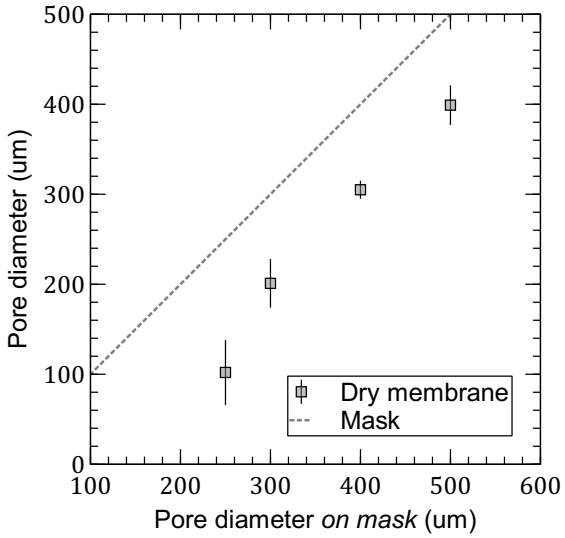

Figure A.7: Effect of mask pore diameter on pore size of cured membrane;
Graph of the pore diameter on the cured membrane as function of pore diameter on the mask used to cure the membrane. Pore diameters were measured on dry membranes (after curing and washing away non-cured precursor). Membranes were cured for 80 s, using masks with different pore sizes, as indicated by the dotted line, a pitch of four times the pore diameter. Squares: Average, error bars: standard deviation based on a sample with n=2.

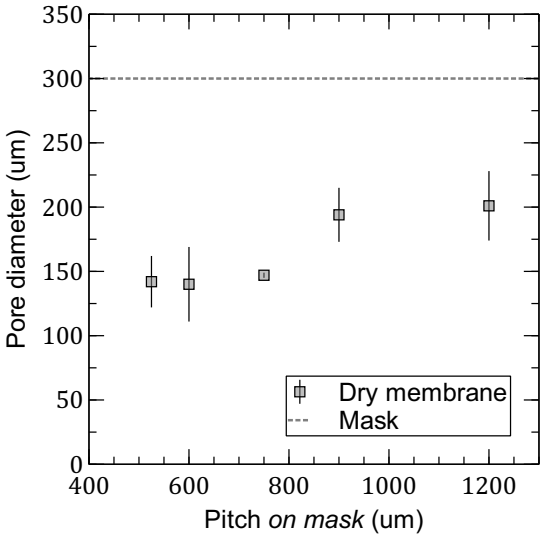

Figure A.8: Effect of mask pitch on pore size of cured membrane;
Graph of the pore diameter on the cured membrane as function of pitch on the mask used to cure the membrane. Pore diameters were measured on dry membranes (after curing and washing away non-cured precursor). Membranes were cured for 80 s, using masks with 300 um pores, as indicated by the dotted line, and different pitches. Squares: Average, error bars: standard deviation based on a sample with n=2.

A.4.2. Membrane inspection to check if pores are open

After curing, all membranes were inspected using an optical microscope. However for membranes with small pores, this inspection did not give conclusive results as to whether the pores were open. By ”open” we mean that the pores run through the entire membrane thickness and are not just dents in the membrane.

To further investigate the pore morphology, membranes were imaged using a white-light interferometer. Imaging was done after curing the membranes, washing away excess precursor and drying the membranes. At this points membranes were still attached to the glass slides that were used in manufacturing. The resulting hight maps of the membranes were interpreted as follows: If it was possible to see down to the bottom of a pore, it was assumed to be open.

Figure A.9 shows a membrane with open pores. This is derived from the black dot that is visible in the centre of each pore on the height map of the membrane. On the height profile plots, it ca be seen that these dots are located at approximately the same height as the slide that supports the membrane. Figure A.10 shows a membrane for which the bottoms of the pores were not visible. From this it cannot be derived that the pores are definitely blocked. It could also be that the aspect ratio of the pore is too high, or there is a residue at the bottom of the pore that prevents reflection. However all pores for which the result was inconclusive, were assumed to blocked. Only curing times and mask designs for which, all pores were open, were included in this work. The manufacturing parameters that were found to give membranes with open pores are listed in table 2. of the paper.

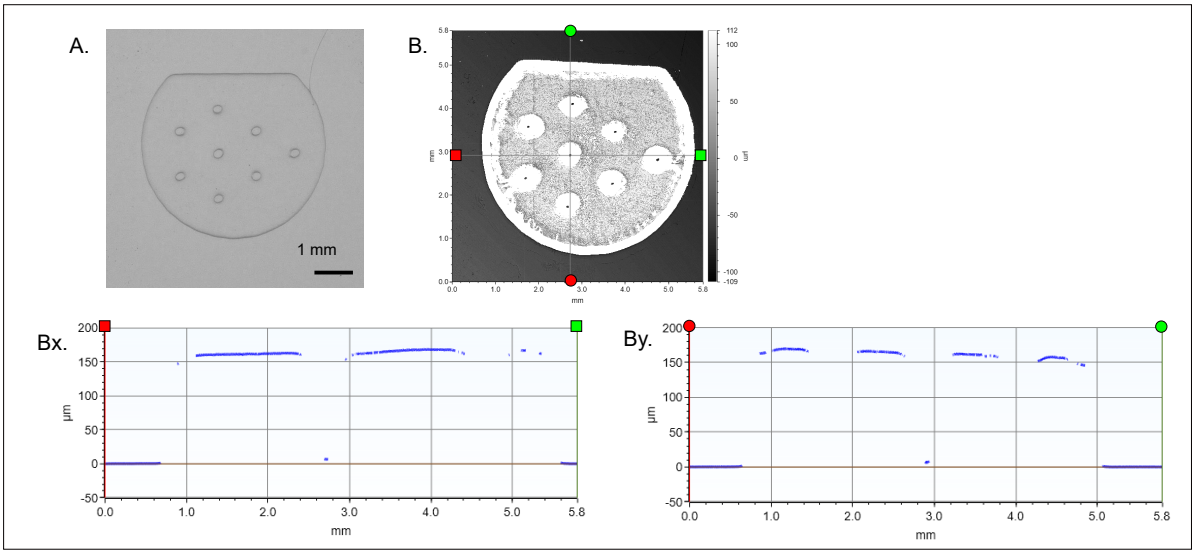

Figure A.9: Images of membrane with open pores.
A. Image taken with optical microscope. B. Height map of membrane, made with white-light interferometry. Bx. Height profile of membrane in x-direction, through central pore. By. Height profile of membrane in y-direction, through central pore. The membrane in these images was cured for 80 s, using a mask with pore diameter = 300 um and pitch = 1200 um.

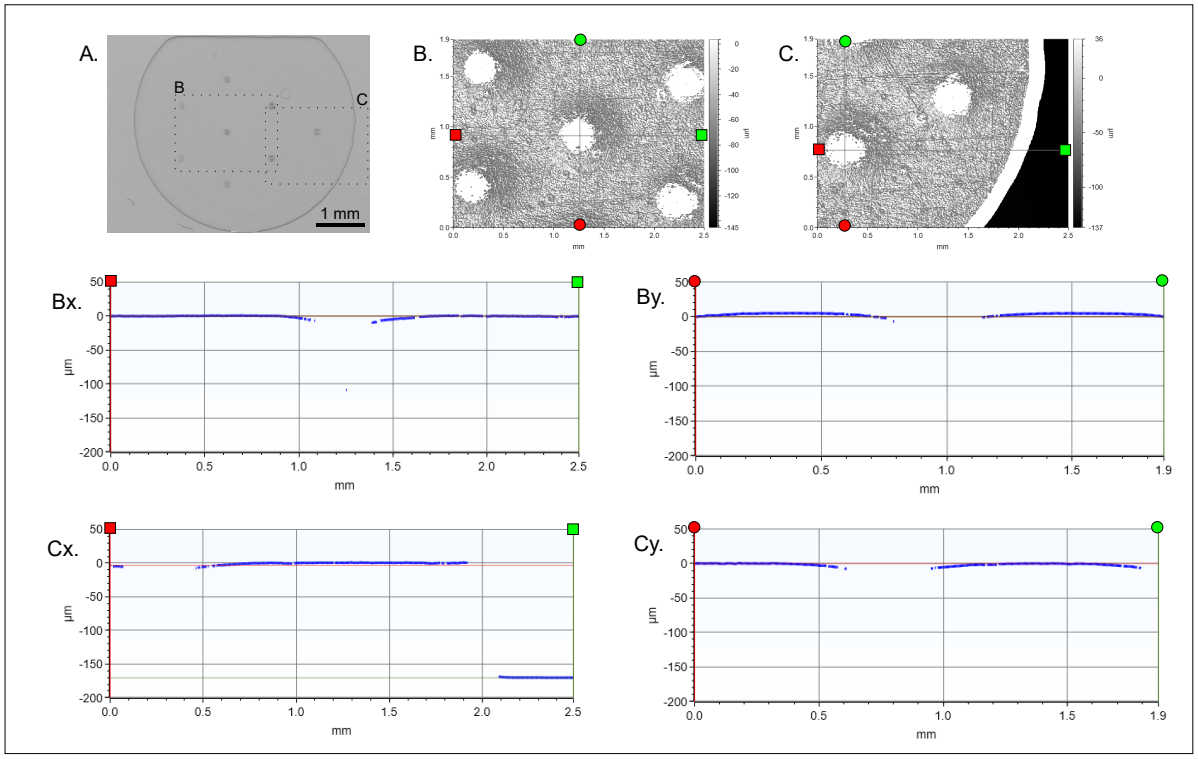

Figure A.10: Images of membrane with pores that are considered blocked.
A. Image taken with optical microscope. B. and C. Height maps of sections of the membrane, made with white-light interferometry. Bx. Height profile of section B in x-direction, through central pore. By. Height profile of section B in y-direction, through central pore. Cx and Cy: height profiles of section C. The membrane in these images was cured for 120 s, using a mask with pore diameter = 300 um and pitch = 1200 um.

B

Simulation of pH-responsive swelling (review)

The aim of this project is to make functional structures from pH responsive materials for integrated fluid control. Simulation of the pH responsive behaviour of these materials can be a useful tool to aid in the design of fluid-controlling structures. Such simulations can be used to investigate how different design parameters affect the performance of a device. Also simulations can aid in the design of experiments and partly replace experimental testing.

Stimuli-responsive hydrogels have been modelled on different scales [78]. Next to this, static and dynamic models can be distinguished and simulation can be done in 1-, 2- or 3-dimensions. A coupled multi-field electro-chemo-mechanical formulation has been developed to a gain more precise insight into phenomena occurring in PEL gels. This formulation can be used to model the geometry, stresses, potentials and concentrations in a system consisting of a hydrogel structure in a bath. It can capture both static and dynamic phenomena, but here only static equilibrium swelling is considered. The coupled electro-chemo-mechanical formulation can be applied in a commercially available software package, Comsol Multiphysics [64, 66], and has been used for simulations in 1-, 2- and 3 dimensions [65].

B.1. Coupled electro-chemo-mechanical formulation

The electro-chemo-mechanical model has been applied in comsol Multiphysics by [65] to simulate pH-responsive swelling of hydrogels in 3D arbitrarily shaped geometries. Before this Suthar have used the same method for 2D simulations [64, 66]. The simulations by Suthar and his colleagues make use of an electro-mechanical model that was described and implemented in 1-dimension by De et al. [16]. Their formulation again closely resembles models by Grimshaw et al. [26] and Wallmersperger et al. [79].

The electro-chemo-mechanical formulation is based on coupled chemical field, electrical field and mechanical equilibrium equations. The model describes the pH- and electric field- responsiveness of PEL hydrogels in static equilibrium. Swelling of the gel begins with a given bath pH. The pH of the bath results in a certain concentration of H^+ ions inside the hydrogel. This leads to the dissociation of electrolyte groups and the concentration H^+ can thus be used to find the concentration of fixed charge groups in the gel. The potential that results from these fixed charges leads to transport of ions between the solution and the gel. The concentration differences between the gel and the solution give rise to a relative osmotic pressure. A mechanical equilibrium then exists between the osmotic pressure urging the gel to swell and the stiffness of the gel network counteracting this swelling. The 1D equations of this electro-chemo-mechanical for acidic gels are derived in the following sections. For basic gels the same theory applies. The model only describes static equilibrium states of swelling, chemical diffusion dynamics and mechanical dynamics are not included. A schematic overview of these equations and their interactions is given in figure B.1.

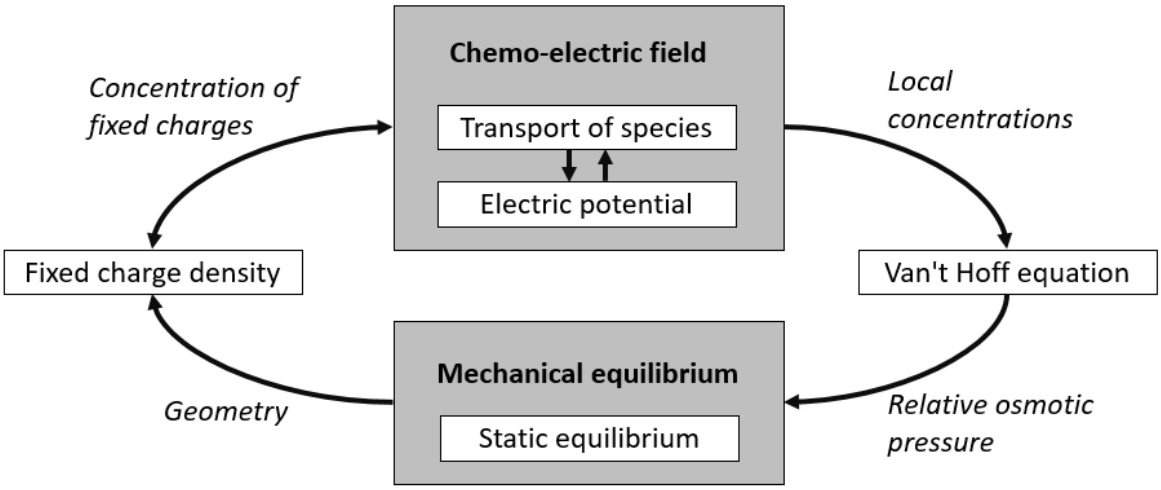

Figure B.1: Schematic overview of the electro-chemo-mechanical model

B.1.1. Dissociation of electrolyte groups

pH-responsive swelling begins when the concentration of H^+ ions[1]) exceeds the value given by the dissociation constant Ka, as described by equation 1.3:

$$K_a = \frac{[A^-][H^+]}{[HA]}$$

The conjugate bases A^- are bound to the hydrogel network, and are therefore referred to as fixed charges. If the pH and the Ka are known, the density of fixed charges inside the hydrogel can be calculated.

Density of fixed charges inside the hydrogel

The number of electrolyte groups in the gel in the initial (dry or unswollen) state N_{EL_0} is equal to the sum of the number of acid groups N_{HA} and the number of dissociated acid groups N_{A^-} at any degree of dissociation and state of swelling.

$$N_{EL_0} = N_{HA} + N_{A^-} \tag{B.1}$$

The number of groups or ions is equal to the concentration of groups times the volume.

$$c_{EL_0} V_0 = ([HA] + [A^-]) V_1 \tag{B.2}$$

Where V_0 is the initial volume of the gel and V_1 is the volume of the swollen gel. This can be rewritten to:

$$[HA] = c_{EL_0} \frac{V_0}{V_1} - [A^-] \tag{B.3}$$

Substituting equation B.3 into equation 1.3 leads to:

$$[A^-] = \frac{V_0}{V_1} \frac{K_a c_{EL_0}}{K_a + [H^+]} \tag{B.4}$$

The concentration of dissociated acid groups is the same as the concentration of fixed charges $[A^-] = c_f$. $\frac{V_0}{V_1}$ is replaced by $\frac{1}{H}$, with H local hydration state of the gel. This results in the equation for the concentration of fixed charge groups in hydrogel.

$$\mathbf{c_f = \frac{1}{H} \frac{K_a c_{EL_0}}{K_a + [H^+]}} \tag{B.5}$$

[1] $pH = -\log[H^+]$

Local hydration

The hydration of the gel is defined by Suthar [66] as the volume ratio of the deformed gel to the initial gel condition.

$$H = \frac{V_1}{V_0} \tag{B.6}$$

H can be determined using the Jacobian of the deformation gradient F. For the deformation of a volume element dV this is:

$$J = \det(F) = \frac{dV_1}{dV_0} \tag{B.7}$$

De et al. [16] use a different definition for H. They define H as the ratio of the volume of fluid to the volume of solid inside the gel.

$$H = \frac{V_1 - V_0}{V_0} \tag{B.8}$$

These two definitions of H are approximately equal if $V_1 \gg V_0$.

B.1.2. Electric field

The fixed charges in the hydrogel and other ionic species in the system contribute to and are affected by an electric potential field. The Poisson equation is used to find the electric potential ϕ for a charge distribution ρ_E.

Electric potential: Poisson equation

The Poisson equation applies if no time varying magnetic fields are present and only irrotational electric fields $\bar{E}$ are considered, so $\nabla \times \bar{E} = 0$ with $\bar{E} = -\nabla\phi$.

$$-\nabla \cdot \varepsilon \nabla\phi = \rho_E \tag{B.9}$$

Equation B.9 is valid for non-uniform electric permittivity ε. The electric permittivity is equal to the relative permitivity of the solvent times the permitivity of vaccuum ($\varepsilon = \varepsilon_s \varepsilon_0$). For uniform fluid properties, the Poisson equation becomes:

$$\nabla \cdot \nabla\phi = \frac{1}{-\varepsilon_s \varepsilon_0} \rho_E \tag{B.10}$$

The charge density of an electrolyte solution is equal to:

$$\rho_E = \sum_k c_k z_k F \tag{B.11}$$

Where the index *k = 1,2,3,...,n* represents the *n* ionic species present in the system, c_k the molar concentration of the *k*th species, z_k the valency of the *k*th species and F the Faraday constant. Similarly, the charge density of the fixed charge groups in the gel is:

$$\rho_E = c_f z_f F \tag{B.12}$$

By combining equations B.10, B.11 and B.12, the one-dimensional Poisson equation for the hydrogel system can be found:

$$\boldsymbol{\frac{\partial^2 \phi}{\partial x^2} = \frac{F}{-\varepsilon_s \varepsilon_0} \left(\sum_k c_k z_k + z_f c_f \right)} \tag{B.13}$$

B.1.3. Chemical field

Transport of species: Nernst-Planck equation

The Nernst-Planck equation describes the transport of a species k in the absence of chemical reactions. For the one-dimensional flux of a species k it reads:

$$J_k(x) = -D_k \frac{\partial c_k(x)}{\partial x} - \frac{z_k F}{RT} D_k c_k \frac{\partial \phi(x)}{\partial x} + c_k v(x) \tag{B.14}$$

The first term represents transport by diffusion, the second migration due to electric fields and the third by convection. D_k is the effective diffusivity of the kth ionic species, R the gas constant, T the temperature and $v(x)$ the fluid velocity.

In equilibrium there is no net transport of species. Furthermore, in the absence of convection the last term disappears. The Nernst-Planck equation becomes:

$$\boldsymbol{-D_k \frac{\partial c_k(x)}{\partial x} - \frac{z_k F}{RT} D_k c_k \frac{\partial \phi(x)}{\partial x} = 0} \tag{B.15}$$

Diffusivity: Einstein relation

The Einstein relation is used to find the effective diffusivity of charged particles. It is:

$$D = \frac{\mu k_B T}{q} \tag{B.16}$$

Using the Faraday constant which represents the charge of a mol of electrons $F = N_A q$, the Boltzmann constant can be written as:

$$k_B = \frac{R}{N_A} = \frac{Rq}{F} \tag{B.17}$$

Combining equations B.16 and B.17, the Einstein relation becomes:

$$\boldsymbol{D_k = \mu_k \frac{RT}{F}} \tag{B.18}$$

B.1.4. Mechanical equilibrium

Osmotic pressure: Van 't Hoff equation

The osmotic pressure Π is calculated using the Van't Hoff equation, which reads:

$$\Pi = i c_{\text{solutes}} RT \tag{B.19}$$

Where i is the dimensionless Van't Hoff index, an empirical constant related to the degree of dissociation of a solute. In this case, since the osmotic pressure is caused by ions which are already dissociated and do not dissociate further, i is assumed to be equal to one.

Swelling of the gel is caused by a difference in osmotic pressure between the environment inside the gel and the surrounding solution. This relative osmotic pressure is:

$$\boldsymbol{P_{\text{osmotic}} = RT \sum_k \left(c_k - c_k^o\right)} \tag{B.20}$$

Where c_k^o is the concentration of the kth ion in the stress-free state in the solution outside the gel.

Mechanical equilibrium equation

In static equilibrium and assuming there are no body forces, the gradient of the Cauchy stress-tensor $\bar{\bar{\sigma}}$ must be zero.

$$\nabla \bar{\bar{\sigma}} = 0 \tag{B.21}$$

The stress tensor in a porous solid has been defined by Biot [11] as

$$\bar{\bar{\sigma}} = \begin{Bmatrix} \sigma_{11} + \sigma_{\text{n}} & \sigma_{12} & \sigma_{13} \\ \sigma_{21} & \sigma_{22} + \sigma_{\text{n}} & \sigma_{23} \\ \sigma_{31} & \sigma_{32} & \sigma_{33} + \sigma_{\text{n}} \end{Bmatrix} \tag{B.22}$$

with symmetry $\sigma_{ij} = \sigma_{ji}$. σ_{n} represents the total normal tension stress applied to the faces a volume element. Thus in this case:

$$\sigma_{\mathrm{n}} = -P_{\mathrm{osmotic}} \tag{B.23}$$

Suthar and his colleagues then write the stress-tensor as [64, 66]:

$$\bar{\bar{\sigma}} = (C\bar{\bar{E}} - P_{\mathrm{osmotic}}I) \tag{B.24}$$

Where C is the fourth-order stiffness tensor and $\bar{\bar{E}}$ is the Green-Lagrange strain tensor. With this the mechanical equilibrium equation becomes:

$$\nabla(C\bar{\bar{E}} - P_{\mathrm{osmotic}}I) = 0 \tag{B.25}$$

For a one-dimensional case this equation is [37]:

$$\frac{\partial}{\partial x}\left((\lambda + 2\mu)\left(\frac{\partial u(x)}{\partial x} + \frac{1}{2}\left(\frac{\partial u(x)}{\partial x}\right)^2\right) - P_{\mathrm{osmotic}}\right) = 0 \tag{B.26}$$

Where λ and μ are the Lamé constants of C, which can be converted from the Young's modulus E and the Poisson's ratio ν using:

$$\lambda = \frac{\nu E}{(1+\nu)(1-2\nu)} \tag{B.27}$$

$$\mu = \frac{E}{2(1+\nu)} \tag{B.28}$$

B.2. Assumptions

Several assumptions are explicitly mentioned in discussions of the electro-chemo-mechanical model or follow implicitly from the theories that are used in the model. Knowledge of these assumptions is important to understand the applicability of the model and to interpret the results of simulations.

Dissociation of electrolyte groups

- In the model the dissociation occurs at the same pH for each electrolyte group in the gel network. However, as discussed in section 1.2.2, in reality the Ka of an individual electrolyte group depends on the dissociation of the surrounding electrolyte groups. This means that in practice two identical, neighbouring electrolyte groups can have different Ka. Thus the dissociation of the electrolyte groups, which drives the pH response, does not occur at a specific pH as described by equation B.5, but rather over a range of pH.

Mechanical equilibrium

- In the mechanical equilibrium as given by equation B.25, it is assumed there are no body forces. Thus stresses due to gravity and electrostatic interactions are not included in this equation.

- The van 't Hoff equation for osmotic pressure is based on ideal solutions (equation B.19). Thus it is assumed that the solute concentration is sufficiently low that the solution can be treated as an ideal solution. Furthermore, ion pairing occurs to some extent in all electrolyte solutions. This causes the measured van 't Hoff factor to be less than that predicted in an ideal solution.

- In this model, swelling of the gel is only driven by osmotic pressure and only counteracted by the elastic stiffness of the network. The effects of changes in the wettability of the gel network, as mentioned in section 1.2.1 are not included.
  As a consequence of this, when defining initial conditions, special attention will need to be paid to how the initial swelling of the gel is included in the model. Three states of the gel can be defined: the dry state, the initial state before swelling and a swollen state. Between the dry state to the initial state, the gel has already absorbed water due to the wettability of the gel network.

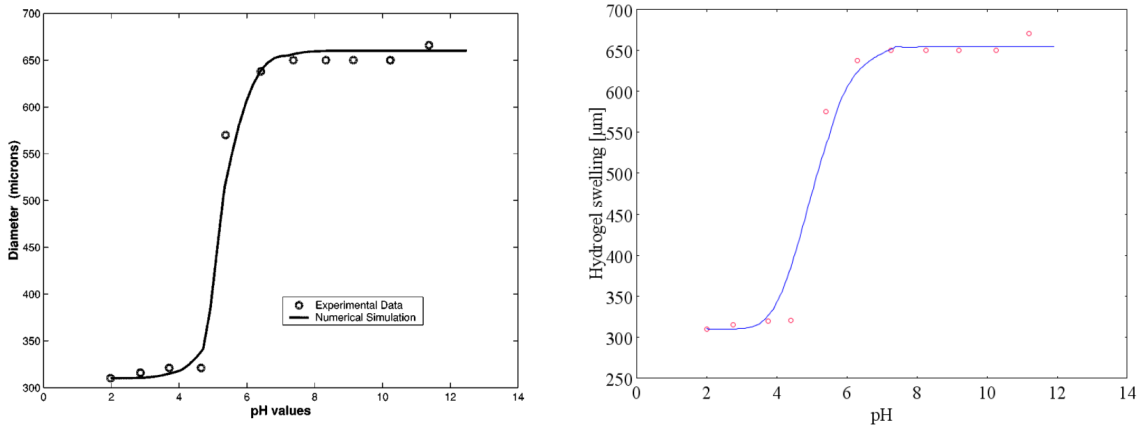

(a) Simulation by De et al. [16]

(b) Simulation by Suthar et al. [64]

Figure B.2: Equilibrium swelling of a 300 □m hydrogel disk. Simulated results versus the experimental results obtained by De et al. [16]. Graphs adapted from [16, 64]

Material

- The material properties of a hydrogel are dependent on the swelling ratio. For the fixed charge density this is included in the model through equation B.5. However also the mechanical properties of the material change with the swelling ratio. This dependency is usually included in the model through linear approximations of measured material behaviour [16, 26].

- The gel is assumed to be a homogeneous material. However hydrogels always exhibit an inhomogeneous cross-link density distribution [50]. The crosslinking density is an important factor that determines the mechanical properties of the material, thus these will also be inhomogeneous.

B.3. Validation

To validate their model, De et al. [16] fabricated cylindrical gel disks inside a micro-channel. The channel allows swelling of the disk in the radial direction but restricts expansion in the height direction. Equilibrium swelling experiments were performed for gels of different diameters: 300 □m, 400 □m, 500 □m and 700 □m for pH variations from 2 to 12.

In their theoretical model, De et al. [16] model the swelling and de-swelling of the hydrogel disks as a one-dimensional problem along the hydrogel's diameter. For the implementation they consider half of the gel diameter (from the centre to the edge), which is sufficient because of symmetry. On the gel-solution edge, they assume a linear variation for the fixed charge concentration, creating a thin boundary layer. De et al. [16] compare their simulations to experimental results for cylindrical gels with diameters of 300 □m, 400 □m, 500 □m and 700 □m for pH variations from 2 to 12. The simulations match closely with the experimental results.

Suthar et al. [64] model the gel disk in 2-D. For this they assume that the planar disc surfaces experience no shear at the interface. The gel disc is assumed to be rotationally symmetric in the xy plane and is therefore modelled with a single quadrant of a circle. The concentration difference at the gel-solution interface is represented by a Heaviside function profile. Suthar et al. [64] compare their simulation to the experimental results obtained by De et al. [16] for a 300 □m hydrogel cylinder. Both simulation and experimental results show a phase transition between the pH 4 and pH 7.

The results of the simulations by De et al. [16] and Suthar et al. [64] are compared to the experimental results obtained by De et al. [16] in figure B.2. Both simulations match the experimental results. However the simulations have slightly different results and the one by De et al. [16] seems to be a more successful match. This might be explained by their different definition of the gel hydration (equations B.6 and B.8) or the difference in the description of the fixed charge concentration at the gel-solution interface.

B.4. Discussion and conclusions

The electro-chemo-mechanical model is very accessible because it can be implemented in a commercially available software package, Comsol Multiphysics. The model can be used to find the stresses, geometry, potentials and concentrations in a system consisting of a hydrogel structure in a bath. It has been used and validated for 1D and 2D simulations of swelling disks and 3D simulations were successfully achieved using Comsol. Based on this, this model seems very suitable for use in this project.

The validation of the model shows a good agreement between simulation and experiments. However the model requires knowledge of the material properties. Material properties of hydrogels typically show great variations, because they are strongly affected by processing factors and composition. The material properties for the materials selected in section 1.3.3 can be found in literature, but a simulation would agree with new experiments more accurately if these properties were measured on the same material that is used in the experiments. However such measurements are not simple as they need to be done in a temperature and pH controlled liquid environment.

The model does not calculate the change in permeability of the hydrogel network that can result from swelling of the hydrogel, as discussed in section 1.1.2. Since the model only concerns static equilibria, the effect of permeability on transport rates is not relevant for the results of the simulations. However, to investigate the effect of swelling of a hydrogel membrane on transport through not only pores in the membrane but also the hydrogel network itself, as shown in figure 1.1, this model is not sufficient.

The model calculates local concentrations and potentials in a hydrogel structure and the surrounding bath. However if this information is not needed, the model could be simplified by imposing a (local) osmotic pressure and only using the mechanical equilibrium equation to find the resulting hydrogel geometry. The coupling between the chemo-electic field and the mechanical equilibrium equation is then lost and the model becomes a purely mechanical problem.

C

Methods

Contents

C.1. UV-curable precursor for pH-responsive polymer hydrogels

Recipe for a liquid, UV-curable, precursor that is used to make cross-linked polymer hydrogels with pH-responsive swelling properties. This recipe was previously described by Liu et al. [39] and Johnson et al. [32]. The precursor solidifies upon irradiation with UV-light, by polymerization and cross-linking through free-radial polymerization reactions. In this it is similar to a negative photo-resist.

Materials

- Chemicals (see table C.1)
- For metering: pipettes (with disposable tips), scale, weighing paper or cup, spatula
- Sonicating bath
- For storage: amber glass bottle and refrigerator
- For rinsing tools: ethanol, soap and water

Compound name	Abbreviation	CAS-No.	wt% (of total)	Amount to make approximately 10 ml
2-Hydroxyethyl methacrylate	HEMA	868-77-9	84.5	8.248 ml
Acrylic acid	AAc	79-10-7	11.7	1.166 ml
Ethylene glycol dimethacrylate	EGDMA	97-90-5	1.0	0.096 ml
2,2-Dimethoxy-2- phenylacetophenone	DMPA	24650-42-8	2.9	0.3193 g

Table C.1: Components of UV-curable precursor for pH-responsive polymer hydrogels.
All chemicals were purchased at Sigma-Aldrich. An inhibitor (4-Methoxyphenol (MEHQ)) was present in the liquid components: 200 ppm in AAc, 250 ppm in HEMA and 90-110 ppm in EGDMA.
Function of each component: HEMA, main component, its crosslinked polymer has hydrogelling behaviour. AAc, electrolyte, creates ph-responsive behaviour. EGDMA, crosslinking agent. DMPA, photo-initiator.

Method

1) Measure components and add to the bottle:
First combine HEMA and AAc in 4:1 mol ratio, then add 1wt % EGDMA and 3 wt % DMPA.
2) Sonicate untill all DMPA crystals are dissolved, approximatly 20 minutes.
3) Store under refrigeration (2-8C), in an amber bottle.

Comments

- The appearance of the final result is a clear, colourless or slightly yellow tinted liquid.
- Dissolving the DMPA crystals may take some time. It can help to leave the bottle overnight to let them dissolve.
- In the articles cited above [32, 39], the chemicals were vacuum-distilled prior to use, most likely to remove the inhibitor. Here this step is skipped, however no significant effects on the result were noticed.

C.2. Fast and low-cost manufacturing of film masks for photolithography

Method for manufacturing film masks for photolithography. This method was inspired by Beebe et al. [8] and previously described by Qin et al. [56].

The masks were designed in freely available Inkscape software and consist of black figures on a white background. Where there is a black figure, the mask will be opaque. It was found that to sufficiently block out the light, two mask layers were needed. Plus sign- shaped symbols were added to all four corners of a mask to facilitate alignment. The designs were saved in pdf format (without rasterization). For the mask designs, see appendix D.

Materials

- PDF files containing 2x the mask design; one as is, one mirrored.
- Transparencies (overhead projector sheets) that are suitable for the printer that is used
- Printer (laser or inkjet, see comments)
- Scissors
- Adhesive tape
- Latex/nitrile gloves

Method

1) Print the two images of the design on the transparencies (in black ink)
2) Cut out both images, leaving a larger margin on one to facilitate taping them together
3) Stack the two prints, with the sides that have ink on them touching, so that they end up on the ”inside” of the mask. Place the piece with the piece with the smaller margin on top of the other one.
4) Manually move the two layers with respect to each other until the features are aligned.
5) Attach the two sides of the mask together using tape; Place a small piece of tape over the two masks, so that half of it is on the top part and half of it is on the larger margin of the bottom part. Do this at two points. Do not fold the tape around the edge.

Comments

- Take care not to get dirt on the masks and wear gloves when assembling and handling the masks to prevent leaving fingerprints. Contamination of the mask can affect its performance.
- A downside of this method is that the mask material is not very durable nor is it resistant to aggressive cleaning.
- It was observed that the two layers of the mask seem to fuse together when exposed to heat and pressure.
- We used a 1200 x 1200 dpi laserprinter (at CSinBKCity, Julianalaan 134, Delft, www.csinbkcity.nl). However in hindsight, an inkjet printer might be more suitable and could eliminate the need for 2 mask layers. The reason for this is that laser printers use toner, which is dry ink powder. This causes the printed areas to be filled with very small pinholes. Inkjet ink is liquid, so it flows to make a solidly opaque feature.
- The minimum feature size that can be achieved with this method depends, among other things, on the resolution of the printer that is used [42]. The minimum feature size achievable with commercially available printers is somewhere between 10 and 50 um. Specialized film-mask manufacturers can produce feature sizes down to 5 um. Here a 1200x1200 dpi printer was used, which means that it can print dots that are about 21 um in size, which will allow reliable printing of 100 um features.

C.3. Disk and membrane manufacturing

The disks and membranes were manufactured using very similar approaches. Disks and membranes were both cured inside a microchannel consisting of a Polydimethylsiloxane (PDMS) bottom, shown in figure C.1, which was closed with a 0.17 mm thick borosilicate glass slide. The main difference between the two approaches was that for the disks, the glass slide was permanently bonded to the PDMS bottom, whereas for the membranes it was not. Therefore after curing the disks remain inside the PDMS-glass microchannel, whereas the membranes are removed from this encasing. Below the processes to manufacture both disks and membranes are described in detail.

C.3.1. Disk and membrane; Preparation

PDMS bottom

The disk and membrane manufacturing processes both start with the same PDMS bottom piece. This is shown in figure C.1. More details on its design can be found in appendix D. The PDMS bottom was made by casting PDMS in a 3D printed mold. This mold was manufactured on a desktop stereolithography system with 30 um lateral and 25 um vertical resolution (Envisiontec Micro Plus HD, material: HTM 140 V2). Before use the PDMS bottom is rinsed first in ethanol and then in DI water.

Channel holder and lid

The disk and membrane manufacturing processes use the same channel holder and lid. These serve to block light from unwanted directions during curing. The lid also helps to align the mask and clamp it to the sample. The channel holder and lid were printed on the same Envisiontech 3D printer as the mold, using lower resolution settings. Their designs are given in appendix D. The channel holder is attached to the bottom of a 100 mm upside down Petri dish, which helps to align it to the centre of the Light curing unit (figure C.4).

Caps

For disk manufacturing, opening are made in the PDMS bottom. Through these the channel can be filled after the PDMS is bonded to the glass coverslip. To close these openings, custom caps were designed (appendix D) and printed on the Envisiontech 3D printer, at the highest resolution settings.

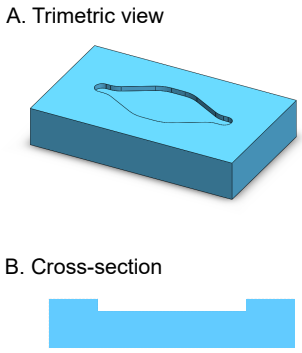

Figure C.1: PDMS bottom piece for disk and membrane curing. The slot is 180 um deep and 6 mm wide (see appendix D). The dimensions in this image are not to scale.

C.3.2. Disk; Pre-curing

Materials

- PDMS bottom
- Glass cover-slip (size: larger than the PDMS bottom, thickness = 0.17 mm)
- 2 blunt needles, sizes 1.3 mm outer diameter (o.d.) (TE Needle 18GA 1/2 Green) and 0.75 mm o.d. (TE Needle GA 1/2 Blue)
- Plasma machine
- Syringe with 0.75 mm o.d. blunt needle
- Precursor

- Channel-holder
- Caps

Method

1) Use the largest of the two blunt needles to punch two holes through the PDMS bottom, one at each end of the channel. Then use the smaller needle to push any remaining PDMS scraps out of each hole. (Figure C.2 B.)
2) Use air plasma treatment to bond the PDMS bottom to a glass coverslip. See appendix C.4 for method.
3) Use the syringe to fill the channel with precursor, close with caps. (Figure C.2 E. and F.)
4) Place the channel into the holder. (Figure C.2 G.)

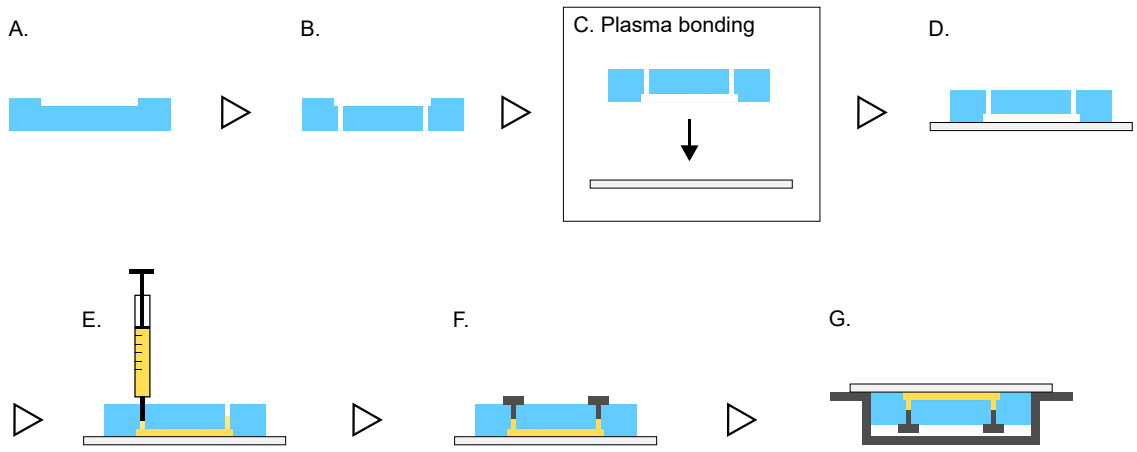

Figure C.2: Disk manufacturing, diagram of pre-curing steps.
The channel holder was attached to a Petri dish, this is only shown in figure C.4 A., not here.

C.3.3. Membrane; Pre-curing

Materials

- PDMS bottom
- PDMS fill pieces (Thin, flat pieces of PDMS, made by casting PDMS in a petri dish and cutting out pieces of the right size.)
- Glass cover-slip (size: larger than the PDMS bottom, thickness = 0.17 mm)
- (Disposable) glass pipette
- Precursor
- Channel-holder

Method

1) Stack PDMS fill pieces inside channel holder and place PDMS bottom on top of stack. The height should be such that the PDMS bottom sticks slightly (approximately 1 mm) out of the channel holder. (Figure C.3 B.)
2) Deposit 1 drop of precursor in the centre of the channel in the PDMS bottom. (Figure C.3 C.)
3) Place the glass coverslip on top of the channel. Do this by first touching one edge to the holder and then gently decreasing the angle between the slip and the holder, thereby lowering the slip until it is flat. (Figure C.3 D. and E.)

C.3.4. Disk and membrane; Curing

Materials

- Channel holder with contents, assembled as described above. As is shown in figure C.4 A., the channel holder is attached to the bottom of an upside-down Petri dish, which helps to align it to the

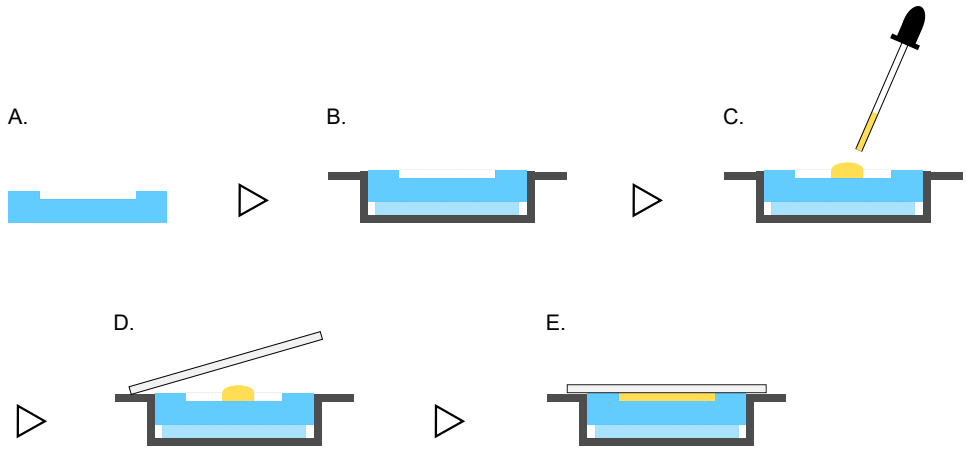

Figure C.3: Disk manufacturing, diagram of pre-curing steps.
The channel holder was attached to a Petri dish, this is only shown in figure C.4 A., not here.

centre of the Light curing unit.
- Lid
- Film mask (appendix C.2).
- Adhesive tape
- Small pegs (like the type used to hang cards)
- UV light source with built in timer (Light curing unit, Photopol A5460(B)).

Method
1) Attach the mask to the lid using adhesive tape.
2) Place the lid on top of the channel holder, so that the mask is in contact with the glass coverslip. (Figure C.4 B.)
3) Use the pegs to clamp the lid to the channel holder, take care to do this evenly. (Figure C.4 C.)
4) Place the channel holder in the centre of the rotating plate inside the Light curing unit and close the door. (Figure C.4 D.)
5) Select the light source (spots only), set the curing time and start the curing process.

Comments
- The UV spots had different light spectra from 320 to 550 nm.
- Curing times were optimized for the mask design, by testing times between 100 and 170 s for the disks and 60 and 100 s for the membranes. More details about this can be found in appendix A.

C.3.5. Disk; Post-curing

Materials
- 2 syringes with 0.75 o.d. blunt needles
- DI water
- Ethanol
- Waste beaker

Method
1) Remove the pegs and take the channel out of the holder
2) Remove caps.
3) Blow non-cured precursor out of channel and into the waste beaker, using a syringe filled with air.
4) Flush the channel (above the waste beaker) using a syringe filled with ethanol (approximately 6 ml.).
5) Blow ethanol out of channel and into waste beaker, using a syringe filled with air.
6) Flush the channel (above the waste beaker) using a syringe filled with DI water (approximately 6 ml.).

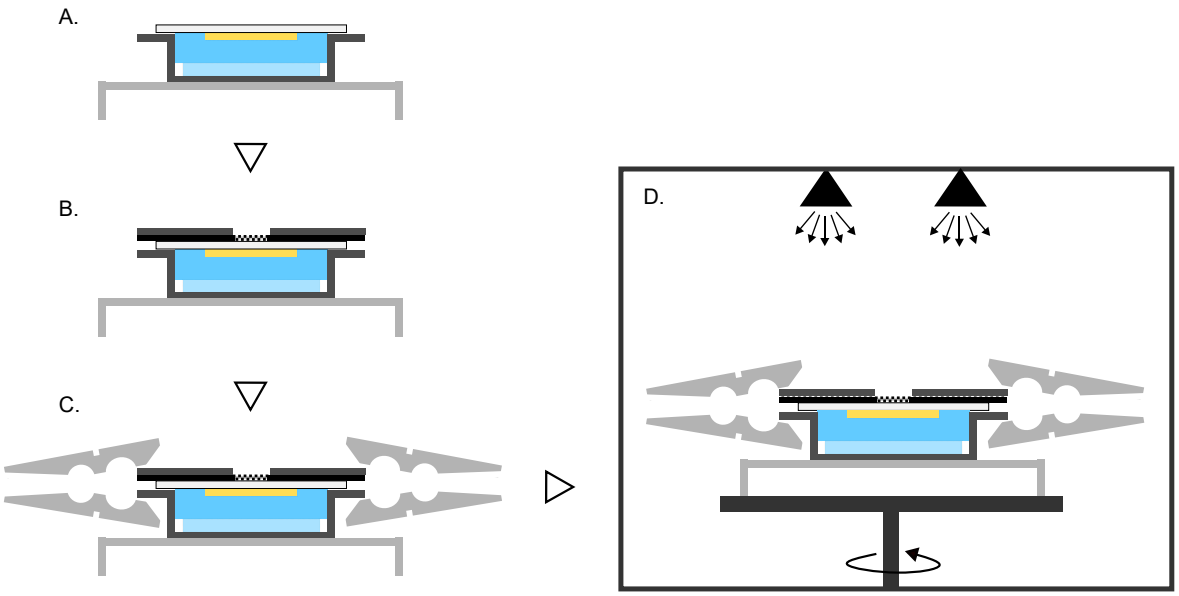

Figure C.4: Disk and membrane manufacturing, diagram of curing steps.

7) Leave the channel filled with DI water and close with the (cleaned) caps.
8) Leave disks to swell in DI water overnight.

Comments
- Use different syringes for ethanol and DI and clean the needles in between steps, to prevent injection of precursor residue back into the channel.
- If any poly(acrylic acid) is left in the system, this can form a gel and block channels when it comes into contact with water. Flooding the system with excess sodium (e.g. a high molarity solution of sodiumchloride) can break bonds in this gel and help unclog the system.

C.3.6. Membrane; Post-curing

Materials
- Small beaker with ethanol
- Small beaker with DI water
- Compressed air source
- Small Petri dish with DI water
- Eppendorf tube (with cap)
- Tweezers (with plastic tips)

Method
1) Remove the pegs and lift the lid and mask off the channel
2) Peel the glass slide off the PDMS, the membrane is attached to the glass slide
3) Use tweezers to pick up the glass slide
4) Submerge the glass slide in the beaker with ethanol, and make a flapping motion, for 10 s
5) Submerge the glass slide in the beaker with DI water, and make a flapping motion, for 10 s
6) Use the dry air to blow off the remaining liquid
7) Let the slide with the membrane dry to the air, after this it can be imaged.

To remove the membrane from the glass slide:
8) Submerge the glass slide with the membrane in a Petri dish with DI water
9) Leave to swell overnight, this releases the membrane from the glass slide
10) The membrane can be removed using tweezers, and placed in a Eppendorf tube filled with DI water or a buffer solution.

Comments
- To get a better grip on the glass slides, it helps to wrap the tips of the tweezers in Parafilm.
- If in step 2) the glass slide is stuck to the PDMS bottom, it helps to take the two out of the channel holder, flip them upside down, and peel the PDMS off of the glass. This is easier because the PSMS is flexible and does not break as easily as the glass.

C.4. PDMS-glass bonding using air plasma

The protocol, as was developed in this project and has been uploaded unto the Polymer Micro and Nano Manufacturing group folder, is included below.

Protocol: PDMS-glass bonding using air plasma

Author: Sophie Soons, last edited: 22/02/2018

Plasma machine: Diener Femto plasma cleaner, in MNE lab, main room (F-0-310), https://mnelab.3me.tudelft.nl/equipment/details/6

Note:

1. It is important not to alter the settings of the flow meters that are on the front of the machine.
2. It is advisable to always test bonding on a scrap of PDMS from the same fabrication batch as your sample, before bonding the actual sample.

Sample preparation

Glass:

- Clean with IPA
- Dry using air gun
- Only handle with clean gloves or tweezers

PDMS:

Cleaning is more difficult so it is easier to take care during the PDMS preparation to avoid contamination, so that cleaning is not needed.

- Make sure molds are clean
- Keep molds and PDMS in clean, closed containers at all times (also during baking)
- Remove any dirt particles using tweezers
- Only handle with clean gloves or tweezers

If this does not give good enough results, try this cleaning protocol:

1. 10 min sonication in ethanol
2. Rinse 2x in DI water
3. Dry using air (N2) gun

Switch on machine

1. Turn power switch on
2. Vent until chamber door can be opened
3. If necessary, clean chamber and tray with a cleanroom-wipe with some IPA

Bonding

1. Load samples:
   Place PDMA samples and glass slides on the tray, surfaces that will be bonded facing upwards. Place tray in plasma chamber.

2. Close door and pump down chamber until the timer turns on. This happens when the pressure reaches about 0.28 mbar. *(press pump, press start)*

3. Set power and time (**40 W**, **1 min**)

4. Bring the plasma chamber to the right pressure:

   To increase pressure in chamber, turn on gas 2 (which is just air) on and quickly turn it off again, so that the pressure is around 3 mbar. *(press gas 2, press gas 2 again)*

5. Switch off the pump (*press pump).*

6. Start plasma treatment:
   Switch on the power. *(press generator)*

   The timer and the generator will automatically switch off when the pressure in the chamber becomes more than 4 mbar. So keep an eye on the pressure and if necessary, use the pump to lower it.

7. As soon as the set time is over, the plasma generation stops automatically.
   Now *press stop, press generator and press vent.* Vent until the door can be opened.

8. Quickly take the tray with the samples from the machine and assemble:
   Bring surfaces together
   Apply gentle, uniform pressure for 10 s. High pressures are not needed and might cause channels to collapse.
   Use a rolling motion when bringing surfaces together to prevent trapping air bubbles.
   Do not move around surfaces after they have first touched.

9. Leave at room temperature for about 15 min. before putting force on the bond.

Switch off machine

10. Place tray back in chamber
11. Close door and pump down until pressure is below 0.2 mbar
12. Switch of pump
13. Switch of machine

Comments

The protocol was developed with the help of Bhattacharya's thesis [10], which investigates how different process parameters affect the quality of the PDMS-glass bond.

C.5. Buffer solutions

A buffer is a solution that can maintain a constant pH. If an acid or base is added to a buffer solution, or it is diluted, the buffer can resist the change in pH to a certain extent. The buffer capacity is a measure of the extent to which a buffer can resist change in pH. A (simple) buffer is usually a solution of a weak acid and (a salt of) its conjugate base. The pH of the buffer can be within one pH unit of the dissociation constant (pKa) of the acid-conjugate base dissociation equilibrium.

To make buffers with a wider range of pH, while keeping the other components of the solution as similar as possible, we used phosphate buffers. Phosphoric acid has three acidic protons, with dissociation constants 2.16, 7.21 and 12.32. [38]. It can be used to create buffers with pH near each of these pKa. The dissociation reactions of phosphoric acid are:

$$\mathrm{H_3PO_4} \rightleftharpoons \mathrm{H_2PO_4^-} + \mathrm{H^+} \qquad \mathrm{pK_a} = 2.16 \tag{C.1}$$

$$\mathrm{H_2PO_4^-} \rightleftharpoons \mathrm{HPO_4^{2-}} + \mathrm{H^+} \qquad \mathrm{pK_a} = 7.21 \tag{C.2}$$

$$\mathrm{HPO_4^{2-}} \rightleftharpoons \mathrm{PO_4^{3-}} + \mathrm{H^+} \qquad \mathrm{pK_a} = 12.32 \tag{C.3}$$

Calculation of components

To calculate the components of a buffer:
1) Decide which weak acid-conjucate base pair you will use and find its pKa.
2) Decide the desired pH. The pH we used are listed in table C.3
3) Decide the desired molarity. We chose $\mathrm{M_{buffer}} = 0.1\mathrm{mol/l}$.
4) For a weak acid with dissociation reaction:

$$\mathrm{HA_{(aq)}} \rightleftharpoons \mathrm{A^-} + \mathrm{H^+} \tag{C.4}$$

The Henderson-Hasselbalch equation gives ratio of $\mathrm{A^-}$ to HA:

$$\mathrm{pH} = \mathrm{pK_a} + \log \frac{[\mathrm{A^-}]}{[\mathrm{HA}]} \tag{C.5}$$

Where [X] indicates the concentration of X.
Then the concentrations can be found using:

$$\mathrm{M_{buffer}} = [\mathrm{HA}] + [\mathrm{A^-}] \tag{C.6}$$

Materials

- Chemicals (see table C.2 and table C.3)
- DI water
- pH meter and corresponding pH probe and storage solution (Hanna Instruments 5522-2)
- Magnetic stirrer
- Scale
- Weighing cups
- Graduated cylinder
- Beakers
- Bottles for storage

Compound name	Abbreviation	CAS-No.
Sodium phosphate monobasic	NaH_2PO_4	13472-35-0
Sodium phosphate dibasic	Na_2HPO_4	7558-79-4
Hydrochloric acid	HCl	7647-01-0
Sodum hydroxide	NaOH	1310-73-2
Sodium chloride	NaCl	7647-14-5

Table C.2: Components of buffer solutions.

pH	Mol per litre of buffer solution					Mass (g) per 100 ml of buffer solution				
	NaH_2PO_4	HCl	Na_2HPO_4	NaOH	NaCl	NaH_2PO_4	HCl	Na_2HPO_4	NaOH	NaCl
1.6	0.1000	0.0784			0.0216	1.5601	0.2859			0.1262
2.5	0.1000	0.0314			0.0686	1.5601	0.1144			0.4011
3.5	0.1000	0.0044			0.0956	1.5601	0.0159			0.5589
5.0	0.0994		0.0006		0.1000	1.5505		0.0087		0.5844
6.1	0.0928		0.0072		0.1000	1.4477		0.1023		0.5844
7.1	0.0563		0.0437		0.1000	0.8783		0.6204		0.5844
8.2	0.0093		0.0907		0.1000	0.1448		1.2878		0.5844
12.2			0.1000	0.0431	0.1000			1.4196	0.1725	0.5844

Table C.3: Components of buffer solutions: Required amounts, as calculated.
Combining NaH_2PO_4 and HCl is analogous to adding NaCl. Therefore different amounts of NaCl are added to each buffer, so that the concentration of NaCl in each buffer becomes 0.1 mol/l.

Method

To prepare 100 ml of a buffer solution:
1) Measure 100 ml of DI water
2) Pour most but not all (about 80 ml) of the water into a beaker with a magnetic stirrer.
3) Submerge the pH probe in the solution
4) Measure all components in separate (labeled) cups
5) Add the NaCl
6) Add one of the other components: Begin with the weak acid or base. If both remaining components are weak, begin with the one that is most difficult to dose, e.g. because it needs the smallest amount, is difficult to dissolve or comes in large grains.
7) Wait until everything is dissolved
8) Add a little bit of the other component, wait for it to dissolve and wait for the pH to stabilize. Repeat untill the desired pH is reached.
9) Add some of remaining DI water to bring the volume up to 100 ml. (This may not require all of the remaining water, because the other components also add volume.)

Comments

- Before using it, check the calibration of the pH meter and recalibrate if necessary. - The required amounts, as given in table C.3, are very small for some buffers. It is difficult to measure this accurately enough. An alternative would be to make a more concentrated buffer and dilute this as needed. - Dissolving the different components (especially sodiumphosphate dibasic) and waiting for the pH to stabilize takes time. It could be better to first dissolve the different components separately, at known concentrations, and then adding these solutions to the buffer. This could also help making the measured amounts more accurate. - The buffers are adjusted until the right pH is reached. The final molarity is not checked, so this could diverge from the intended value.

C.6. Image analysis

C.6.1. Disk area

Image analysis method to measure disk area on image taken with optical microscope. This method was used for all disk measurements, except for the disk diameter measurements that were used to find the optimal curing time for the disks. These are the measurements plotted in figures A.1, A.6 and A.3. The image analysis method uses free ImageJ (also named Fiji) software.

Method

1) Open image in ImageJ
2) Set scale (and make global).
3) Transform image to greyscale (Image>Type>8-bit). (Figure C.5 B.)
4) Threshold to create binary image (Image>Adjust>Threshold) (Figure C.5 C.)
5) Check binary image for gaps in the outline of the disk or bridges between the disk and surrounding areas. Manually correct these using the pencil or paintbrush tool (Figure C.5 Ci. and Di.). If multiple concentric disk outlines are visible, use the outermost outline.
6) Measure area using the analyze particles function (Analyze>Analyze particles). Select Show: Bare outlines. And use the image of the outlines to check if the measurement was correct. (Figure C.5 E.)

Comments

- The appearance of the image and thus the required threshold (step 4) depend on the brightness of the image. This is influenced by the sample itself, the objective, lighting and microscope software settings. Therefore the same lighting, software settings and threshold value were used as much as possible.
- Also all images were taken using the same objective and processed using the same scale settings. Therefore any error in the scale setting is the same for all measurements.
- Where possible, Batch processing Macro's were written and used to speed up the analysis process.

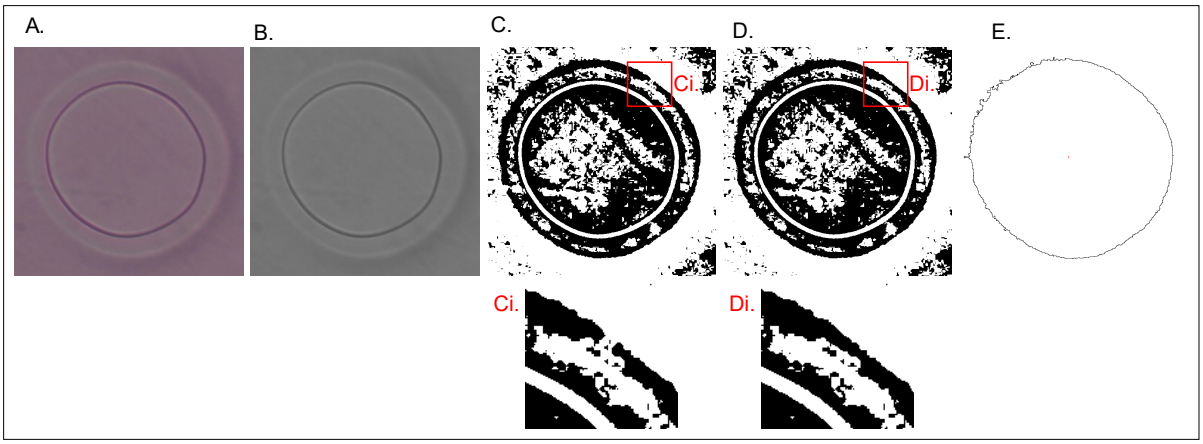

Figure C.5: Illustration of method to measure disk area using image analysis in ImageJ.
A. Original image. B. Greyscale image. C. Binary image Ci. Section of C. showing a gap in the disk outline, that needs correction. D. Binary image with manually executed corrections. Di. Section of D. showing the same area as Ci., after correction. E. Outline of the measured disk area.

C.6.2. Disk diameter - simpler method

Image analysis method to measure disk diameter on image taken with optical microscope. The method uses the built in 3-point circle measurement tool of a Motic microscope. This method was only applied for the disk diameter measurements that were used to find the optimal curing time for the disks. These are the measurements plotted in figures A.1, A.6 and A.3.

With (overly) long curing times, disks were found to develop star-like spikes. This makes measurement of the diameters of the outer border and inner ring more difficult. The following workaround is used:

For round disk:

Outer border: Measurement circle touches border at three points, that are spread out over circumference, and encloses the border.
Inner ring: Measurement circle touches ring at three points, that are spread out over circumference, and encloses the ring.

For disk with star-like spikes (occurs when curing time is too high):
Outer border: Measurement circle touches border at three points (at the tips of spikes), that are spread out over circumference, and encloses the border, including the spikes.
Inner ring: Measurement circle touches ring at three points, that are spread out over circumference. These points are located at the bottom of the valleys between spikes. The measurement circle encloses all (lowest points of) the valleys, but does not encircle all spikes.

Method
1) Open the image in 'Motic Images Plus 2.0' software
2) Set the scale, by selecting the objective with which the image was taken.
3) Select the three point measurement tool, which lets you define a circle by selecting three points that are located on the circle.
4) Use this tool to draw circles around the inner ring and outer border, following the rules described above. The software returns the size of the circles.

Comments
This method is faster than the above method to measure the disk area, but it is less accurate, because most disks are not perfectly circular.

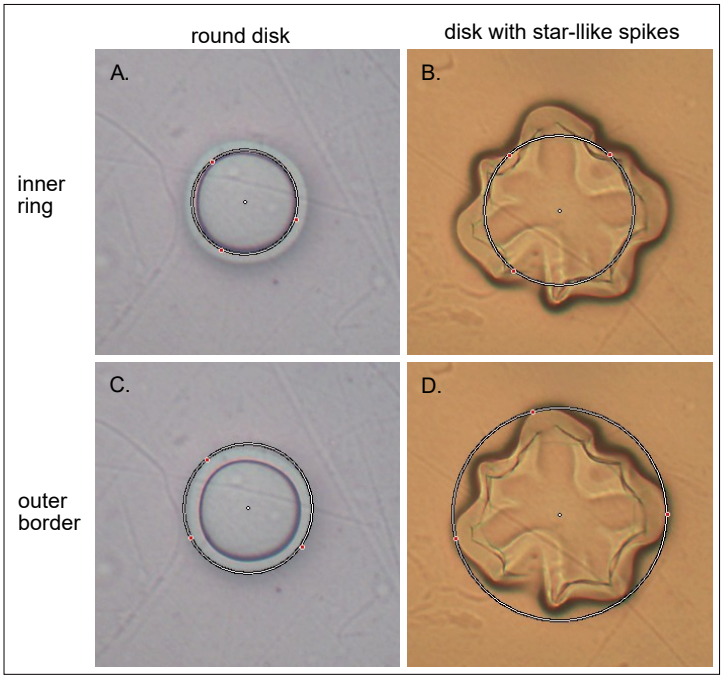

Figure C.6: Illustration of method to measure disk size using Motic software.

C.6.3. Membrane pore area

Image analysis method to measure pore area on image taken with optical microscope. The image analysis method uses free ImageJ (also named Fiji) software. Membranes were always imaged from the same side, which is facilitated by the the asymmetric membrane design. The same pore, in the centre of the membrane, was measured on all membranes (figure C.7 A.).

Method
1) Open image in ImageJ
2) Set scale (and make global).
3) If necessary enhance contrast to improve visibility of the pore.
4) Select the area inside the pore using the ”Selection brush tool”. Use the innermost outline of the pore (figure C.7 C.). To make it easier to make an accurate selection, adjust the brush size and the cursor speed.
5) Measure the area of the selected region (Analyze>Measure).
Alternatively: convert the selection to a binary image, as shown in figure C.7 D. (Edit>Selection>Create Mask) and use the Analyze particles function to measure the area.

Comments
- All images were taken using the same objective and processed using the same scale settings.

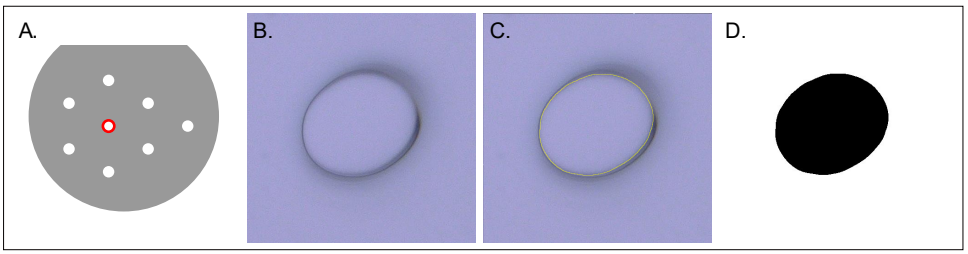

Figure C.7: Illustration of method to measure pore area using image analysis in ImageJ.
A. Schematic indicating the position of the central pore, which was used for the pore size measurements on each membrane. B. Original pore image C. Pore image on which the area inside the pore is selected using the ”Selection brush tool”. D. Binary image showing the selected pore area.

C.6.4. Membrane pitch

Image analysis method to measure pitch on image taken with optical microscope. The method uses the built in software of a Keyence VHX microscope. Membranes were always imaged from the same side, which is facilitated by the the asymmetric membrane design. On all membranes the same two pores were used for this measurement, as indicated in figure C.8 A.

Method
1) Open the image in the VHX-6000 Communication software
2) Select Measure/Comment
3) Zoom in to the pores of interest
4) Use the ”2 Centres” tool to measure the pitch. This tool lets you define two circles by selecting three points per circle that are located on the circle (figure B.). It then draws these two circles on the image and returns the distance between the centres of these two circles (figure C.).

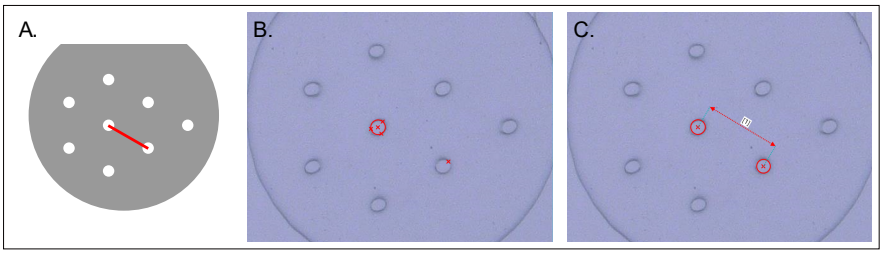

Figure C.8: Illustration of method to measure pitch.
A. Schematic indicating the position of the two pores that were used for the pitch measurement on each membrane. Images B. and C. Illustrate how the ”2 Centres” tool is used to measure the pitch.

D

Designs

Contents

D.1. Disk masks

A. Mask design to create three disks.
B. Mask design to create one disk.

The + signs in the corners of the masks are used to align the two mask layers. The white bar can be written on to label the mask.

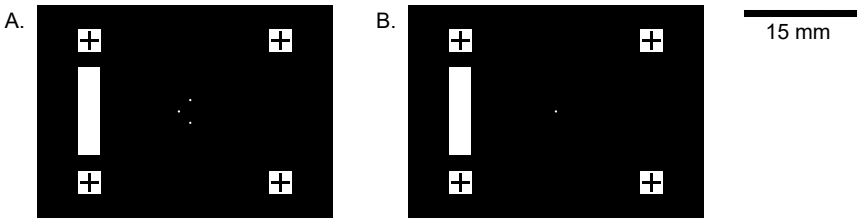

D.2. Membrane masks

A. Mask for membrane with no pores.
B. Masks for membranes with varying pitch.
C. Masks for membranes with varying pore diameter.

Each mask has a label at the bottom to identify the mask design. The first number is the pore diameter in micron, the second number is the pitch, as a function of the pore diameter. The + signs in the corners of the masks are used to align the two mask layers. The white bar at the top is placed to help recognize the orientation of the mask. The dotted circle is used to align the mask with respect to the lid of the channel holder.

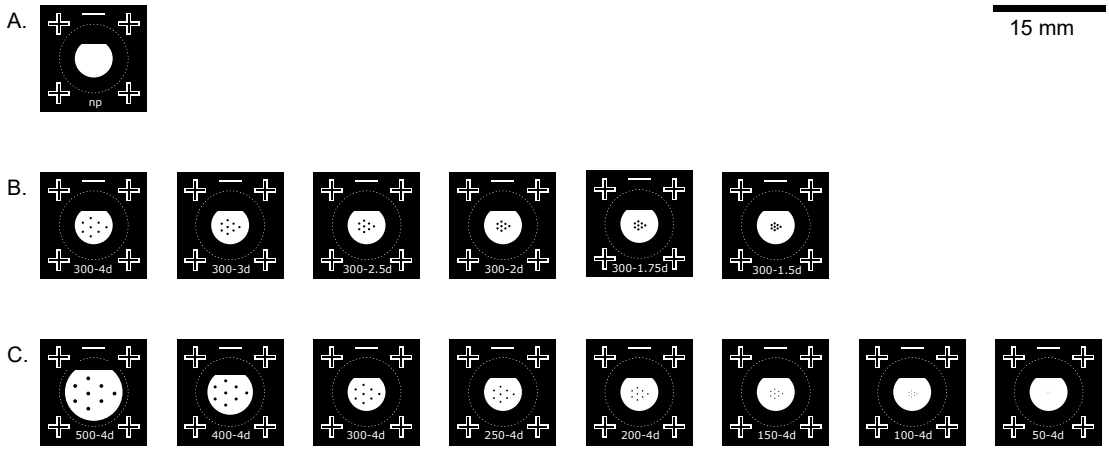

D.3. Mold for PDMS bottom piece

Purpose: Mold used for PDMS replication to make the PDMS bottom piece that is used in disk and membrane manufacturing.

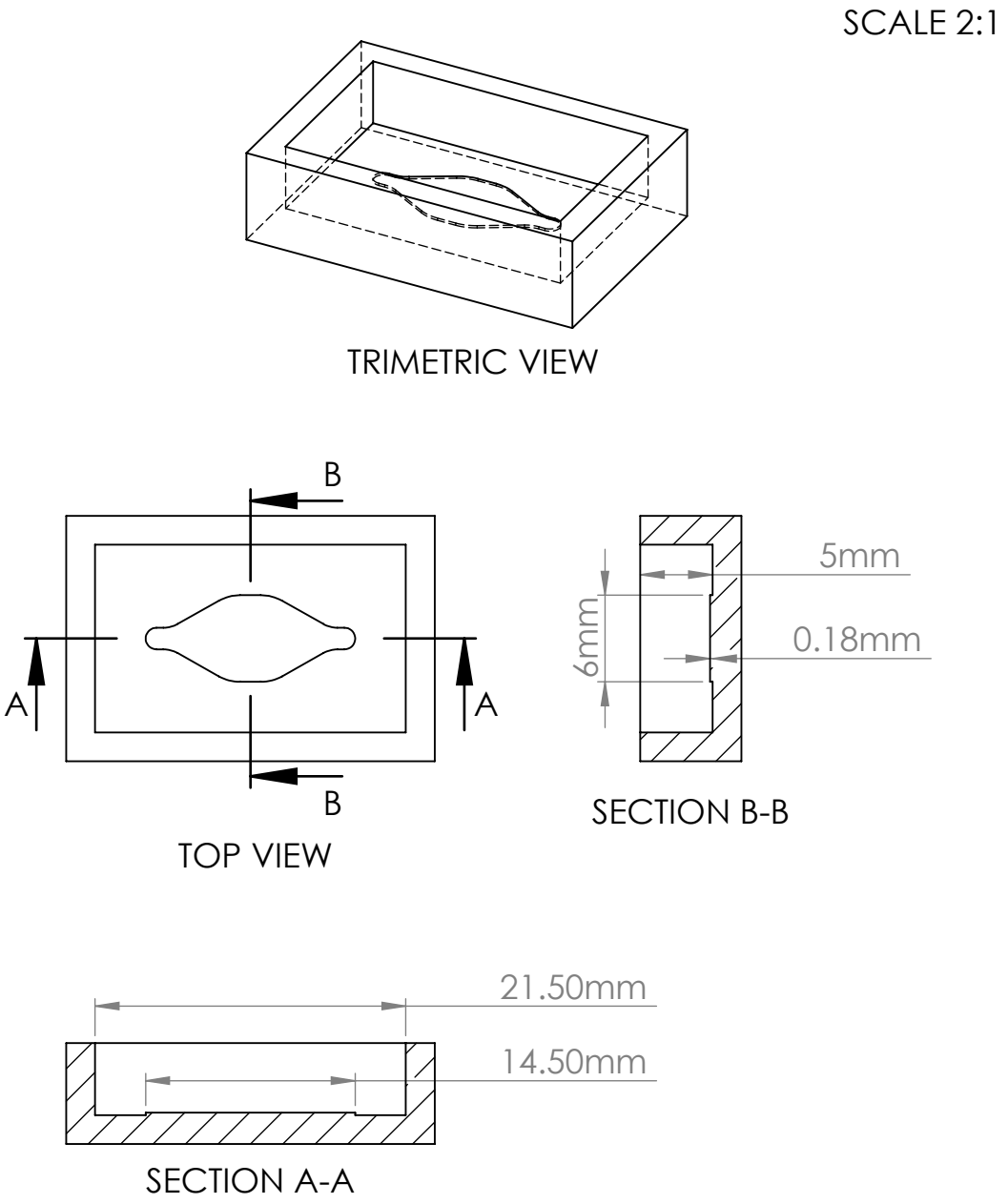

D.4. Cap

Purpose: To close off the the openings through the PDMS through which a microchannel can be accessed.

SCALE 10:1

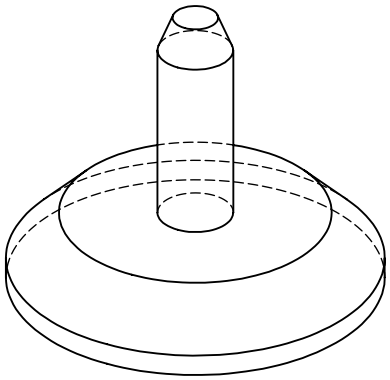

TRIMETRIC VIEW

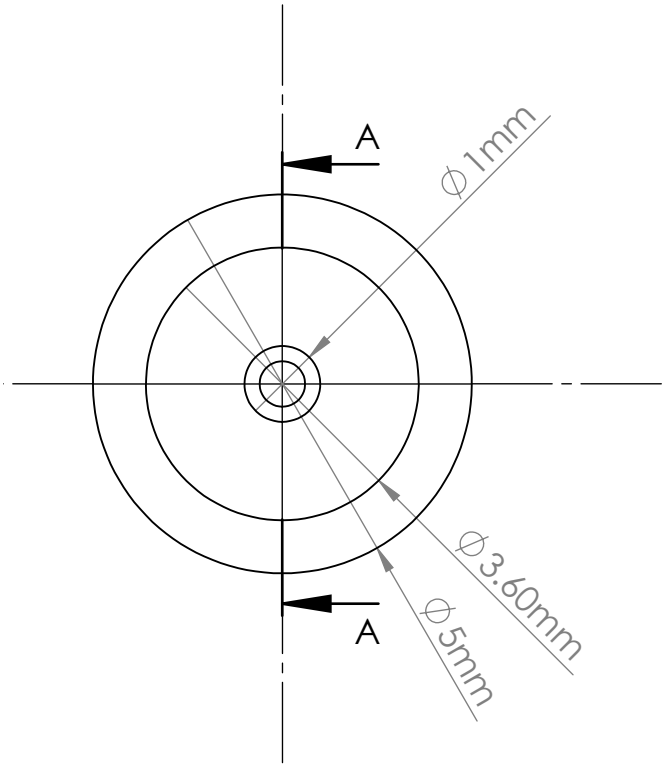

TOP VIEW

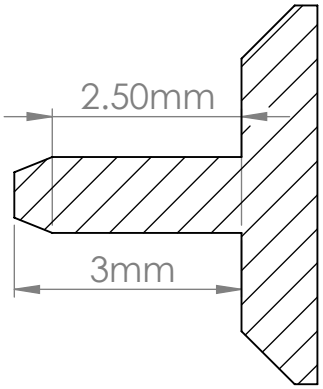

SECTION A-A

D.5. Channel holder (for curing process)

Purpose: To block unwanted light during curing.

SCALE 1:1

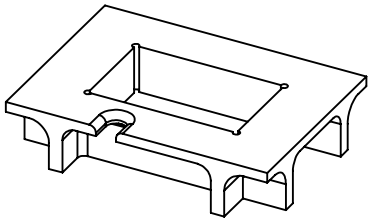

TRIMETRIC VIEW

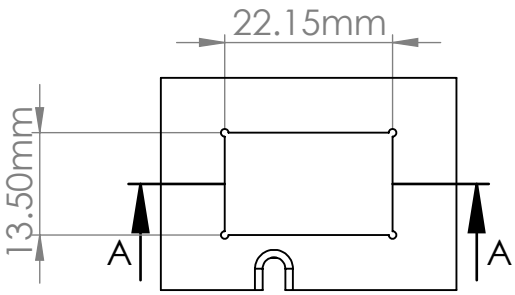

TOP VIEW

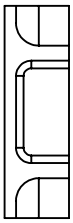

SIDE VIEW

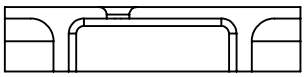

SIDE VIEW

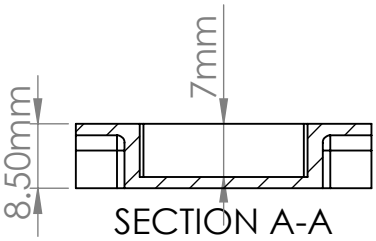

SECTION A-A

D.6. Lid for channel holder

Purpose: To hold mask in place and block unwanted light during curing.

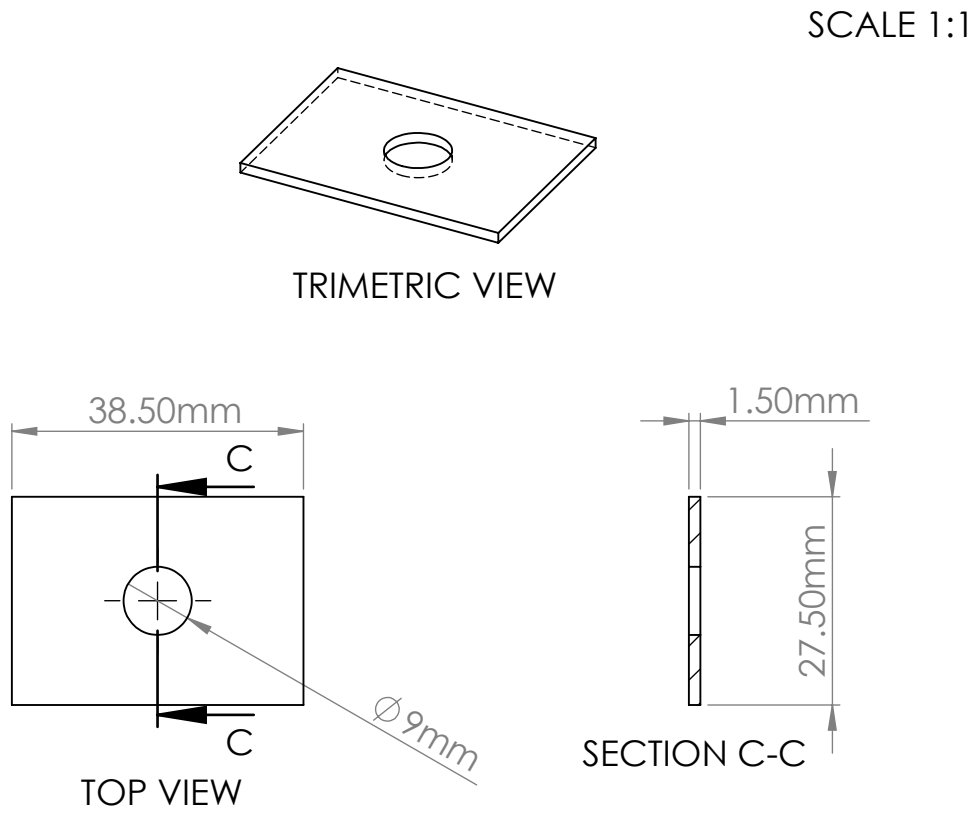

D.7. Channel holder for microscopy

Purpose: to keep a channel containing hydrogel disks stable and horizontal during inspection.

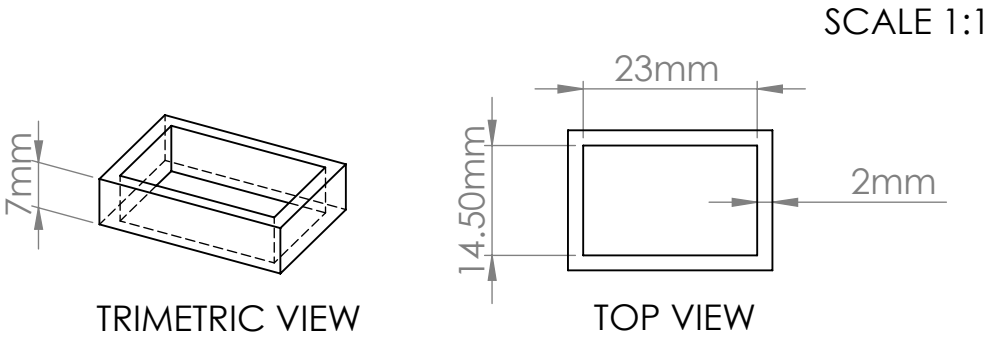

Bibliography

[1] SIGMA-ALDRICH / MERCK. URL www.sigmaaldrich.com.

[2] Hydrophilic Polymers. Technical report, Sigma-Aldrich (is now Merck), 2017. URL http://www.sigmaaldrich.com/materials-science/material-science-products.html?TablePage=16372116.

[3] Enas M. Ahmed. Hydrogel: Preparation, characterization, and applications: A review. *Journal of Advanced Research*, 6(2):105–121, 2015. ISSN 20901232. doi: 10.1016/j.jare.2013.07.006. URL http://dx.doi.org/10.1016/j.jare.2013.07.006.

[4] J. V. Alemán, A. V. Chadwick, J. He, M. Hess, K. Horie, R. G. Jones, P. Kratochvíl, I. Meisel, I. Mita, G. Moad, S. Penczek, and R. F. T. Stepto. Definitions of terms relating to the structure and processing of sols, gels, networks, and inorganic-organic hybrid materials (IUPAC Recommendations 2007). *Pure and Applied Chemistry*, 79(10):1801–1829, 2007. ISSN 1365-3075. doi: 10.1351/pac200779101801. URL http://www.degruyter.com/view/j/pac.2007.79.issue-10/pac200779101801/pac200779101801.xml.

[5] M. Alger. *Polymer Science Dictionary*. Chapman & Hall, 2nd edition, 1996. ISBN 9780412608704.

[6] P. Auroy, L. Auvray, and L. Léger. Characterization of the brush regime for grafted polymer layers at the solid-liquid interface. *Physical Review Letters*, 66(6):719–722, 1991. ISSN 00319007. doi: 10.1103/PhysRevLett.66.719.

[7] David J. Beebe, J S Moore, Q Yu, Robin H. Liu, M L Kraft, B H Jo, and C Devadoss. Microfluidic tectonics: a comprehensive construction platform for microfluidic systems. *Proceedings of the National Academy of Sciences of the United States of America*, 97(25):13488–93, 2000. ISSN 0027-8424. doi: 10.1073/pnas.250273097. URL http://www.pnas.org/content/97/25/13488.full.

[8] David J. Beebe, Jeffrey S. Moore, Joseph M Bauer, Qing Yu, Robin H. Liu, Chelladurai Devadoss, and Byung-Ho Jo. Functional hydrogel structures for autonomous flow control inside microfluidic channels. *Nature*, 404(6778):588–590, 2000. ISSN 1476-4687. doi: 10.1038/35007047. URL http://www.nature.com/doifinder/10.1038/35007047{%}5Cnpapers3://publication/doi/10.1038/35007047.

[9] Arnaud Bertsch and Philippe Renaud. Chapter 1.2 - Microstereolithography. In *Three-Dimensional Microfabrication Using Two-Photon Polymerization*, pages 20–44. Elsevier Inc., 2016. ISBN 9780323353212. doi: 10.1016/B978-0-323-35321-2/00002-9. URL http://dx.doi.org/10.1016/B978-0-323-35321-2/00002-9.

[10] Shantanu Bhattacharya. *Plasma bonding of Poly(dimethyl)siloxane and glass surfaces and its application to microfluidics*. PhD thesis, 2003.

[11] M. A. Biot. Theory of elasticity and consolidation for a porous anisotropic solid. *Journal of Applied Physics*, 26(2):182–185, 1955. ISSN 00218979. doi: 10.1063/1.1721956.

[12] Michael S. Bodnarchuk, Kay E. B. Doncom, Daniel B. Wright, David M. Heyes, Daniele Dini, and Rachel K. O'Reilly. Polyelectrolyte pKa from experiment and molecular dynamics simulation. *RSC Adv.*, 7(32):20007–20014, 2017. ISSN 2046-2069. doi: 10.1039/C6RA27785C. URL http://xlink.rsc.org/?DOI=C6RA27785C.

[13] Lisa Brannon-Peppas and Nikolaos A. Peppas. Equilibrium Swelling Behavior of pH-Sensitive Hydrogels. *Chemical Engineering*, 46(3):715–722, 1991. ISSN 00092509. doi: 10.1016/0009-2509(91)80177-Z. URL http://www.sciencedirect.com/science/article/B6TFK-444P1P4-H1/2/e866d771afcdad2db5bfa0e86fa92cc6.

[14] Enrica Caló and Vitaliy V. Khutoryanskiy. Biomedical applications of hydrogels: A review of patents and commercial products. *European Polymer Journal*, 65:252–267, 2015. ISSN 00143057. doi: 10.1016/j.eurpolymj.2014.11.024.

[15] Jonathan (University of Manchester) Clayden, Nick (University of Liverpool) Greeves, and Stuart (University of Cambridge) Warren. Acidity, basicity, and pKa. In *Organic Chemistry*, chapter 8, pages 163 – 181. Oxford university press, 2nd edition, 2012.

[16] Sudipto K. De, N. R. Aluru, B. Johnson, W. C. Crone, David J. Beebe, and J. Moore. Equilibrium swelling and kinetics of pH-responsive hydrogels: Models, experiments, and simulations. *Journal of Microelectromechanical Systems*, 11(5):544–555, 2002. ISSN 10577157. doi: 10.1109/JMEMS.2002.803281.

[17] J. de Jong, R. G. H. Lammertink, and M. Wessling. Membranes and microfluidics: a review. *Lab on a Chip*, 6(9):1125, 2006. ISSN 1473-0197. doi: 10.1039/b603275c. URL http://xlink.rsc.org/?DOI=b603275c.

[18] Haitao Dong, Hongbo Du, Xianghong Qian, Haitao Dong, Hongbo Du, and Xianghong Qian. Theoretical Prediction of p K Values for Methacrylic Acid Oligomers Using Combined Quantum Mechanical and Continuum Solvation Methods Theoretical Prediction of p K a Values for Methacrylic Acid Oligomers Using Combined Quantum Mechanical and Continuum Sol. pages 12687–12694, 2008. doi: 10.1021/jp807315p.

[19] Jean-Pierre Fouassier and Jacques Lalevee. Photopolymerizaton and Photo-Cross-Linking. In *Photoinitiators for Polymer Synthesis: Scope, Reactivity and Efficiency*, pages 3–20. Wiley-VCH Verlag GmbH & Co KGaA, 1st edition, 2012.

[20] Sami Franssila. Advanced Lithography. In *Introduction to Microfabrication*, pages 115 – 126. John Wiley & Sons, Ltd, 2nd edition, 2010.

[21] Sami Franssila. Optical Lithography. In *Introduction to Microfabrication*, pages 103–113. John Wiley & Sons, Ltd, 2nd edition, 2010.

[22] Sami Franssila. Polymer Microprocessing. In *Introduction to Microfabrication*, pages 203 – 223. John Wiley & Sons, Ltd, 2nd edition, 2010.

[23] S H Gehrke, J P Fisher, M Palasis, and M E Lund. Factors determining hydrogel permeability. *Annals of the New York Academy of Sciences*, 831(508):179–207, 1997. ISSN 00778923. doi: 10.1111/j.1749-6632.1997.tb52194.x.

[24] R Gemeinhart and Chunqiang Guo. Fast Swelling Hydrogel Systems. In Nobuhiko Yui, Randall J. Mrsny and Kinam Park, editors, *Reflexive Polymers and Hydrogels: Understanding and Designing Fast Responsive Polymeric Systems*, chapter 13, pages 245–257. CRC Press LLC, 2004. ISBN 0849314879. doi: doi:10.1201/9780203485354.ch13.

[25] Venkateshwarlu Gopishetty, Yuri Roiter, Ihor Tokarev, and Sergiy Minko. Multiresponsive biopolyelectrolyte membrane. *Advanced Materials*, 20(23):4588–4593, 2008. ISSN 09359648. doi: 10.1002/adma.200801610.

[26] P. E. Grimshaw, J. H. Nussbaum, A. J. Grodzinsky, and M. L. Yarmush. Kinetics of electrically and chemically induced swelling in polyelectrolyte gels. *The Journal of Chemical Physics*, 93(6):4462–4472, 1990. ISSN 0021-9606. doi: 10.1063/1.458729. URL http://aip.scitation.org/doi/10.1063/1.458729.

[27] Hongyan He, Xia Cao, and L. James Lee. Design of a novel hydrogel-based intelligent system for controlled drug release. *Journal of Controlled Release*, 95(3):391–402, 2004. ISSN 01683659. doi: 10.1016/j.jconrel.2003.12.004.

[28] Derek S Hernandez and Jason B Shear. Mask-Directed Micro-3D Printing. In *Three-Dimensional Microfabrication Using Two-Photon Polymerization*, pages 102–118. Elsevier Inc., 2016. ISBN 9780323353212. doi: 10.1016/B978-0-323-35321-2/00006-6. URL http://dx.doi.org/10.1016/B978-0-323-35321-2/00006-6.

[29] J. F. Hester, S. C. Olugebefola, and A. M. Mayes. Preparation of pH-responsive polymer membranes by self-organization. *Journal of Membrane Science*, 208(1-2):375–388, 2002. ISSN 03767388. doi: 10.1016/S0376-7388(02)00317-4.

[30] Allan S. Hoffman. Hydrogels for biomedical applications. *Advanced Drug Delivery Reviews*, 64 (SUPPL.):18–23, 2012. ISSN 0169409X. doi: 10.1016/j.addr.2012.09.010. URL http://dx.doi.org/10.1016/j.addr.2012.09.010.

[31] Dongeun Huh, Yu Suke Torisawa, Geraldine A. Hamilton, Hyun Jung Kim, and Donald E. Ingber. Microengineered physiological biomimicry: Organs-on-Chips. *Lab on a Chip*, 12(12):2156–2164, 2012. ISSN 14730189. doi: 10.1039/c2lc40089h.

[32] B. Johnson, David J. Beebe, and W. C. Crone. Effects of swelling on the mechanical properties of a pH-sensitive hydrogel for use in microfluidic devices. *Materials Science and Engineering C*, 24(4):575–581, 2004. ISSN 09284931. doi: 10.1016/j.msec.2003.11.002.

[33] Do Hyun Kang, Sang Moon Kim, Byungjun Lee, Hyunsik Yoon, and Kahp-Yang Suh. Stimuli-responsive hydrogel patterns for smart microfluidics and microarrays. *Analyst*, 138(21):6230–42, 2013. ISSN 1364-5528. doi: 10.1039/c3an01119d. URL http://www.ncbi.nlm.nih.gov/pubmed/24029824.

[34] Sang Moon Kim, Do Hyun Kang, Jai Hyun Koh, Hyo Seon Suh, Hyunsik Yoon, Kahp-Yang Suh, and Kookheon Char. Thermoresponsive switching of liquid flow direction on a two-face prism array. *Soft Matter*, 9(16):4145, 2013. ISSN 1744-683X. doi: 10.1039/c3sm27901d. URL http://xlink.rsc.org/?DOI=c3sm27901d.

[35] G. Kocak, C. Tuncer, and V. Bütün. pH-Responsive polymers. *Polym. Chem.*, 8(1):144–176, 2017. ISSN 1759-9954. doi: 10.1039/C6PY01872F. URL http://xlink.rsc.org/?DOI=C6PY01872F.

[36] Adam C Lee and Gordon M Crippen. Predicting pK by Molecular Tree Structured Fingerprints and PLS. *J. Chem. Inf. Comput. Sci.*, 43:870–879, 2003. doi: 10.1021/ci900209w.

[37] H Li, TY Ng, YK Yew, and KY Lam. Modeling and simulation of the swelling bahavior of pH-stimulus-responsive hydrogels. *Biomacromolecules*, 6:109–120, 2005.

[38] David R. (National Institute of Standards Lide and Technology), editors. *CRC Handbook of Chemistry and Physics*. CRC Press, 84th editi edition, 2003.

[39] Robin H. Liu, Qing Yu, and David J. Beebe. Fabrication and characterization of hydrogel-based microvalves. *Journal of Microelectromechanical Systems*, 11(1):45–53, 2002. ISSN 10577157. doi: 10.1109/84.982862.

[40] Gabriel S. Longo, Monica Olvera De La Cruz, and I. Szleifer. Molecular theory of weak polyelectrolyte gels: The role of pH and salt concentration. *Macromolecules*, 44(1):147–158, 2011. ISSN 00249297. doi: 10.1021/ma102312y.

[41] Chris A Mack and Finle Technologies. Optical Proximity Effects, part 1. (Spring), 1996. ISSN 1074407X.

[42] Marc J Madou. Lithography (Part I). In *Fundamentals of Microfabrication and Nanotechnology, volume II*, pages 2 – 147. 2011.

[43] Arvind M. Mathur, Shailender K. Moorjani, and Alec B. Scranton. Methods for Synthesis of Hydrogel Networks: A Review. *Journal of Macromolecular Science, Part C: Polymer Reviews*, 36(2):405–430, 1996. ISSN 1532-1797. doi: 10.1080/15321799608015226. URL http://www.tandfonline.com/doi/abs/10.1080/15321799608015226.

[44] A. D. McNaught, A. Wilkinson, M. Nic, J. Jirat, B. Kosata, and A. Jenkins. *IUPAC. Compendium of Chemical Terminology, 2nd ed. (the "Gold Book")*. Blackwell Scientific Publications, Oxford, 2006. ISBN 0-9678550-9-8. doi: https://doi.org/10.1351/goldbook. URL http://goldbook.iupac.org.

[45] Sergiy Minko. Responsive polymer brushes. *Polym. Rev.*, 46(Copyright (C) 2012 American Chemical Society (ACS). All Rights Reserved.):397–420, 2006. ISSN 1558-3724. doi: 10.1080/15583720600945402.

[46] Nanoscribe. Data Sheet Photonic Professional, 2016.

[47] John W. Nicholson. Polymerisation Reactions. In *The Chemistry of Polymers*, pages 23 – 41. Royal Society of Chemistry, 4th edition, 2012.

[48] Lucie Nova, Filip Uhlik, and Peter Kosovan. Local pH and effective pKa of weak polyelectrolytes – insights from computer simulations. *Phys. Chem. Chem. Phys.*, (2):14376–14387, 2017. ISSN 1463-9076. doi: 10.1039/C7CP00265C. URL http://pubs.rsc.org/en/Content/ArticleLanding/2017/CP/C7CP00265C.

[49] Mangala S. Oak, Takaomi Kobayashi, Hong Ying Wang, Takahiro Fukaya, and Nobuyuki Fujii. pH effect on molecular size exclusion of polyacrylonitrile ultrafiltration membranes having carboxylic acid groups. *Journal of Membrane Science*, 123(2):185–195, 1997. ISSN 03767388. doi: 10.1016/S0376-7388(96)00214-1.

[50] O Okay. General Properties of Hydrogels. In Gerald Gerlach and Karl-Friedrich Arndt, editors, *Hydrogel Sensors and Actuators*, pages 1–14. Springer, 2010. ISBN 978-3-540-75644-6. doi: 10.1007/978-3-540-75645-3. URL http://link.springer.com/10.1007/978-3-540-75645-3.

[51] Maxim Orlov, Ihor Tokarev, Andreas Scholl, Andrew Doran, and Sergiy Minko. pH-responsive thin film membranes from poly(2-vinylpyridine): Water vapor-induced formation of a microporous structure. *Macromolecules*, 40(6):2086–2091, 2007. ISSN 00249297. doi: 10.1021/ma062821f.

[52] K. Pal, A. K. Banthia, and D. K. Majumdar. Polymeric Hydrogels: Characterization and Biomedical Applications. *Designed Monomers & Polymers*, 12(3):197–220, 2009. ISSN 1385772X. doi: 10.1163/156855509X436030. URL http://www.tandfonline.com/doi/full/10.1163/156855509X436030.

[53] Yong Soon Park, Yoshihiro Ito, and Yukio Imanishi. pH-Controlled Gating of a Porous Glass Filter by Surface Grafting of Polyelectrolyte Brushes. *Chemistry of Materials*, 9(14):2755, 1997. ISSN 0897-4756. doi: 10.1021/cm970034e.

[54] Nikolaos A. Peppas. Kinetics of Smart Hydrogels. In Nobuhiko Yui, Randall J. Mrsny and Kinam Park, editors, *Reflexive Polymers and Hydrogels: Understanding and Designing Fast Responsive Polymeric Systems*, chapter 7. CRC Press LLC, 2004. ISBN 0849312876. doi: 10.1016/B978-1-4160-4210-5/00011-6.

[55] Olga E. Philippova, Dominique Hourdet, Roland Audebert, and Alexei R. Khokhlov. pH-Responsive Gels of Hydrophobically Modified Poly(acrylic acid). *Macromolecules*, 30(26):8278–8285, 1997. ISSN 0024-9297. doi: 10.1021/ma970957v. URL http://pubs.acs.org/doi/abs/10.1021/ma970957v.

[56] Dong Qin, Younan Xia, and George M. Whitesides. Advanced Materials. *Advanced MaterialsMaterials*, 9(11):639–643, 1997.

[57] Jetse Reijenga, Arno van Hoof, Antonie van Loon, and Bram Teunissen. Development of methods for the determination of pKa values. *Analytical Chemistry Insights*, 8(1):53–71, 2013. ISSN 11773901. doi: 10.4137/ACI.S12304.

[58] F. Rodriguez, C. Cohen, Cristopher K. Ober, and Lynden A. Archer. Some general properties of polymer systems. In *Principles of Polymer Systems*, pages 413 – 434. 2003.

[59] Janusz M. Rosiak and Fumio Yoshii. Hydrogels and their medical applications. *Nuclear Instruments and Methods in Physics Research, Section B: Beam Interactions with Materials and Atoms*, 151(1-4):56–64, 1999. ISSN 0168583X. doi: 10.1016/S0168-583X(99)00118-4.

[60] Eric K. Sackmann, Anna L. Fulton, and David J. Beebe. The present and future role of microfluidics in biomedical research. *Nature*, 507(7491):181–189, 2014. ISSN 14764687. doi: 10.1038/nature13118. URL http://dx.doi.org/10.1038/nature13118.

[61] Dirk Schmaljohann. Thermo- and pH-responsive polymers in drug delivery. *Advanced Drug Delivery Reviews*, 58:1655–1670, 2006. doi: 10.1016/j.addr.2006.09.020.

[62] Sigma-Aldrich. Photoinitiators: UV absorption Spectra. ISSN 0196-6553. URL https://www.sigmaaldrich.com/content/dam/sigma-aldrich/docs/Aldrich/Brochure/al{_}pp{_}spectra.pdf.

[63] Martien A. Cohen Stuart, Wilhelm T. S. Huck, Jan Genzer, Marcus Müller, Cristopher K. Ober, Manfred Stamm, Gleb B. Sukhorukov, Igal Szleifer, Vladimir V. Tsukruk, Marek Urban, Françoise Winnik, Stefan Zauscher, Igor Luzinov, and Sergiy Minko. Emerging applications of stimuli-responsive polymer materials. *Nature Materials*, 9(2):101–113, 2010. ISSN 1476-1122. doi: 10.1038/nmat2614. URL http://www.nature.com/doifinder/10.1038/nmat2614.

[64] Kamlesh J Suthar, Derrick C Mancini, and Muralidhar K Ghantasala. Simulation of the effect of different parameters on the swelling characteristics of a pH-sensitive hydrogel. *Proceedings of SPIE-The International Society for Optical Engineering*, 7644:764418, 2010. ISSN 0277-786X; 978-0-8194-8059-0. doi: 10.1117/12.849138.

[65] Kamlesh J Suthar, Derrick C Mancini, Muralidhar K Ghantasala, Advanced Photon Source, and Physical Sciences. The Swelling Responsiveness of pH-Sensitive Hydrogels in 3D Arbitrary Shaped Geometry. pages 1–6, 2013.

[66] Kamleshkumar J Suthar. *Simulation, Synthesis, and Characterization of Hydrogels and Nanocomposite Gels*. PhD thesis, Western Michigan University, 2009. URL http://scholarworks.wmich.edu/dissertations.

[67] Masao Tamada, Masaharu Asano, Reimar Spohr, Johann Vetter, Christine Trautmann, Masaru Yoshida, Ryouichi Katakai, and Hideki Omichi. Preparation of hydrolyzed pH responsive ion track membrane. *Macromol. Rapid Commun.*, 51:47–51, 1995.

[68] Benjamin G Tehan, Edward J Lloyd, Margaret G Wong, Will R Pitt, John G Montana, and David T Manallack. Estimation of pK a Using Semiempirical Molecular Orbital Methods . Part 1 : Application to Phenols and Carboxylic Acids . *Quant. Struct.-Act. Relat.*, 21:457–472, 2002. ISSN 09318771. doi: 10.1002/1521-3838(200211)21:5<457::AID-QSAR457>3.0.CO;2-5.

[69] Yuksel Temiz, Robert D. Lovchik, Govind V. Kaigala, and Emmanuel Delamarche. Lab-on-a-chip devices: How to close and plug the lab? *Microelectronic Engineering*, 132:156–175, 2015. ISSN 01679317. doi: 10.1016/j.mee.2014.10.013.

[70] Ihor Tokarev, Maxim Orlov, and Sergiy Minko. Responsive polyelectrolyte gel membranes. *Advanced Materials*, 18(18):2458–2460, 2006. ISSN 09359648. doi: 10.1002/adma.200601288.

[71] Ihor Tokarev, Maxim Orlov, Evgeny Katz, and Sergiy Minko. An electrochemical gate based on a stimuli-responsive membrane associated with an electrode surface. *Journal of Physical Chemistry B*, 111(42):12141–12145, 2007. ISSN 15206106. doi: 10.1021/jp0757208.

[72] Ihor Tokarev, Venkateshwarlu Gopishetty, Jian Zhou, Marcos Pita, Mikhail Motornov, Evgeny Katz, and Sergiy Minko. Stimuli-responsive hydrogel membranes coupled with biocatalytic processes. *ACS Applied Materials and Interfaces*, 1(3):532–536, 2009. ISSN 19448244. doi: 10.1021/am800251a.

[73] Faheem Ullah, Muhammad Bisyrul Hafi Othman, Fatima Javed, Zulkifli Ahmad, and Hazizan Md Akil. Classification, processing and application of hydrogels: A review. *Materials Science and Engineering C*, 57:414–433, 2015. ISSN 09284931. doi: 10.1016/j.msec.2015.07.053.

[74] Marek W Urban. *Biologically Responsive Polymers*. The Royal Society of Chemistry, 2016. ISBN 978-1-84973-656-5.

[75] Marek W. Urban. Stimuli-responsive Materials in Medical Therapy. In *Stimuli-Responsive Materials*, pages 254–286. Royal Society of Chemistry, 2016.

[76] Marek W Urban. *Stimuli-responsive Surfaces and Interfaces*. The Royal Society of Chemistry, 2016. ISBN 978-1-84973-656-5.

[77] Marek W Urban. *What is Stimuli Responsiveness?* The Royal Society of Chemistry, 2016. ISBN 978-1-84973-656-5.

[78] Thomas Wallmersperger. Modelling and Simulation of the Chemo-Electro-Mechanical Behaviour. In Gerald Gerlach and Karl-Friedrich Arndt, editors, *Hydrogel Sensors and Actuators*, pages 137 – 163. Springer, 2010. ISBN 978-3-540-75644-6. doi: 10.1007/978-3-540-75645-3. URL http://link.springer.com/10.1007/978-3-540-75645-3.

[79] Thomas Wallmersperger, Bernd Kröplin, Jens Holdenried, and Rainer W. Guelch. Coupled multi-field formulation for ionic polymer gels in electric fields. *Proceedings of SPIE*, 4329(Smart Structures and Materials 2001: Electroactive Polymer Actuators and Devices), 2001.

[80] Daniel Wandera, S. Ranil Wickramasinghe, and Scott M. Husson. Stimuli-responsive membranes. *Journal of Membrane Science*, 357(1-2):6–35, 2010. ISSN 03767388. doi: 10.1016/j.memsci.2010.03.046. URL http://dx.doi.org/10.1016/j.memsci.2010.03.046.

[81] Evan M. White, Jeremy Yatvin, Joe B. Grubbs, Jenna A. Bilbrey, and Jason Locklin. Advances in smart materials: Stimuli-responsive hydrogel thin films. *Journal of Polymer Science, Part B: Polymer Physics*, 51(14):1084–1099, 2013. ISSN 08876266. doi: 10.1002/polb.23312.

[82] Fumiki Yanagawa, Shinji Sugiura, and Toshiyuki Kanamori. Hydrogel microfabrication technology toward three dimensional tissue engineering. *Regenerative Therapy*, 3:45–57, 2016. ISSN 2352-3204. doi: 10.1016/j.reth.2016.02.007. URL http://dx.doi.org/10.1016/j.reth.2016.02.007.

[83] Jing Zhang and Nikolaos A. Peppas. Synthesis and Characterization of pH- and Temperature-Sensitive Poly (methacrylic acid)/ Poly (N -isopropylacrylamide) Interpenetrating Polymeric Networks. *Macromolecules*, 33:102–107, 2000. ISSN 0024-9297. doi: 10.1021/ma991398q.